CSIRO Marine Laboratories
Report 223

# Wave Climate Measurements in the Southern Ocean

J.S. Reid and C.B. Fandry

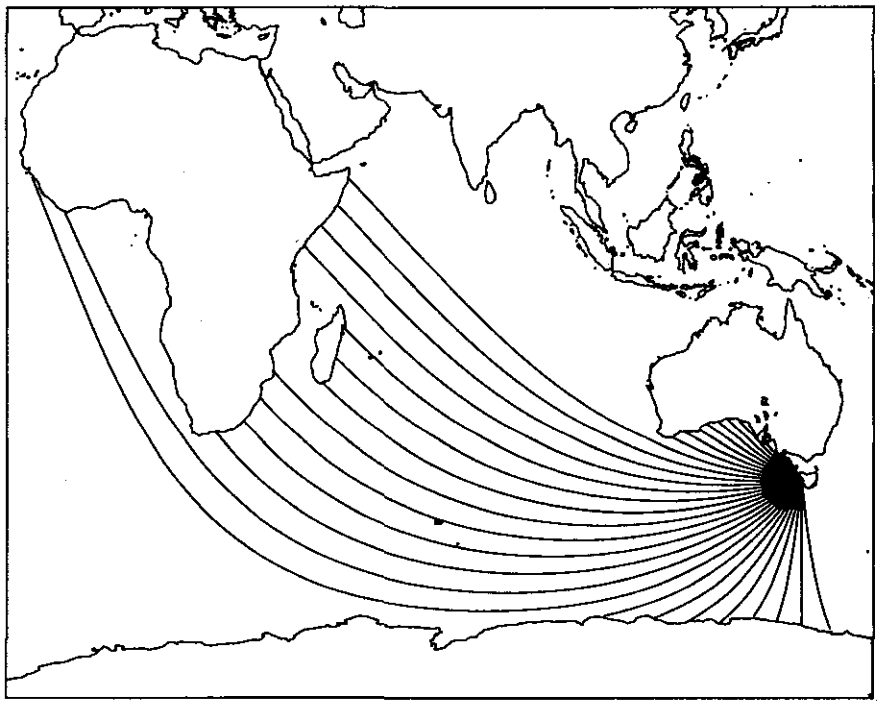

CSIRO
AUSTRALIA

1994

CSIRO Marine Laboratories - Report 223

# Wave Climate Measurements in the Southern Ocean

J.S.Reid and C.B.Fandry

November 1994

## Abstract

Wave observations from four sites in the Southern Ocean off the Tasmanian west coast in the period July 1985 to December 1993 are presented. Twenty four time domain and frequency domain "burst" or sample statistics were selected and their distributions and interrelationships analysed. Wave data were also recorded simultaneously at different sites allowing the spatial coherence of burst statistics and spectral variances to be examined. It is concluded that average differences in energy in different spectral bands may be due to focussing effects of bottom topography.

The dependence of burst statistics and average spectra on wind velocity is examined. The variance of the vertical acceleration of the sea surface i.e. the fourth spectral moment of sea surface elevation was found to be well correlated with onshore wind speed. The major effect of onshore winds was to enhance a pre-existing swell. During offshore winds the swell peak was diminished by the wind. During high offshore winds a wind-sea peak was superimposed on the diminished swell peak.

The effect of using intermittently collected data rather than continuously collected data to estimate the return period of sample statistics is discussed. In order to use intermittent data for this purpose the mean duration of extreme events must be known or estimated. The one hundred year return period significant wave height for the west coast site is estimated to be 15.7 metres. A maximum significant wave height of 13.59 metres was observed in the course of this study. The largest single wave height measured was 19.83 metres.

**National Library of Australia Cataloguing-in-Publication**

Reid, J.S. (John Sinclair)
Wave Climate Measurements in the Southern Ocean

ISBN 0 643 05623 8.

1. Ocean waves - Antarctic Ocean - Statistics. 2. Ocean circulation - Antarctic Ocean - Statistics. 3. Submarine topography. I Fandry, C. B. (Chris B.).
II. CSIRO. Marine Laboratories. III. Title. (Series: Report (CSIRO Marine Laboratories) ; 223).

551.470209167

# Contents

# List of Figures

# List of Tables

# 1 Introduction

In July 1985 the Division of Oceanography embarked on a wave observation program with the deployment of two "Waverider" buoys in the Southern Ocean near Cape Sorell on the west coast of Tasmania. A map showing this site in a larger context is shown in Figure 1. Great circle fetches from the site generally extend through the Southern Ocean to South Africa and Madagascar. For a small range of azimuths near 215°, fetches extend 15,000 Km into the South Atlantic.

Very few systematic observations had been made of the wave climate of the Southern Ocean in the Australian region. What data did exist from, for example, lighthouse reports, has been shown to be inconsistent and unreliable (Underwood, 1987). In subsequent years measurements were made at other sites: further north near Cape Grim and in Storm Bay (Figure 2).

These observations are used to assess both typical and extreme sea states at these sites and for estimating spatial, seasonal and interannual variations in wave conditions in the Tasmanian region.

The program concluded in December 1993 when the Storm Bay buoy ceased operation.

# 2 The Measurement Program

## 2.1 Equipment

Throughout the program "Waverider" buoys and "Diwar" receivers manufactured by Datawell bv of Haarlem, The Netherlands were used to make the observations.

The Waverider buoy consists of a metal sphere, 70 cm in diameter which floats half submerged and which is attached to a mooring by means of a rubber tether. As it moves an accelerometer inside the sphere senses the vertical component of the motion. The sensitivity of the accelerometer to rotations and horizontal motions is greatly reduced by mounting it on a damped gimbaled platform. The accelerometer signal is integrated electronically inside the buoy to convert it to a signal representing the vertical displacement of the buoy and this, in turn, is converted to a frequency modulated tone which is continuously broadcast as an HF radio signal via a low power transmitter and a quarter-wave whip antenna

mounted on top of the buoy. On shore the signal is detected by the "Diwar" radio receiver and converted to digital form.

A personal computer was programmed to interrogate the receiver and to accept and save the digitized data. Generally a modem was also connected to the personal computer. This enabled data to be retrieved from the shore base by means of the public telephone system. At other times data were retrieved via floppy disk.

Each buoy was calibrated prior to deployment. This was done by means of a specially built apparatus which allowed the buoy to be rotated in a vertical circle 1.515 m in radius. The buoy was constrained to be oriented vertically while it was rotated to simulate its motion in the sea. The period of the rotation could be varied continuously from 2.7 seconds to over 40 seconds.

Calibration was carried out at eight or so spot frequencies. The calibration curve closely resembled the manufacurer's specifications and the calibration factor never varied by more than four percent from the nominal value of one bit per cm.

## 2.2 Deployment

Buoys were deployed in three areas, Cape Grim ("CG"), Cape Sorell ("CS") and Storm Bay ("SB") as shown in Figure 2. These areas are shown in greater detail in Figures 3, 4 and 5 in which the locations of the buoys are shown. In Figure 3 buoys were deployed at sites "G" and "H" and the shore base was located at the Cape Grim Baseline Air Pollution Station at "CG". In Figure 4 buoys were deployed at sites "A","B","C" and "D" and the shore base was located in the township of Strahan. A wind tower was located at Granville Harbour, "GH" in the diagram. Figure 5 shows the location of the buoy at "W" near Wedge Island and the shorebase at "F". The precise location of these mooring sites are listed in Table 1.

For simplicity the sites will be aggregated into four sites, viz:

| | |
|---|---|
| Cape Grim | G,H |
| Cape Sorell (100m) | B,C |
| Cape Sorell (50m) | A,D |
| Storm Bay | W |

Although the buoys broadcast their data continuously only short samples or "bursts" of data were digitized and saved by the computer for further

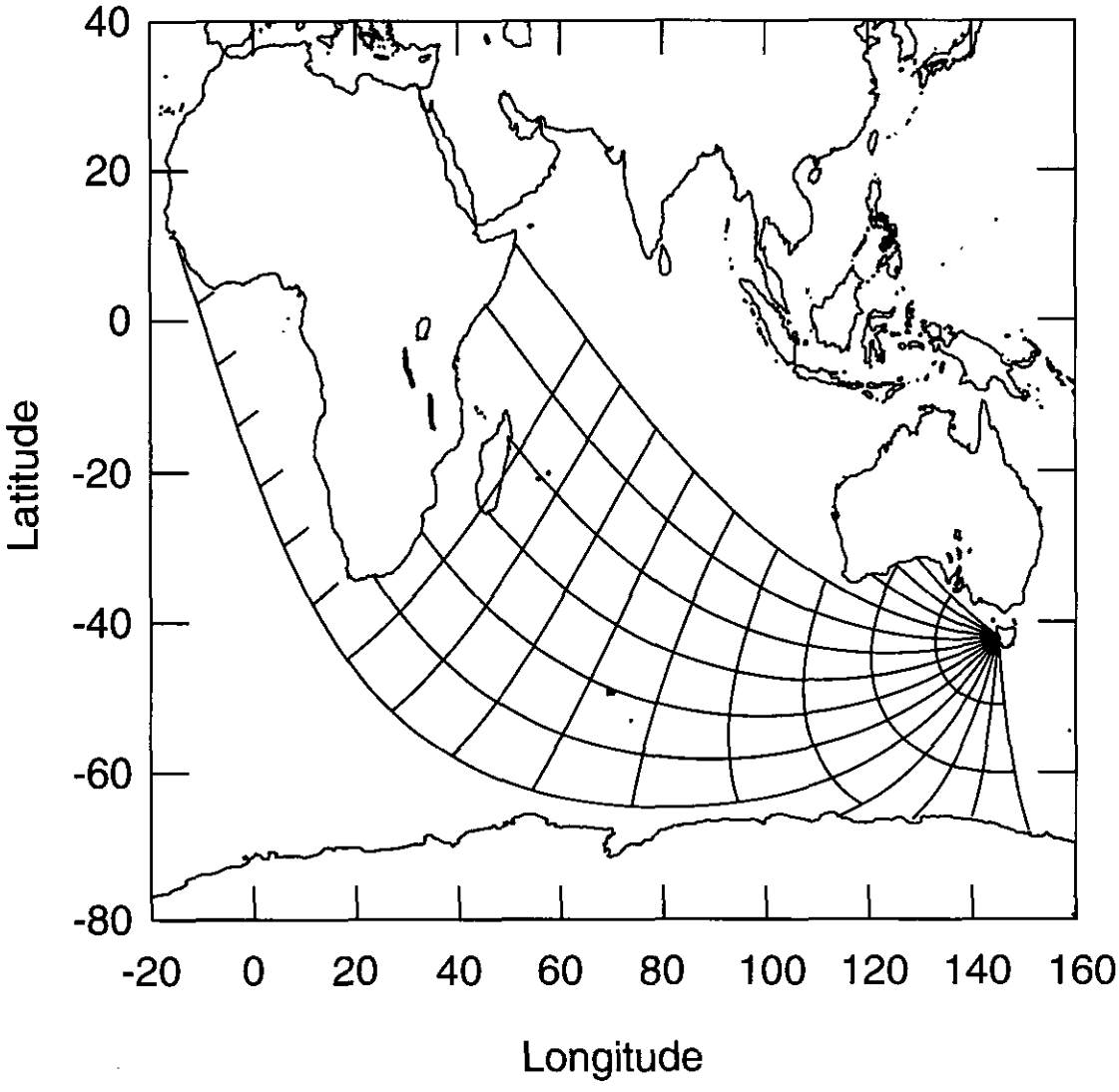


Figure 1: Map showing the Cape Sorell study sites in a world context. Great circle fetches to the site for azimuths ranging from 175° to 305° by 10° intervals are shown. Range marks are drawn every 1000 Km along the great circles.

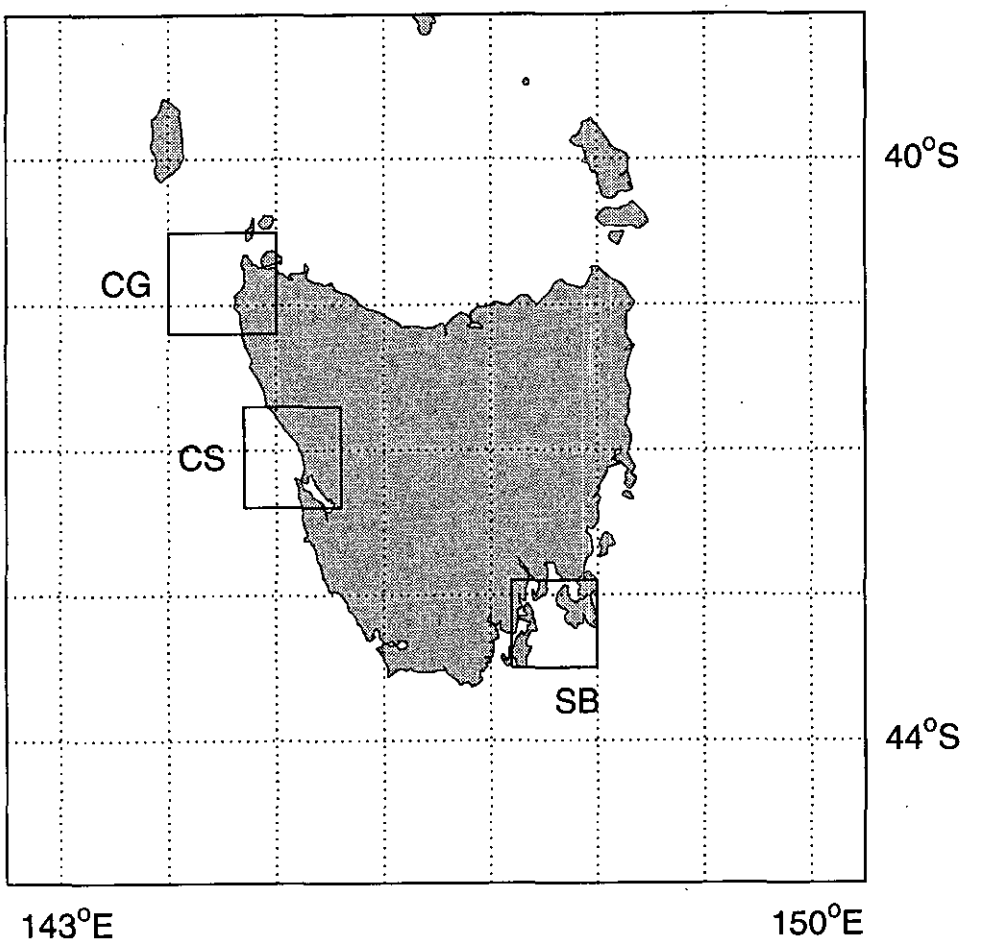


Figure 2: Tasmania showing the three study regions, Cape Grim, "CG", Cape Sorell, "CS" and Storm Bay, "SB".

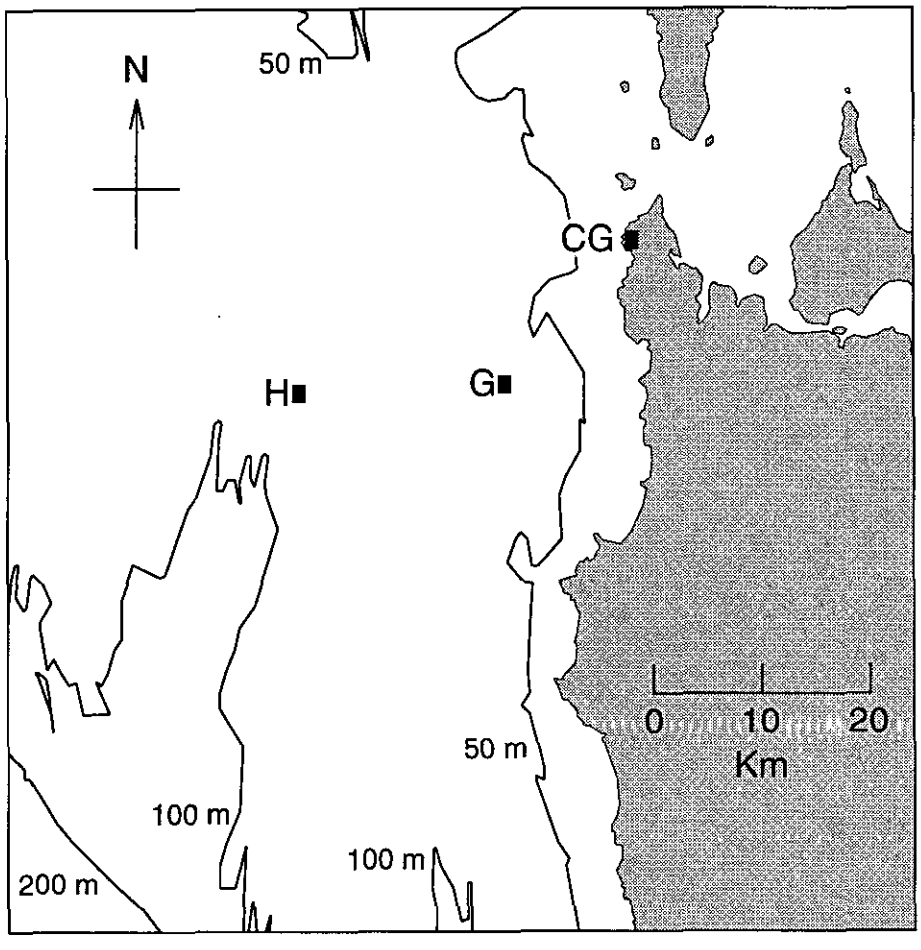


Figure 3: The Cape Grim study region showing the two sites used, "G" and "H". The shore base was locate at the Cape Grim Air Polluution Baseline Monitoring Station, "CG". Depth contours at 50m, 100m and 200m are shown.

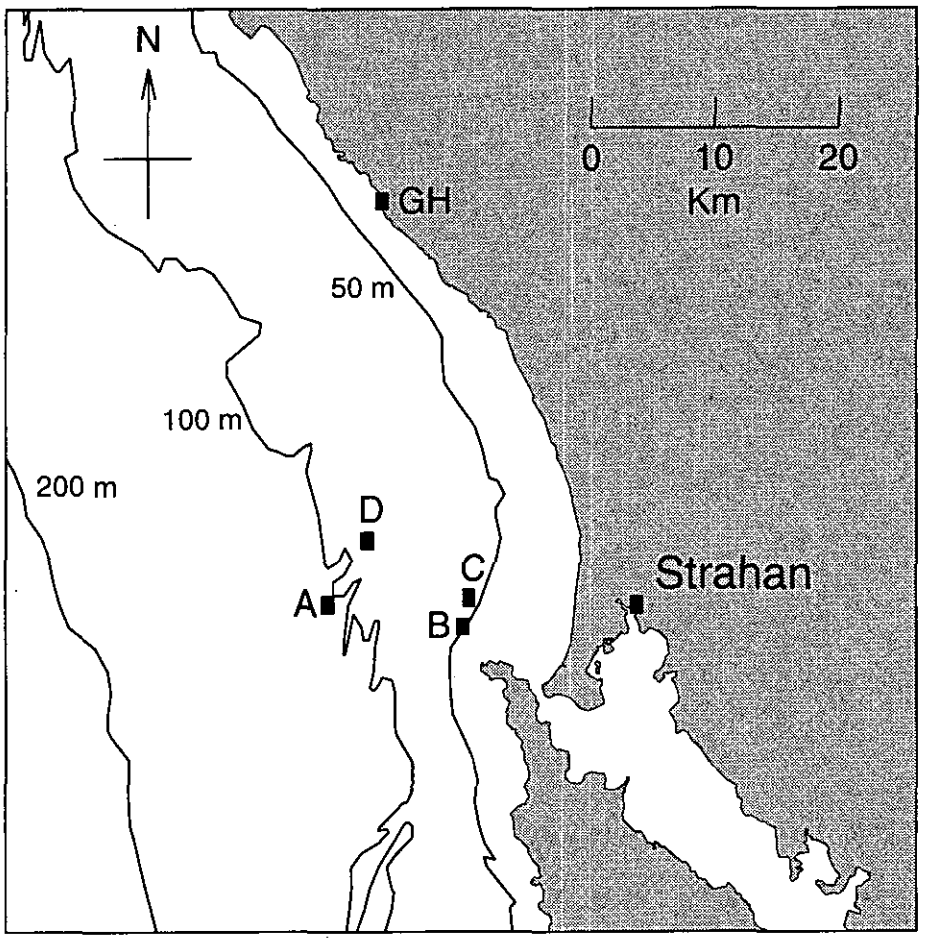


Figure 4: The Cape Sorell study region showing the four buoy sites used, "A","B","C" and "D". Wind data were obtained from Granville Harbour, "GH". The shore base was situated in the township of Strahan. Depth contours at 50m, 100m and 200m are shown.

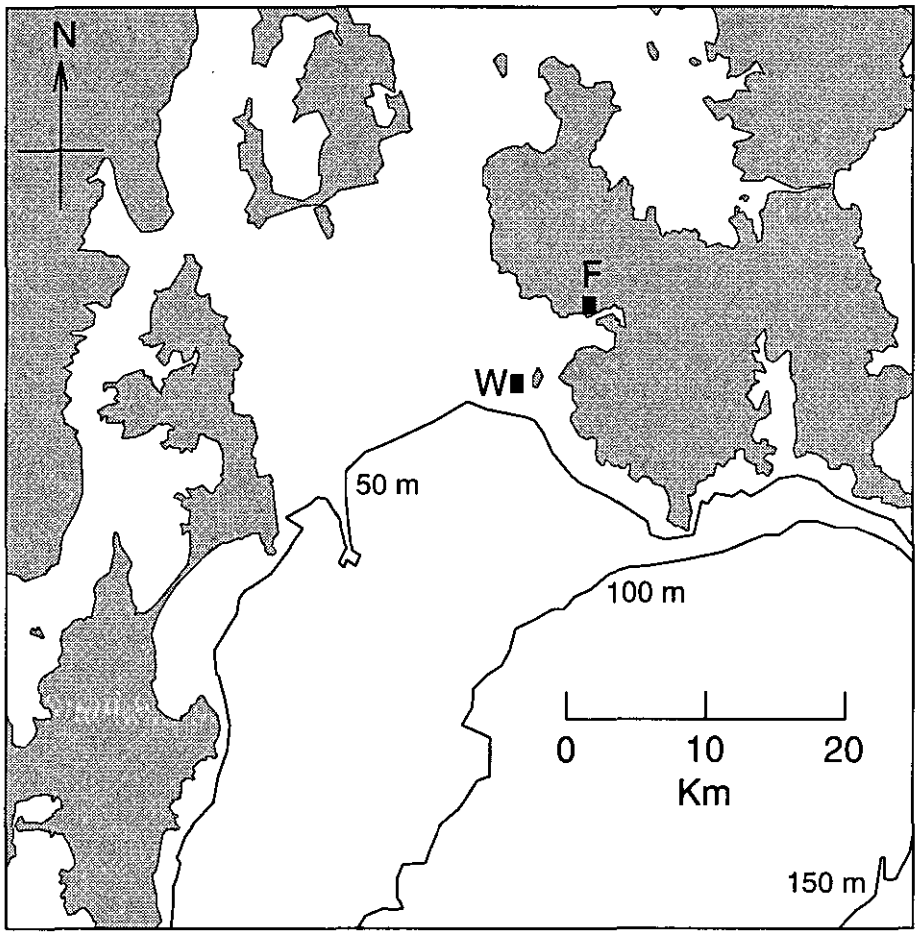


Figure 5: The Storm Bay study region showing the buoy site near Wedge Island, "W", and the shore base at the Nubeena Fish Farm, "F". Depth contours at 50m, 100m and 150m are shown.

| label | latitude | | | longitude | | | depth |
|---|---|---|---|---|---|---|---|
| | deg | min | | deg | min | | metres |
| A | 42 | 9.0 | S | 145 | 1.0 | E | 100 |
| B | 42 | 10.0 | S | 145 | 9.0 | E | 50 |
| C | 42 | 8.7 | S | 145 | 9.4 | E | 50 |
| D | 42 | 6.1 | S | 145 | 3.3 | E | 100 |
| G | 40 | 47.0 | S | 145 | 33.0 | E | 65 |
| H | 40 | 47.4 | S | 145 | 19.3 | E | 97 |
| W | 43 | 8.6 | S | 145 | 39.1 | E | 40 |

Table 1: Waverider buoy sites

analysis. During the first few months of the program a burst comprising 1024 measurements of sea surface height sampled at 2.56 samples per second was saved every two hours. After 18 November 1985 the bursts were doubled in length and sampled less frequently, viz, every three hours. The sampling rate of 2.56 Hz remained unchanged.

Figure 6 shows schematically the periods during which data were gathered from the various sites. These periods are shown more precisely in Table 2. The gaps are chiefly due to equipment failures, usually flat batteries or buoys coming adrift from moorings. Mooring failure was particularly prevalent in the Cape Grim area. On five out of six occasions when moorings failed the missing buoy was found and recovered by fishermen. Five buoys in all were purchased and of these only one was lost without trace in the course of the project.

Bursts of sea surface height data collected in this way were saved on hard disk as a number of "archives" and backed up onto exabyte tape. The archives were then used to provide a database of burst statistics. There were 101 megabytes in the archives and 24 megabytes in the database.

## 2.3 Data Quality

The "Diwar" receivers used in the project had the advantage of providing a built-in data quality assessment. This took the form of an "unlocked" indication which is passed to the computer by the setting of an "unlocked" bit in the data word. The term "unlocked" refers to the failure of the phase-locked loop in the receiver to lock onto the frequency modulated audio tone generated by the buoy. This occurred when the strength of the radio signal was weak or when radio interference was present. Experience showed that the unlocked flag was a very reliable indicator of suspect data. An

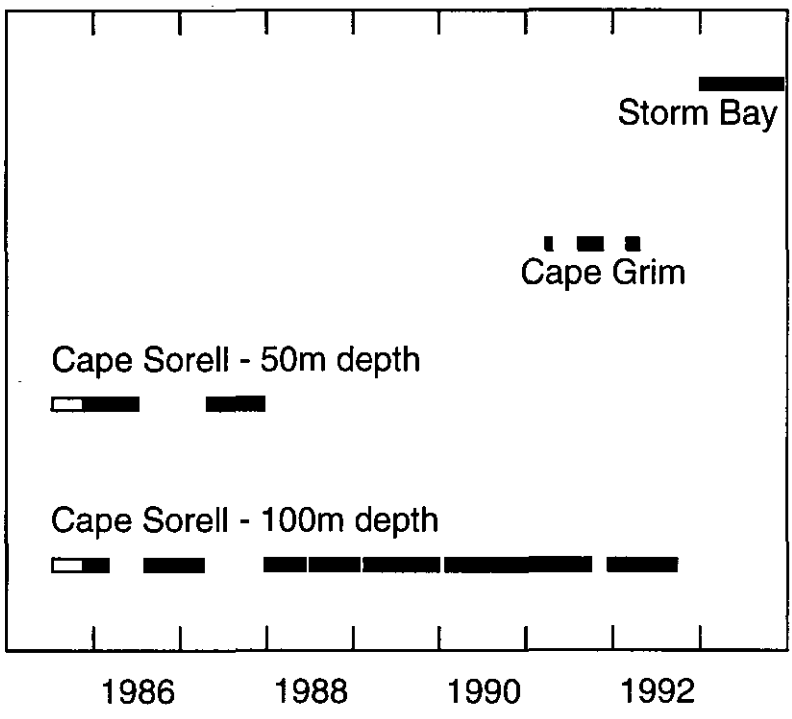


Figure 6: Deployment of wave buoys at the four sites. The filled rectangles indicate the intervals and locations at which 800 second long bursts of data were collected every 3 hours. The empty rectangles indicate the intervals and locations at which 400 second bursts were collected every 2 hours.

| site | from | to | samples/burst | burst rate |
|---|---|---|---|---|
| A | 11/7/85 | 18/11/85 | 1024 | 2 hourly |
| A | 18/11/85 | 2/3/86 | 2048 | 3 hourly |
| A | 4/8/86 | 9/4/87 | 2048 | 3 hourly |
| B | 11/7/85 | 18/11/85 | 1024 | 2 hourly |
| B | 18/11/85 | 7/7/86 | 2048 | 3 hourly |
| C | 27/4/87 | 21/12/87 | 2048 | 3 hourly |
| D | 22/12/87 | 11/6/88 | 2048 | 3 hourly |
| D | 1/7/88 | 25/1/89 | 2048 | 3 hourly |
| D | 15/2/89 | 29/12/89 | 2048 | 3 hourly |
| D | 26/1/90 | 29/9/91 | 2048 | 3 hourly |
| D | 12/12/91 | 24/9/92 | 2048 | 3 hourly |
| H | 28/3/91 | 21/4/91 | 2048 | 3 hourly |
| H | 12/8/91 | 20/11/91 | 2048 | 3 hourly |
| G | 2/3/92 | 20/4/92 | 2048 | 3 hourly |
| W | 1/1/93 | 14/12/93 | 2048 | 3 hourly |

Table 2: Waverider buoy deployment

| | Jan | Feb | Mar | Apr | May | Jun | Jul | Aug | Sep | Oct | Nov | Dec |
|---|---|---|---|---|---|---|---|---|---|---|---|---|
| 1985 | - | - | - | - | - | - | 29.0 | 75.5 | 68.3 | 78.8 | 77.7 | 47.2 |
| 1986 | 18.1 | - | 76.6 | 75.8 | 89.1 | 86.3 | 14.1 | - | - | - | - | - |
| 1987 | - | - | - | 5.0 | 94.8 | 97.5 | 96.0 | 98.8 | 98.3 | 98.4 | 97.9 | 66.9 |

Table 3: Percentages of good data recovery from Cape Sorell (50m)

| | Jan | Feb | Mar | Apr | May | Jun | Jul | Aug | Sep | Oct | Nov | Dec |
|---|---|---|---|---|---|---|---|---|---|---|---|---|
| 1985 | - | - | - | - | - | - | 27.4 | 77.2 | 72.8 | 80.4 | 79.3 | 42.3 |
| 1986 | 55.2 | 37.5 | 4.8 | - | - | - | - | 83.9 | 87.5 | 79.4 | 88.3 | 81.0 |
| 1987 | 55.6 | 8.5 | 76.6 | - | - | - | - | - | - | - | - | 28.6 |
| 1988 | 95.2 | 96.6 | 94.4 | 86.3 | 91.5 | 32.9 | 85.9 | 63.3 | 60.0 | 56.9 | 54.6 | 78.6 |
| 1989 | 46.8 | 41.1 | 74.6 | 66.3 | 77.0 | 80.8 | 70.2 | 77.0 | 68.8 | 68.5 | 88.3 | 73.8 |
| 1990 | 11.7 | 64.3 | 0.4 | 37.5 | 52.0 | 59.6 | 58.5 | 35.5 | 92.5 | 98.8 | 80.0 | 98.0 |
| 1991 | 59.7 | 97.8 | 98.4 | 67.5 | 85.9 | 86.3 | 95.6 | 81.0 | 80.8 | - | - | 61.3 |

Table 4: Percentages of good data recovery from Cape Sorell (100m)

| | Jan | Feb | Mar | Apr | May | Jun | Jul | Aug | Sep | Oct | Nov | Dec |
|---|---|---|---|---|---|---|---|---|---|---|---|---|
| 1991 | - | - | 10.9 | 56.7 | - | - | - | 42.3 | 83.3 | 89.1 | 41.3 | - |
| 1992 | - | - | 95.2 | 62.5 | - | - | - | - | - | - | - | - |

Table 5: Percentages of good data recovery from Cape Grim

| | Jan | Feb | Mar | Apr | May | Jun | Jul | Aug | Sep | Oct | Nov | Dec |
|---|---|---|---|---|---|---|---|---|---|---|---|---|
| 1993 | 98.8 | 98.7 | 99.6 | 100.0 | 100.0 | 98.8 | 98.8 | 99.2 | 100.0 | 99.2 | 93.3 | 42.3 |

Table 6: Percentages of good data recovery from Storm Bay

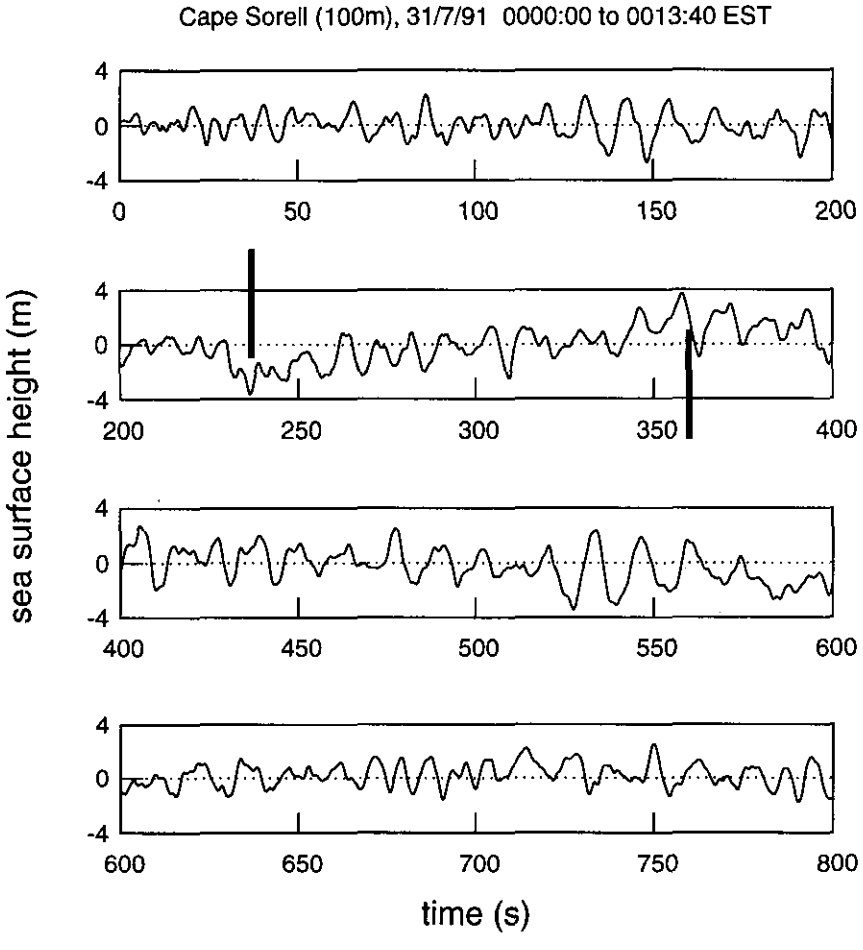


Figure 7: A time series of sea surface height showing anomolous buoy behaviour after 240 seconds and 360 seconds (vertical bars).

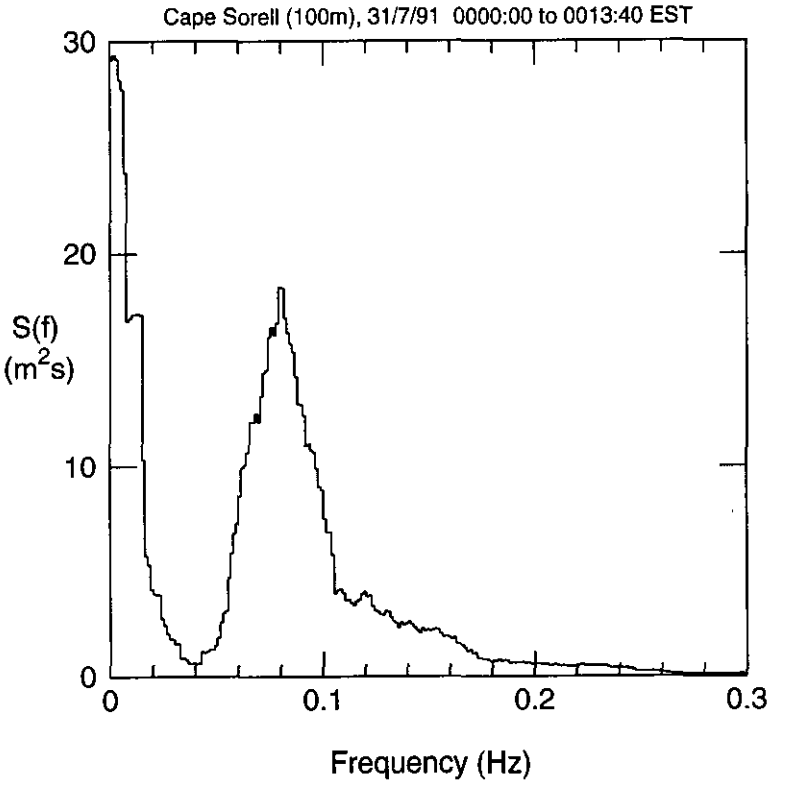


Figure 8: The variance density spectrum of the time series displayed in the previous figure showing spurious low frequency noise below .04 Hz

exception occurred when buoy batteries were low. As the voltage dropped the receiver would report the presence of long period waves with a "saw tooth" appearance which were obviously spurious. This fault only occurred when the buoy batteries were almost exhausted but it was not accompanied by an "unlocked" indication.

Bursts which showed the low battery symptoms were eliminated from the archives. Those which showed one or more "unlocked" data words were saved and the "unlocked" count was passed to the database record for that burst. Burst statistics for bursts with a non-zero unlocked count were eliminated from the statistical comparisons discussed below.

Data recovery may be defined as the percentage of bursts in each week for which good data was obtained and for which the unlocked count was zero. Data recovery defined in this way are displayed in Tables (5) to (6). The low recovery from mid 1988 to mid 1990 at Cape Sorell was due to interference from distant broadcast stations brought about by good ionospheric propagation conditions during the sunspot maximum. The problem was remedied by replacing the receiving antenna with one with better directional characteristics.

## 2.4 The Twisted Suspension Problem

A minor aspect of data quality is the twisted suspension effect. According to the manufacturer when a Waverider buoy is rotated the suspension in the gimbaled mount can become twisted. This results in the generation of a spurious signal with a period of about 40 seconds. A burst showing this effect is plotted as a time series in Figure 7. Its variance density spectrum is shown in Figure 8 The effect is manifested as a long slow trough near $t = 240$ and a peak near $t = 360$ seconds in Figure 7. Although these may look real they have periods in excess of 50 seconds which is below the low frequency cut-off of the buoy. The spectrum of the time series in Figure 8 shows a large amount of noise at frequencies below 0.04 Hz due to this effect.

Since the frequencies at which this effect occurs are below the lowest frequency at which ocean surface waves are observed it does not present a serious problem. Nevertheless it was certainly present in much of the data collected during this program. Indeed it was present in both of the first buoys put out from the moment they were first deployed.

# 3 Statistics

## 3.1 Definitions

A wide variety of sample statistics describing sea state have come into use over the years and there are a number of definitions of them. Here the definitions given by PIANC (1973) are generally followed.

Each archived "burst" of data consisted of 2048 readings of sea surface elevation (or 1024 prior to 18/11/85) sampled at the rate of 2.56 samples per second. The statistics from each burst were saved in a single record in a database. Prior to deriving the statistics a mean level was computed and subtracted from each data point which was then multiplied by the calibration factor for that particular buoy.

### 3.1.1 Time domain statistics

Various wave height statistics are defined by PIANC such as the maximum upcrossing wave height, $H_{mu}$, the maximum wave trough depth , $a_{tmax}$ etc. and these are listed in Table 7. Here $a_{tmax}$ is taken as positive for convenience of display.

Two statistics termed "significant wave height" are defined, viz: $H_\sigma$ and $H_{\frac{1}{3}}$. The former and more recent definition is

$$H_\sigma = 4\sigma \tag{1}$$

where $\sigma$ is the sample standard deviation of sea surface height given by

$$\sigma^2 = \sum_{i=1}^{N} z_i^2 \tag{2}$$

where $z_i$ is the (zero mean) value of sea surface height returned at time $(i-1)\Delta t$ after commencement of the burst, where $\Delta t$ is the sampling interval.

Under the older definition, $H_{\frac{1}{3}}$ is defined as the average height of the one third highest downcrossing waves (Sverdrup and Munk, 1947). In practice the two are highly correlated and almost equal numerically.

The mean zero crossing period, $T_z$ , is defined by

$$T_z = 2\frac{t_N - t_1}{N_z - 1} \tag{3}$$

| symbol | name | units |
|---|---|---|
| $H_{mu}$ | Maximum upcrossing wave height | $m$ |
| $H_{md}$ | Maximum downcrossing wave height | $m$ |
| $H_\sigma$ | Significant wave height (standard deviation) | $m$ |
| $H_m$ | Spectral moment wave height | $m$ |
| $a_{cmax}$ | Maximum wave crest height | $m$ |
| $a_{tmax}$ | Maximum wave trough depth | $m$ |
| $H_{\frac{1}{3}}$ | Significant wave height (1/3 highest waves) | $m$ |
| $T_{\frac{1}{3}}$ | Significant wave period | $s$ |
| $T_z$ | Mean zero crossing period | $s$ |
| $T_c$ | Mean crest to crest period | $s$ |
| $T_p$ | Spectral peak period | $s$ |
| $T_{-1}$ | Minus oneth spectral mean period | $s$ |
| $T_1$ | First spectral mean period | $s$ |
| $T_2$ | Second spectral mean period | $s$ |
| $T_4$ | Fourth spectral mean period | $s$ |
| $m_{-1}$ | Minus oneth spectral moment | $m^2 s$ |
| $m_0$ | Zeroth spectral moment | $m^2$ |
| $m_1$ | First spectral moment | $m^2 s^{-1}$ |
| $m_2$ | Second spectral moment | $m^2 s^{-2}$ |
| $m_4$ | Fourth spectral moment | $m^2 s^{-4}$ |
| $\epsilon$ | Spectral width parameter | - |
| $P$ | Energy Flux | $KWm^{-1}$ |
| $H_{sw}$ | Swell height (.04 to .12 Hz) | $m$ |
| $H_{ws}$ | Wind sea height (.2 to .6 Hz) | $m$ |

Table 7: Burst statistics

where $t_1$ and $t_N$ are the times of the first and last zero crossings in the burst and $N_z$ is the number of zero crossings (both up and down).

### 3.1.2 Frequency domain statistics

Frequency domain statistics all depend on the estimation of a variance spectrum of each burst. The burst data sequence was multiplied by a ten percent raised cosine window (modified Hanning window) and the resulting sequence transformed using an N point fast Fourier transform where $N = 1024$ or 2048. The squared modulus of the transform then yields a 1025 long periodogram, $P_n$ , of the data from zero to the Nyquist frequency, $f_N = 1.28$ Hz, with a frequency resolution, $\delta f$, of 1/800 Hz for the 2048 long bursts. By the power theorem the sum of the terms in the periodogram,

$\sum P_n$ , is equal to the variance of sea surface height, $\sigma^2$, defined by equation (2). The fraction of the variance associated with the frequency range $< f_1, f_2 >$ can be defined as

$$V < f_1, f_2 >= \sum_{n=n_1}^{n_2} P_n \tag{4}$$

where

$$n_i = Int[f_i/\delta f] + 1 \tag{5}$$

where $Int$ means "the integer part of".

The various spectral moments, $m_q$ , are defined by

$$m_q = \sum_{n=n_1}^{n_2} [(n-1)\delta f]^q P_n \tag{6}$$

where $n_2 = N/2 + 1$ corresponds to the Nyquist frequency. The lower bound, $n_1$ , should be zero. However owing to the prevalence of the twisted suspension error discussed above it is more convenient to set $n_1$ to a value corresponding to a frequency of 0.04 Hz, i.e. to 33 for the 2048 long bursts.

Frequency domain statistics with the dimensions of height can be defined. These include $H_m$ , the "zeroth moment" wave height defined by

$$H_m = 4\sqrt{m_0} \tag{7}$$

Since $m_0 = \sigma^2$, $H_m$ should be identical with $H_\sigma$. Small discrepancies will occur due to the windowing process and due to the fact that $n_1$ was chosen to be non-zero in (6) above. In fact comparison of $H_m$ with $H_\sigma$ provides a measure of the degree to which the twisted suspension error affects the wave height statistics.

Other height-like frequency domain statistics can be found by summing the periodogram across a specific frequency band to find the variance in the band as in (4), then taking four times the square root by analogy with (7). These include $H_{sw}$ and $H_{ws}$ a "swell" height and "wind sea" height found by summing the periodogram across the ranges 0.04 to 0.12 Hz and 0.2 Hz to 0.6 Hz respectively. The justification for these range boundaries arises from the observed correlation or anticorrelation of the variance with the wind as discussed in Section 4 below.

Various spectral time parameters may be defined by

$$T_q = (\frac{m_0}{m_q})^{\frac{1}{q}} \tag{8}$$

where $q = -1, 1, 2$ and 4. The statistic $T_{-1}$ is included because it relates to the energy flux or "wave power", $P$, an important quantity in wave power applications. The quantity $P$ is defined as the mean power flux per unit length of wavefront and is given by

$$P = \rho g^2 m_{-1}/2 \tag{9}$$

where $\rho$ is the density of sea water and $g$ is the acceleration due to gravity (Mollison, 1986). It follows that

$$P = \rho g^2 m_0 T_{-1} \tag{10}$$

Perhaps the most fundamental frequency domain time parameter is the spectral peak period, $T_p$, defined as

$$T_p = \frac{1}{f_p} \tag{11}$$

The spectral peak frequency,$f_p$ is given by

$$f_p = (n_{max} - 1)\delta f \tag{12}$$

where $n_{max}$ is the value of n for which the periodogram, $P_n$, is a maximum. In practice $T_p$ is a rather noisy parameter, reflecting the noisiness of the unsmoothed periodogram, $P_n$. Various schemes have been proposed for smoothing $T_p$ including curve fitting to $P_n$ in the vicinity of its maximum. However no smoothing or curve fitting was carried out to determine $T_p$ in the present study.

Various spectral width parameters can be derived from the moments $m_q$, for example the broadness factor, $\epsilon$, where

$$\epsilon = \sqrt{\frac{1 - m_2}{m_0 m_4}} \tag{13}$$

Owing to the fact that bursts acquired before 18 November 1985 were only half the length of later bursts, some burst statistics for this period were not strictly comparable with those of later bursts. For example the ratio of $H_{mu}$ to $H_\sigma$ will increase with increasing burst length. For this reason these data were excluded from the statistical calculations discussed below.

Unfortunately the biggest waves were recorded during this early period. This will be discussed further in Section 5.

## 3.2 Distributions of sample statistics

Histograms showing the distributions of various burst statistics for each of the four sites are shown in Figures 9 to 32.

The main parameters of these distributions are shown in Tables 8 to 12.

Some of these are grouped to give the equivalent parameters for all four sites in Table 12.

In Figures 9 to 32 only the distributions of Storm Bay statistics differ noticeably from those from the other three sites on the west coast. This is particularly true of the various wave height statistics and of the spectral moments. These differences are born out by the distribution statistics shown in Tables 8 to 11. The mean, median and modal heights for Storm Bay are just under half of the values for the west coast sites. The higher ordinates in the histograms also reflect this; because the spread of values is less there are proportionately more values in each bin.

The slight differences in distribution among the different west coast sites are unlikely to be real and reflect the different time intervals in which the data were gathered. Many more values contributed to the histograms for the Cape Sorell (100m) site and these are consequently less "noisy".

The period statistics show less variation among the different sites. The distributions of spectral peak period, $T_p$, shown in Figure 19 have a noisy appearance. This is an artefact caused by harmonics of $\delta f$ "beating" with the bin width.

The statistic, $T_p$, is defined by equation (11) in which $f_p$ can only take values which are integral multiples of $\delta f$. Consequently $T_p$ is also restricted to certain values. In the range 10 sec$< T_p <$ 20 sec the spacing of these fixed values of $T_p$ is similar to the spacing of the bin boundaries and a bin may fortuitously have more fixed values falling within it than its neighbour. Such a bin would capture a greater percentage of the total of $T_p$ values.

The most skewed statistics are $m_{-1}$ and its multiple $P$, the wave energy flux, for which the mean is two or three times the mode.

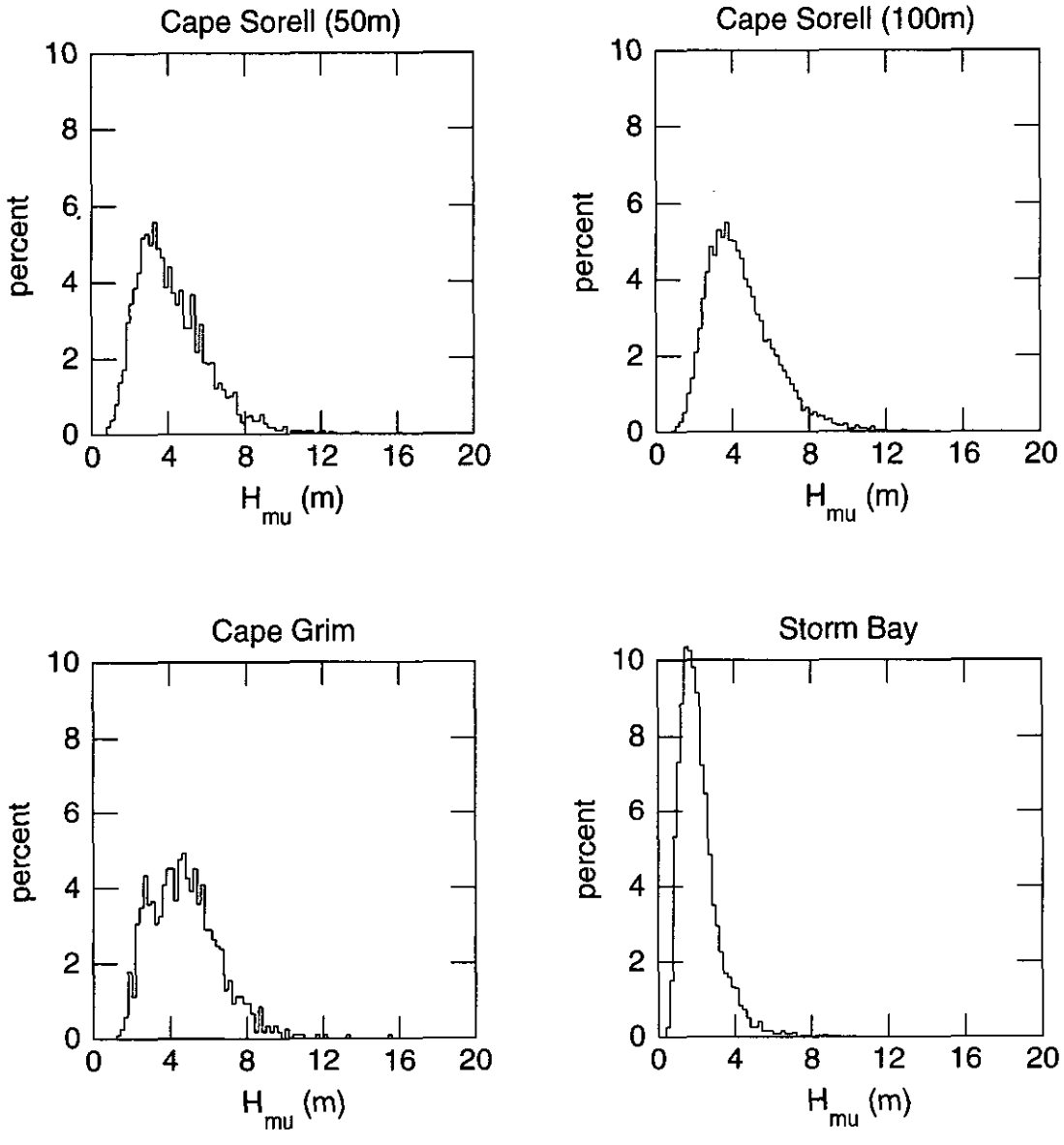


Figure 9: Histograms showing distribution of maximum upcrossing wave height.

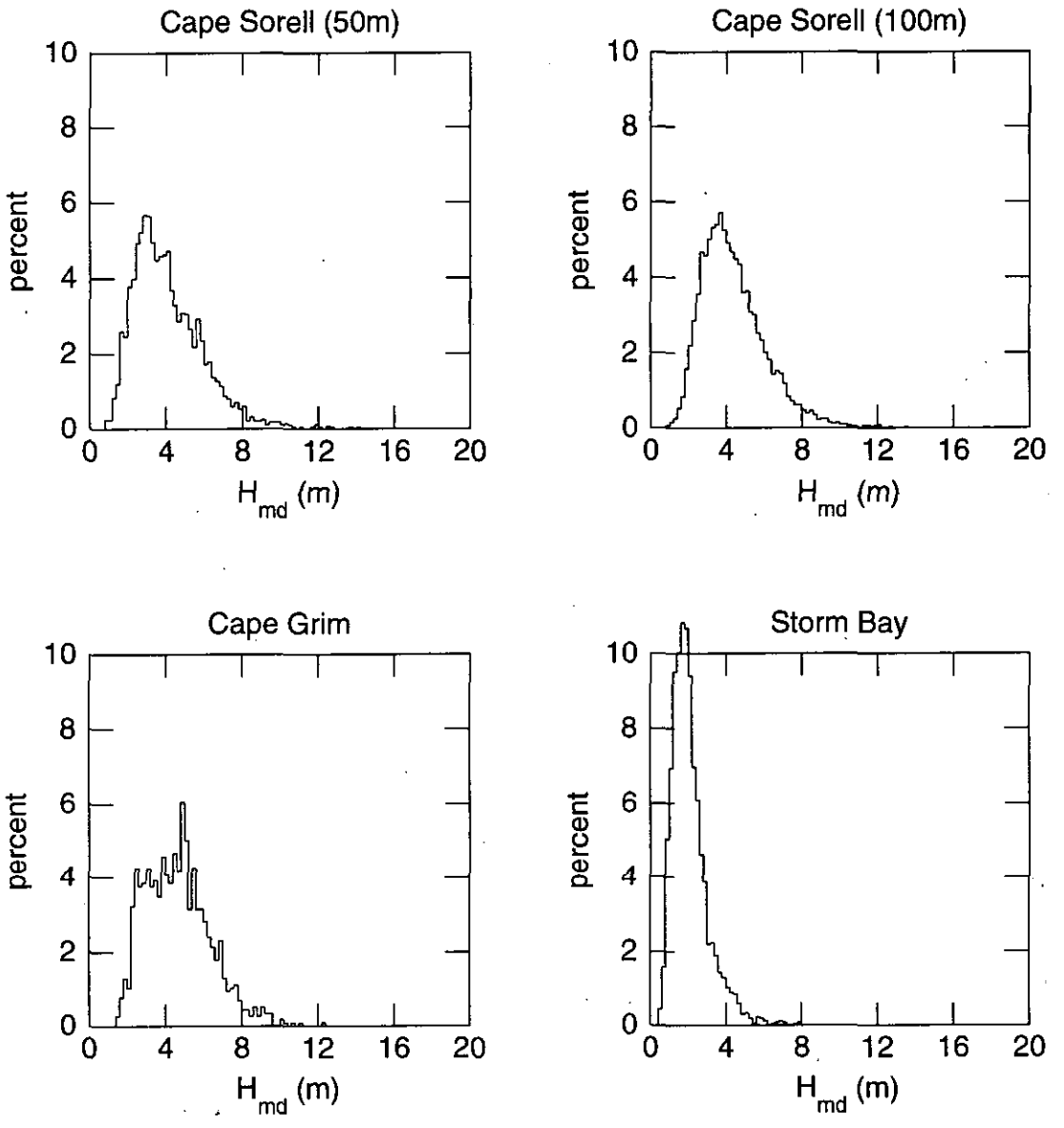


Figure 10: Histograms showing distribution of maximum downcrossing wave height.

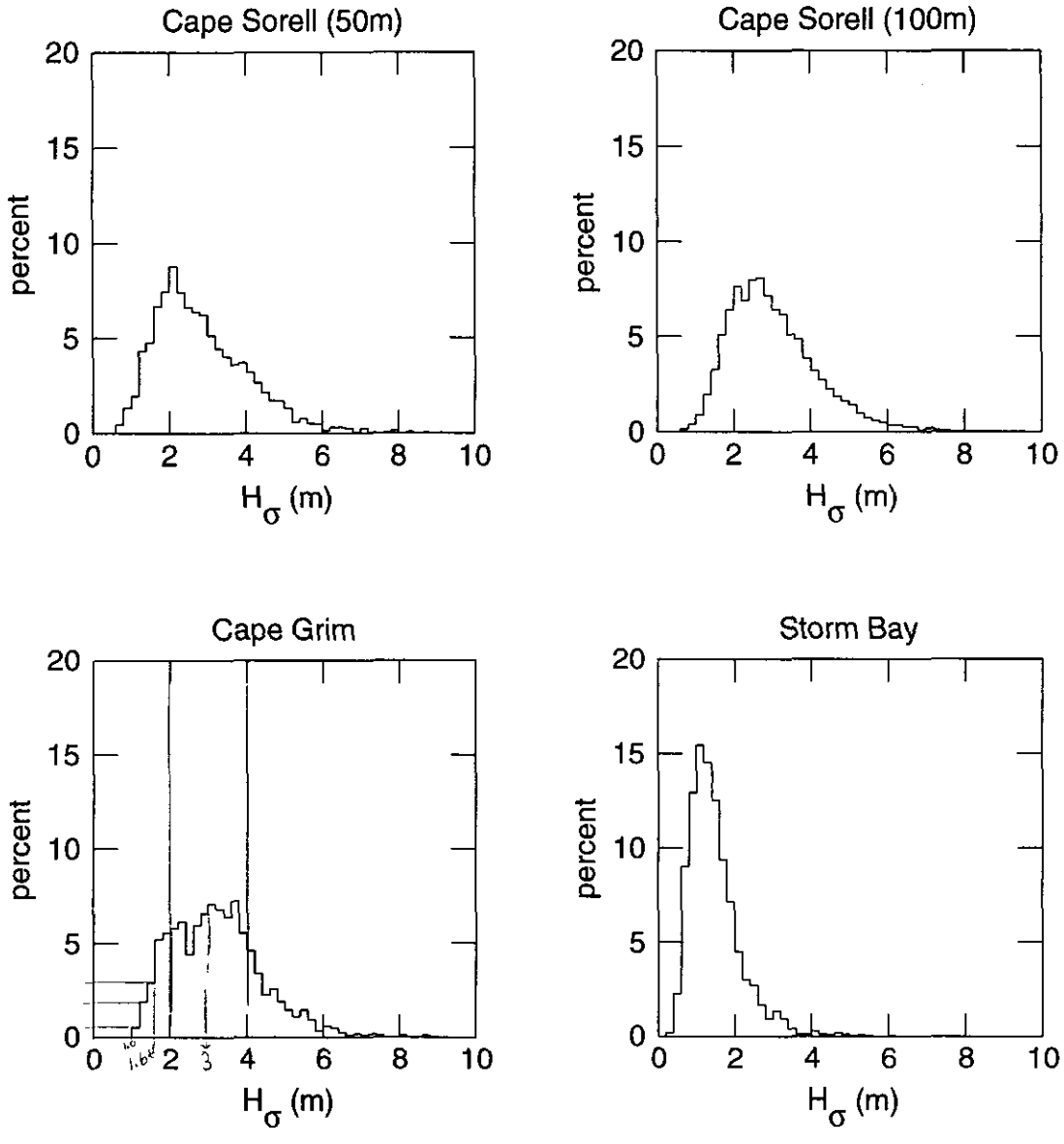


Figure 11: Histograms showing distribution of significant wave height.

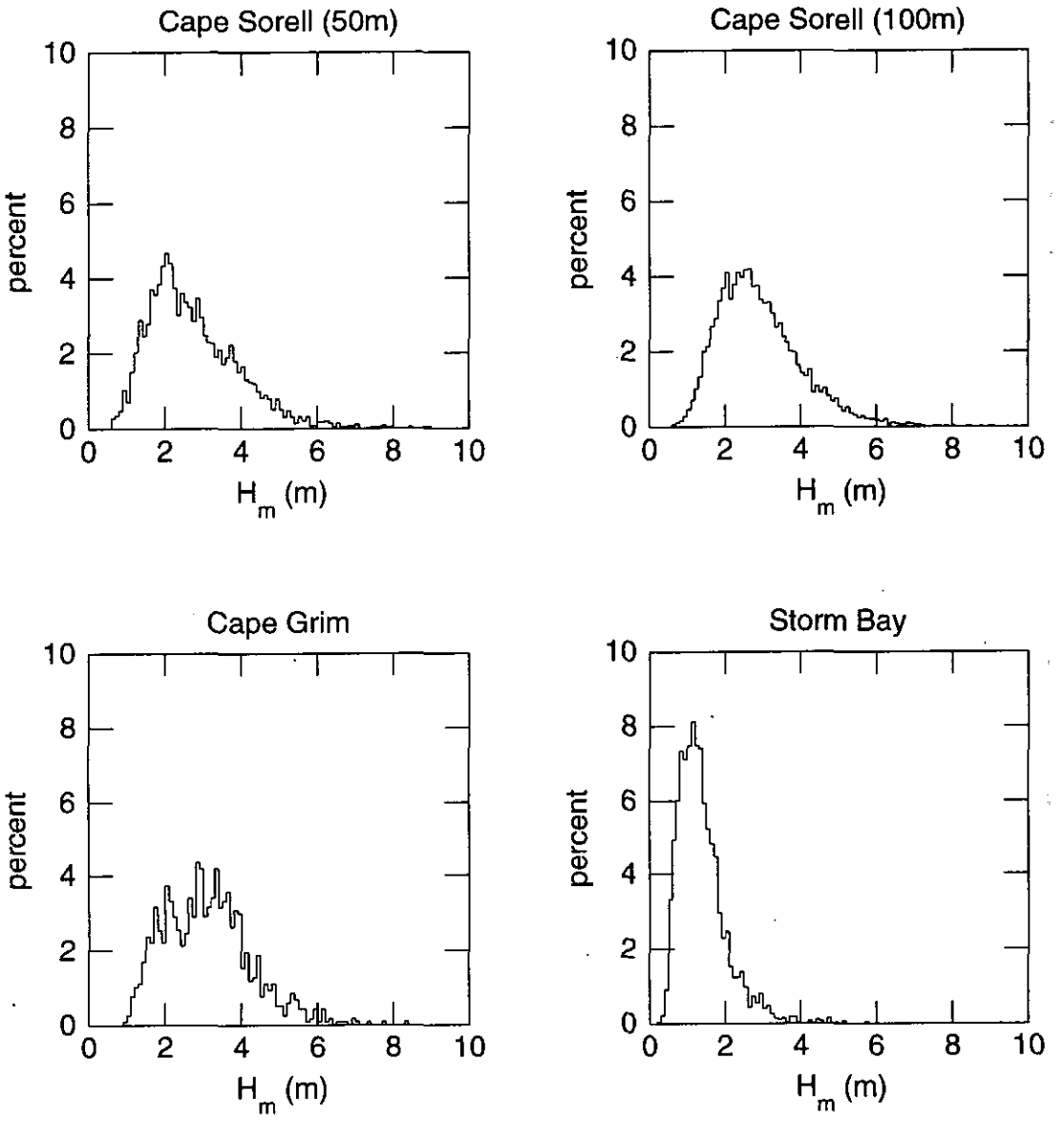


Figure 12: Histograms showing distribution of spectral moment wave height.

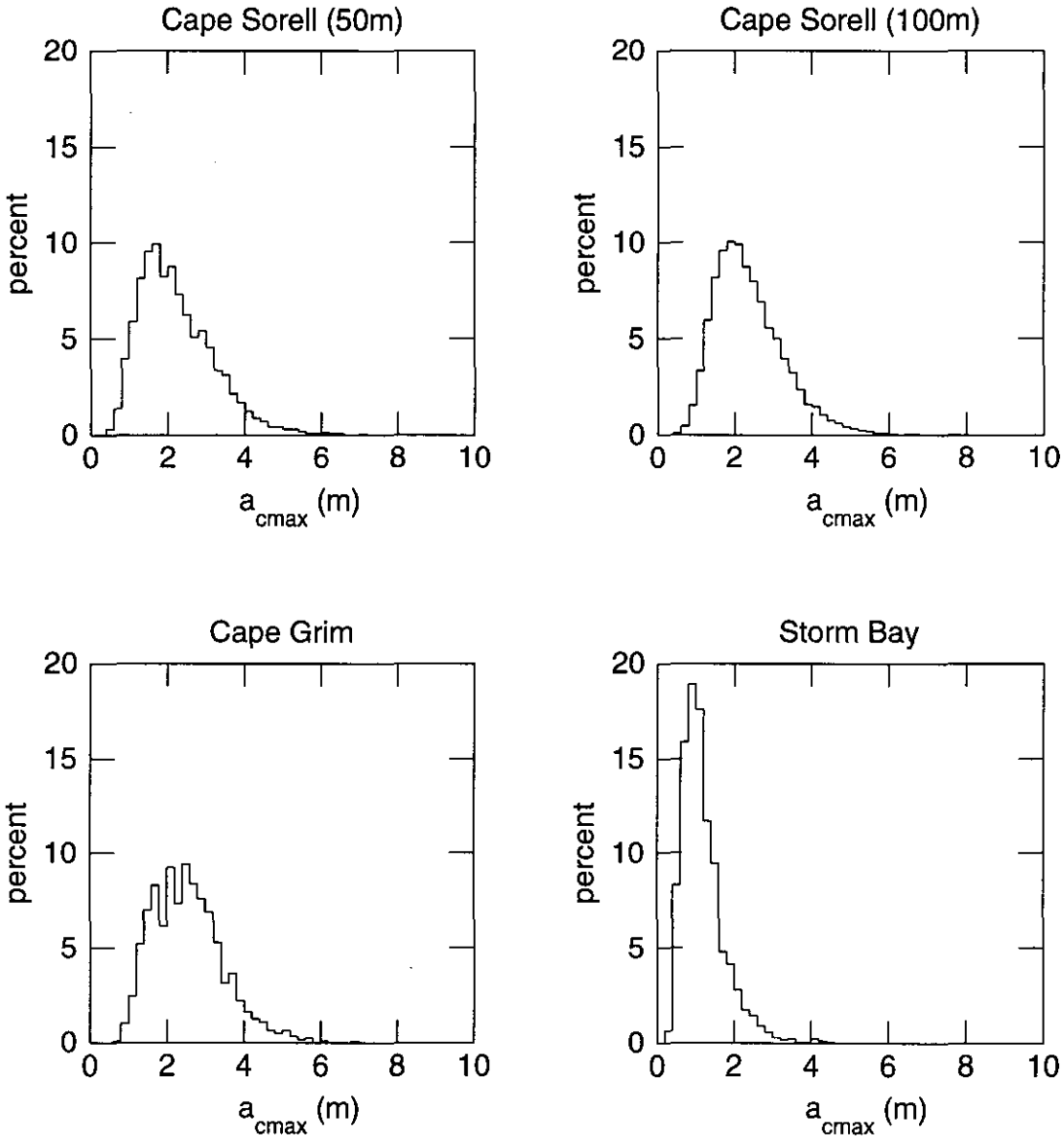


Figure 13: Histograms showing distribution of maximum zerocrossing wave crest height.

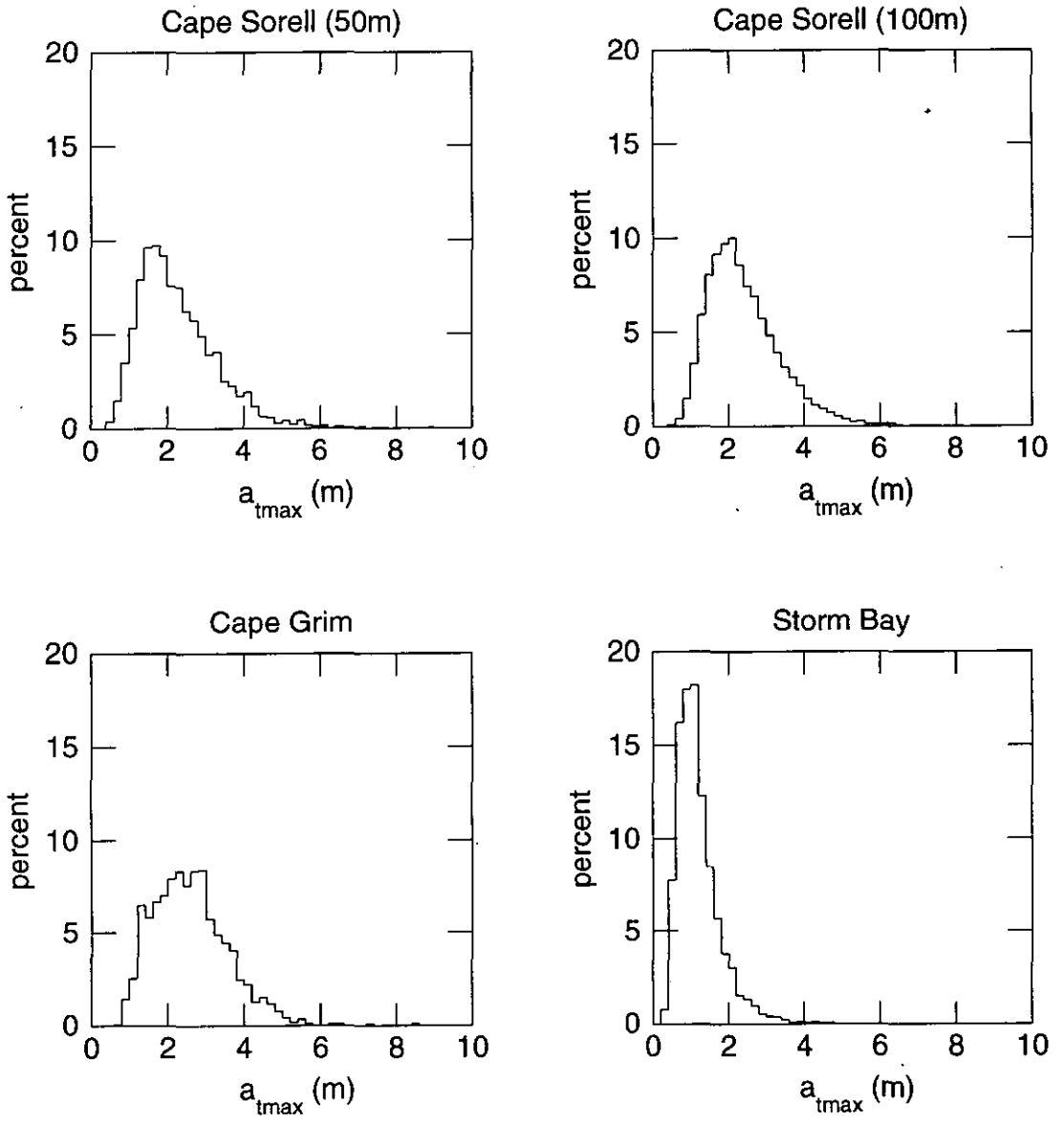


Figure 14: Histograms showing distribution of maximum zerocrossing wave trough depth.

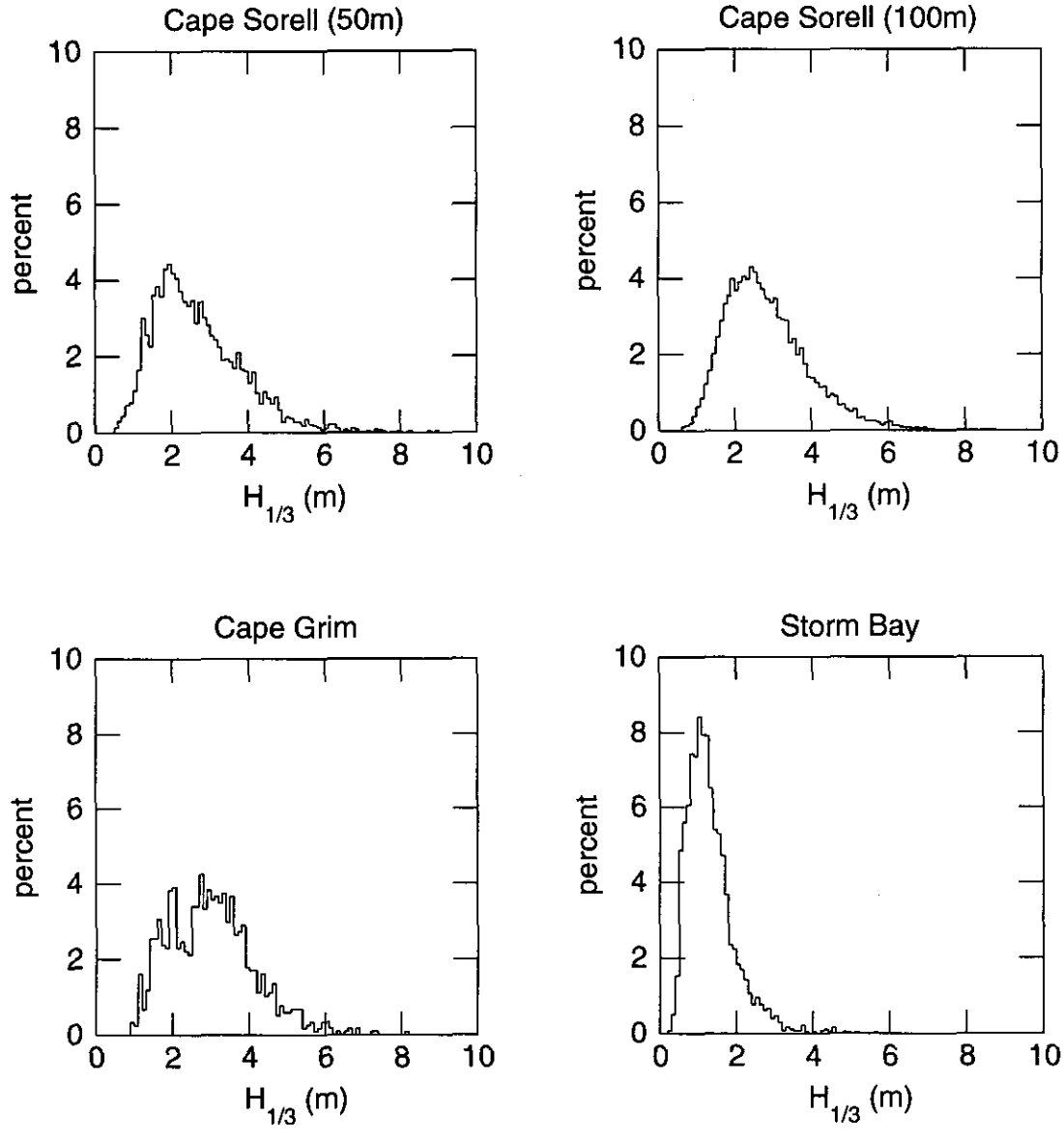


Figure 15: Histograms showing distribution of significant wave height (1/3 highest waves).

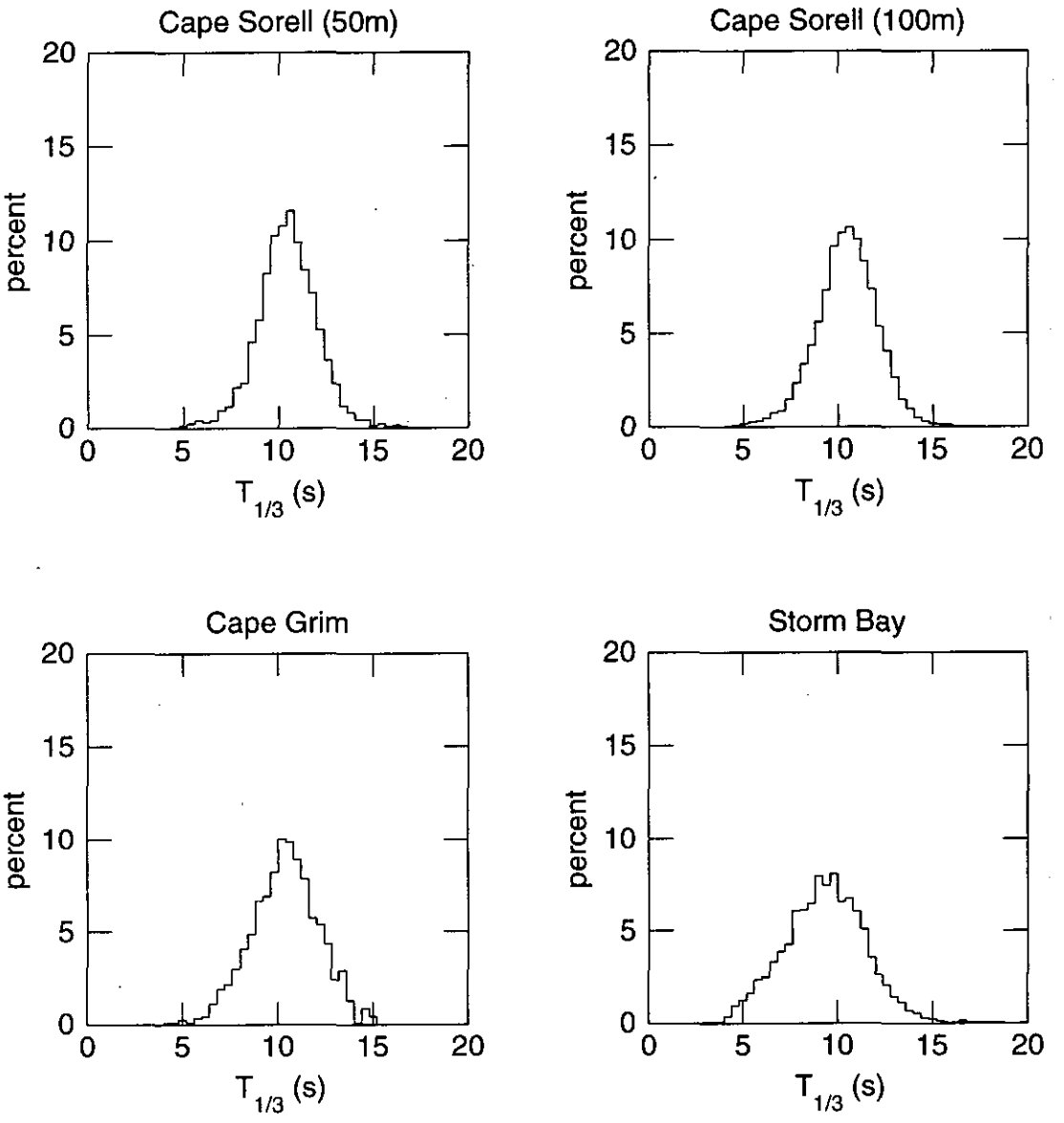


Figure 16: Histograms showing distribution of significant wave period.

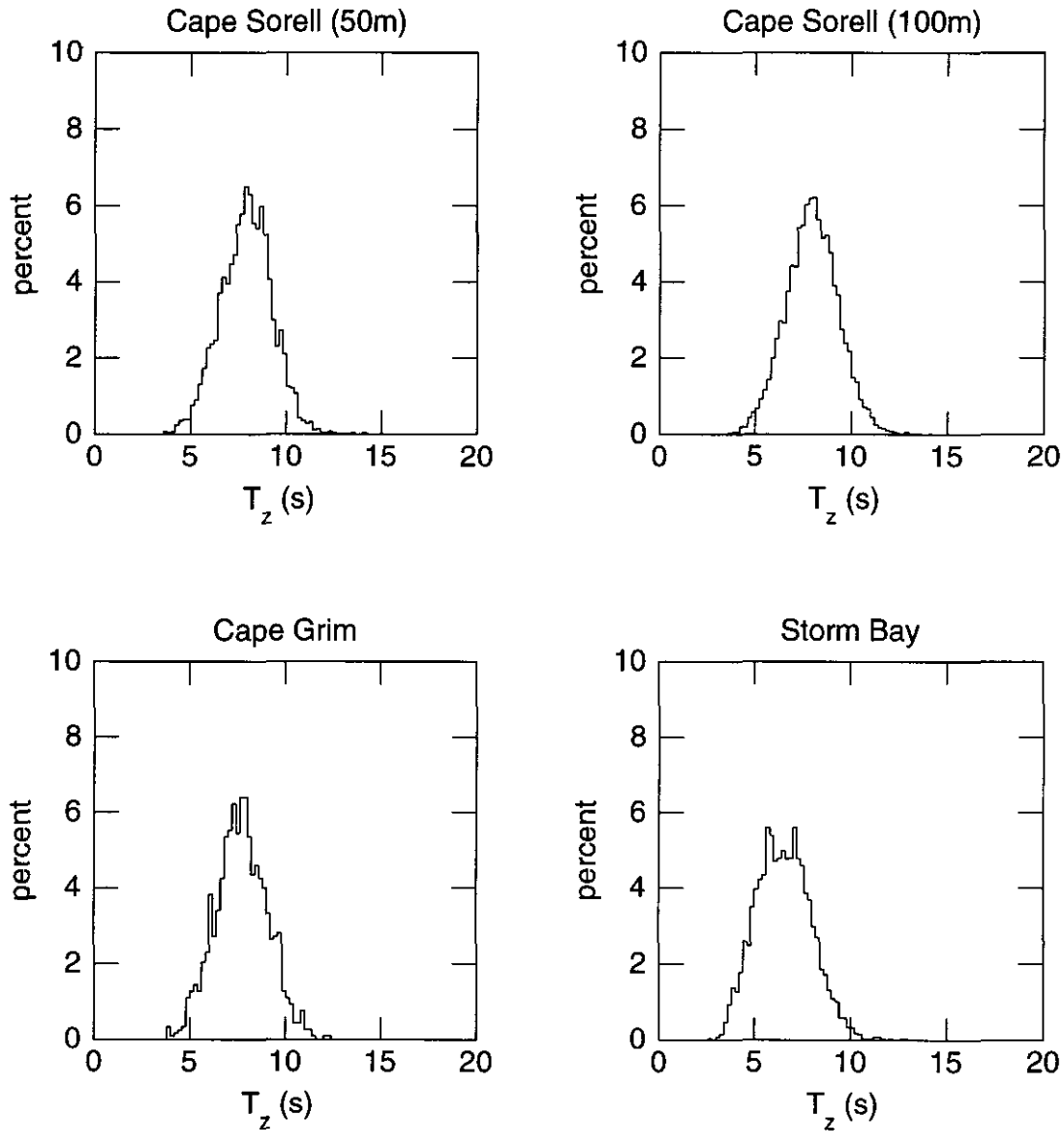


Figure 17: Histograms showing distribution of mean zero crossing period.

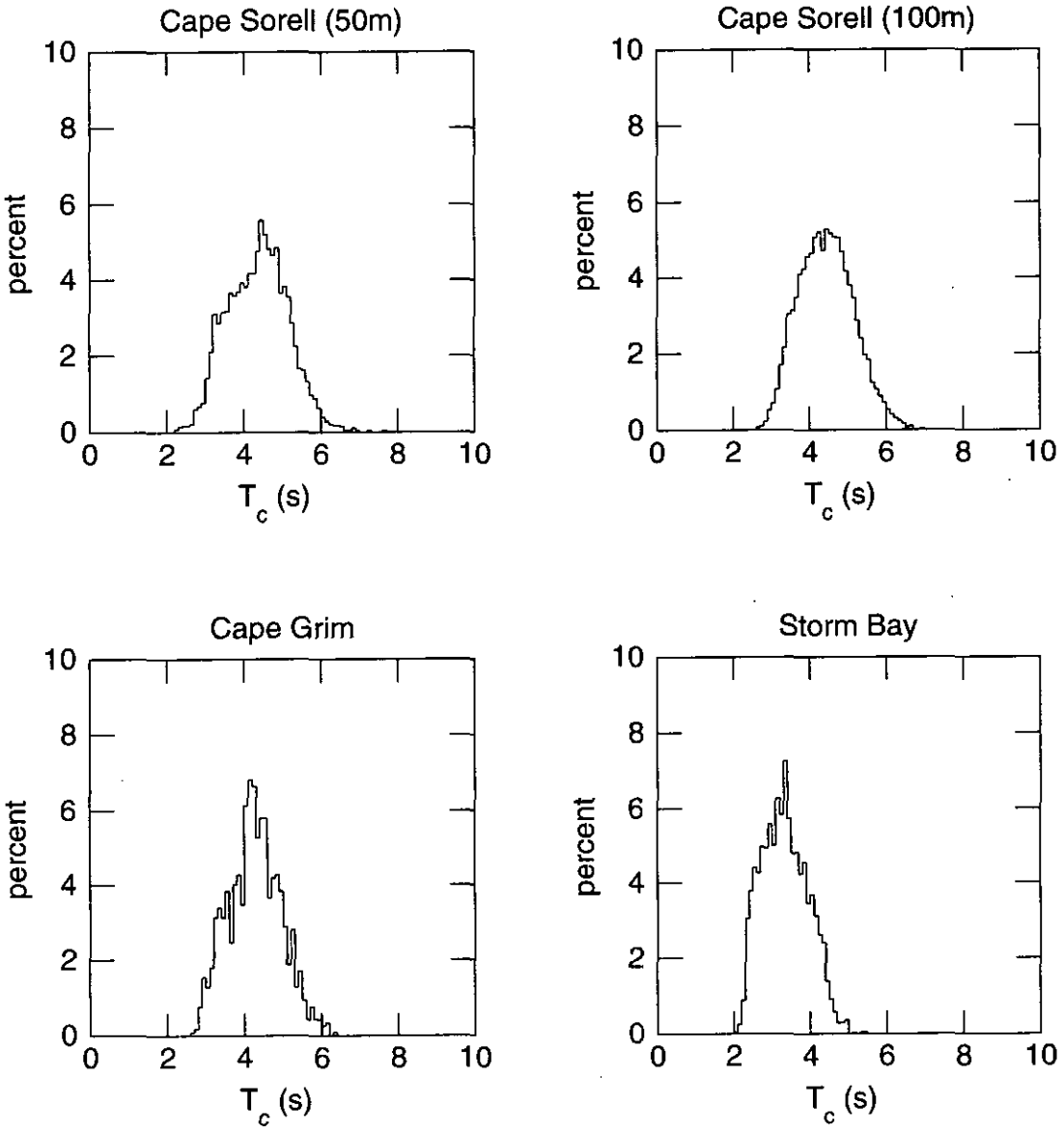


Figure 18: Histograms showing distribution of mean crest to crest period.

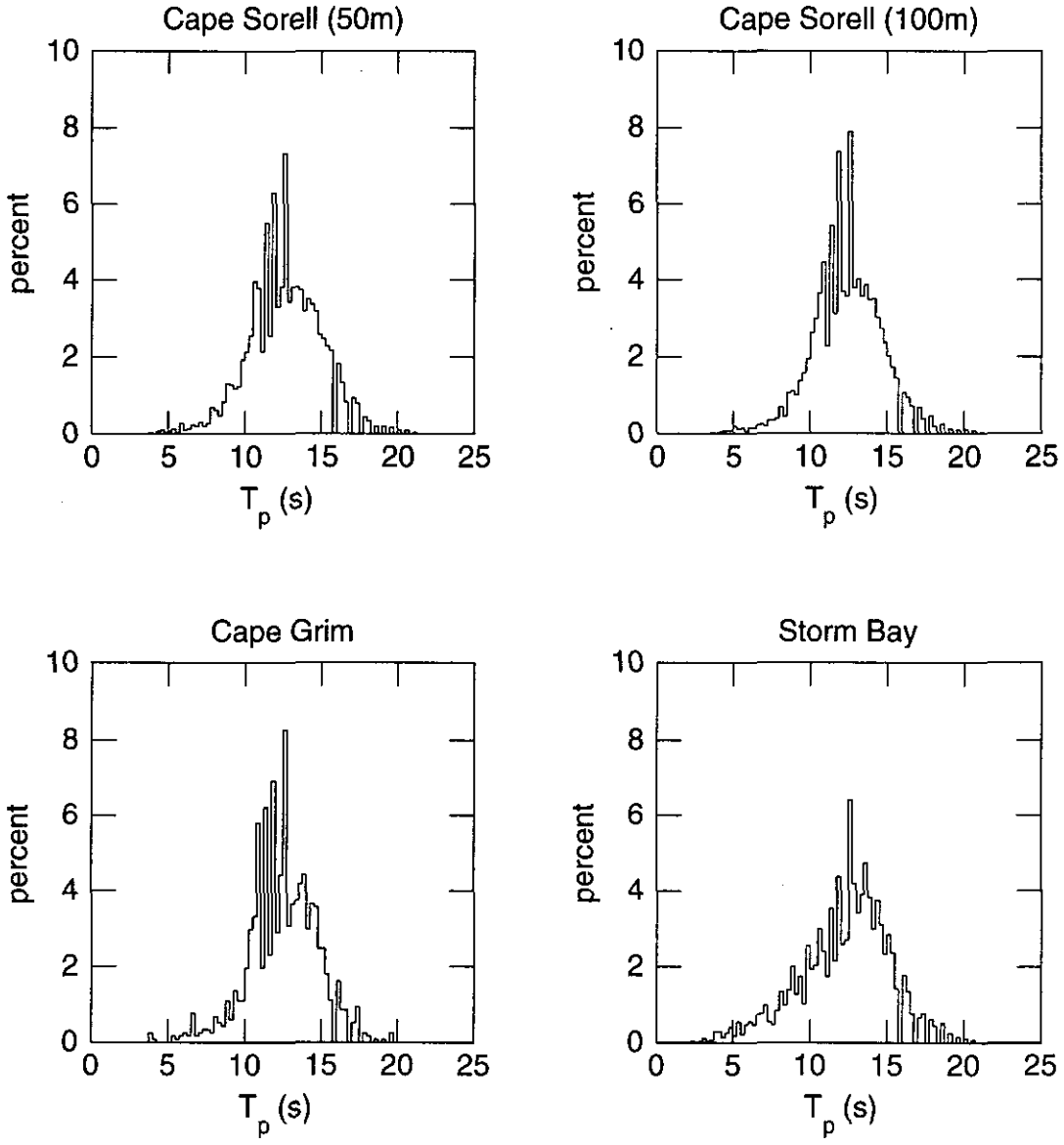


Figure 19: Histograms showing distribution of spectral peak period.

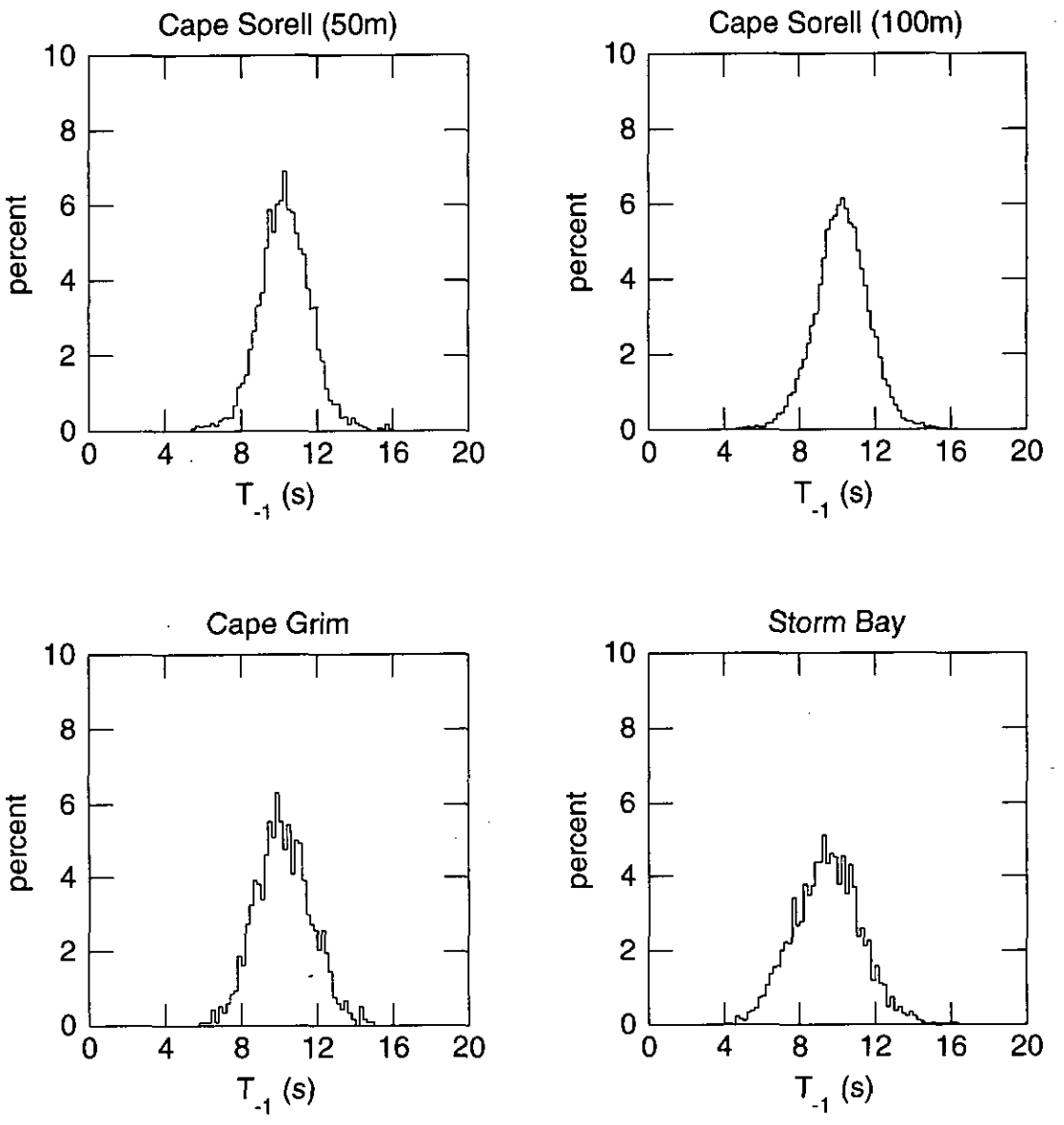


Figure 20: Histograms showing distribution of spectral mean period, $T_{-1}$.

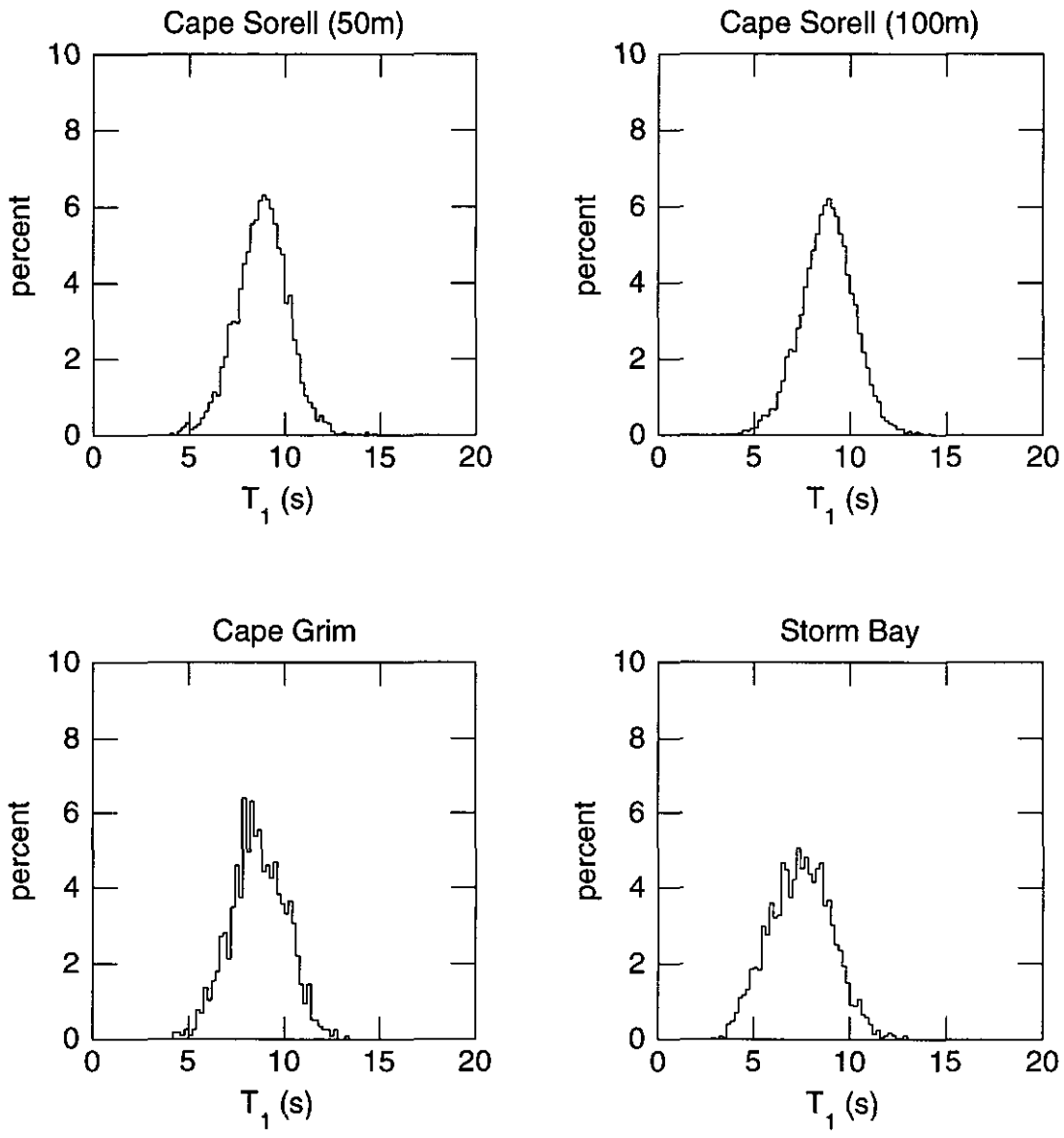


Figure 21: Histograms showing distribution of spectral mean period, $T_1$.

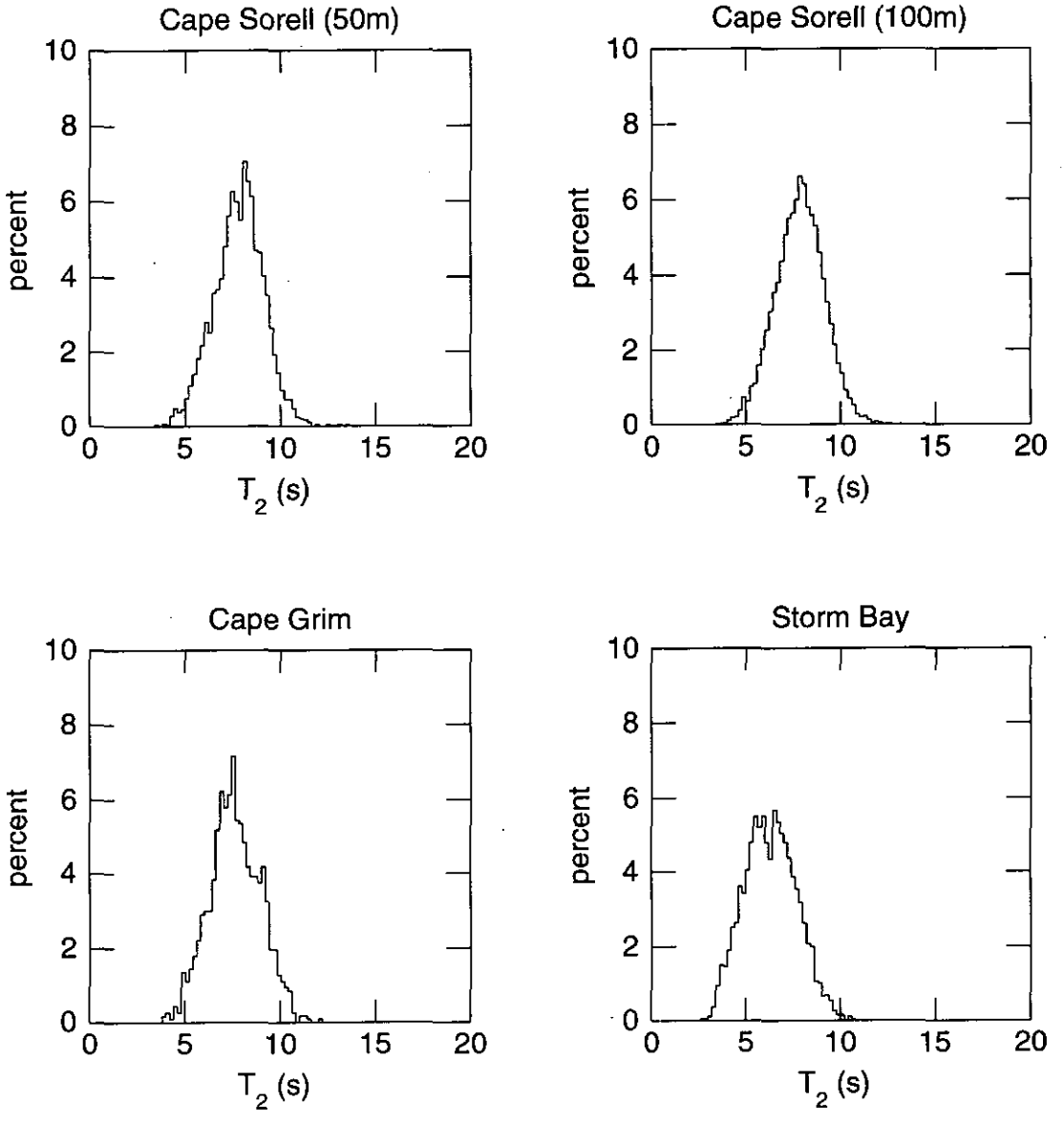


Figure 22: Histograms showing distribution of spectral mean period, $T_2$.

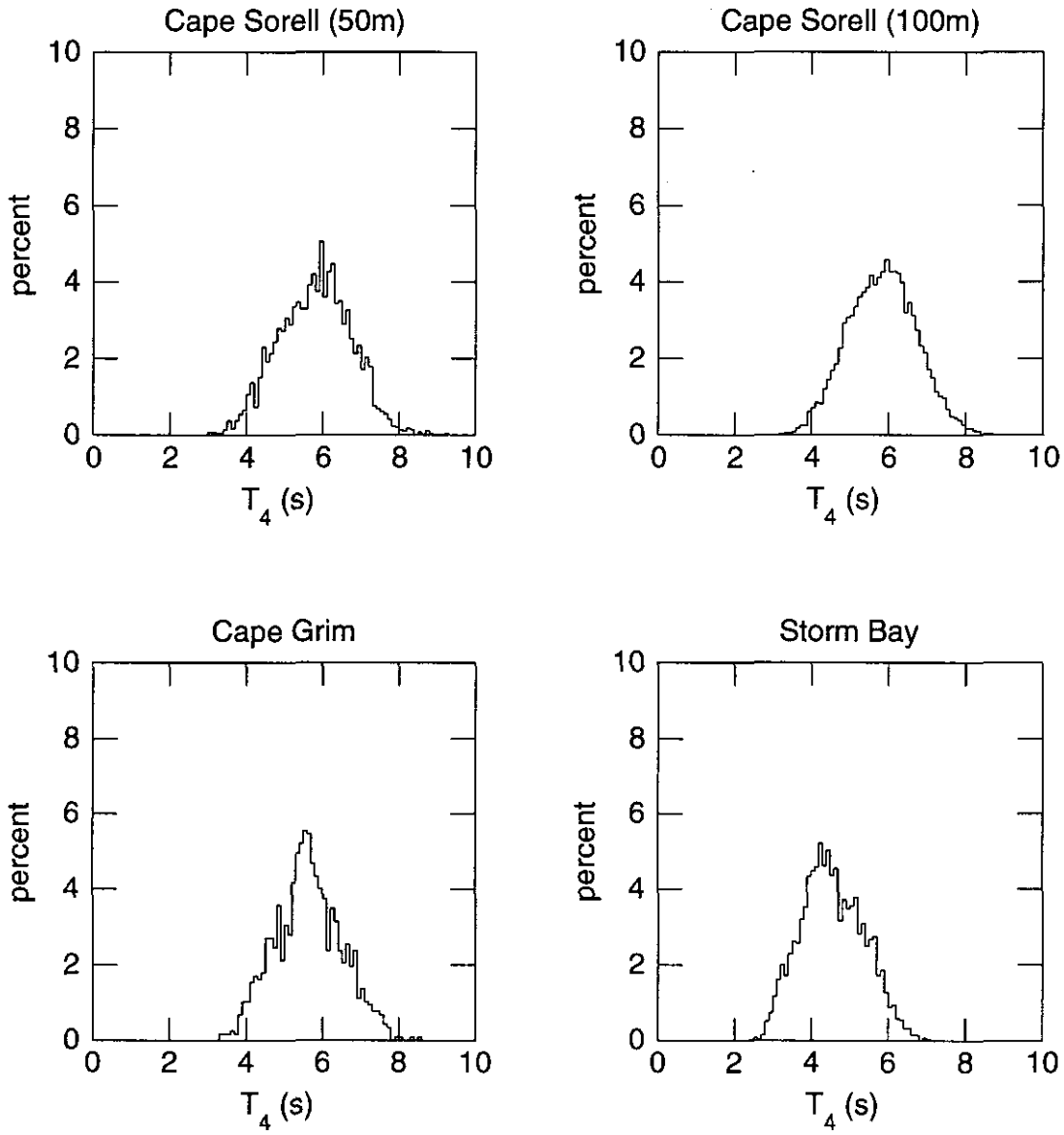


Figure 23: Histograms showing distribution of spectral mean period, $T_4$.

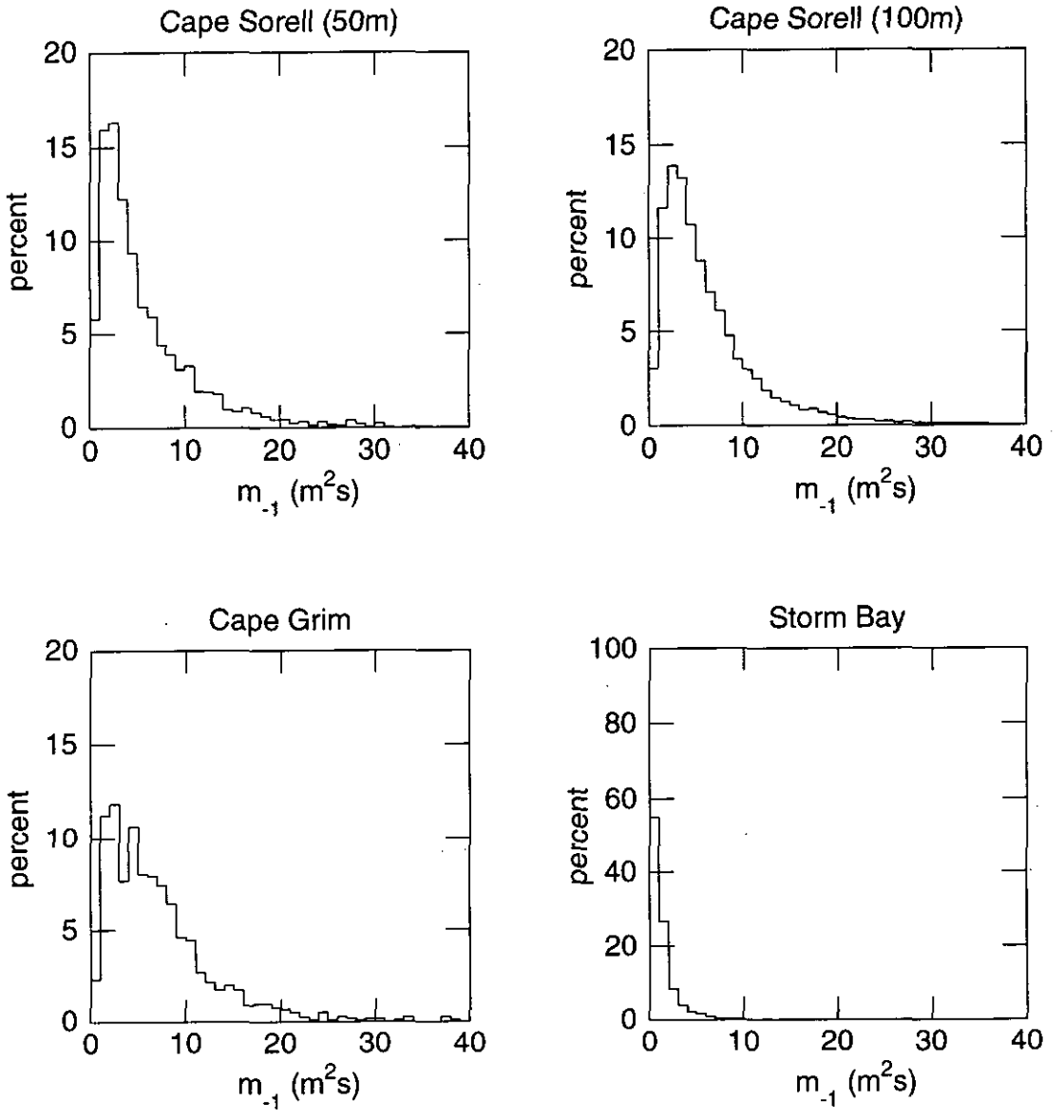


Figure 24: Histograms showing distribution of spectral moment, $m_{-1}$.

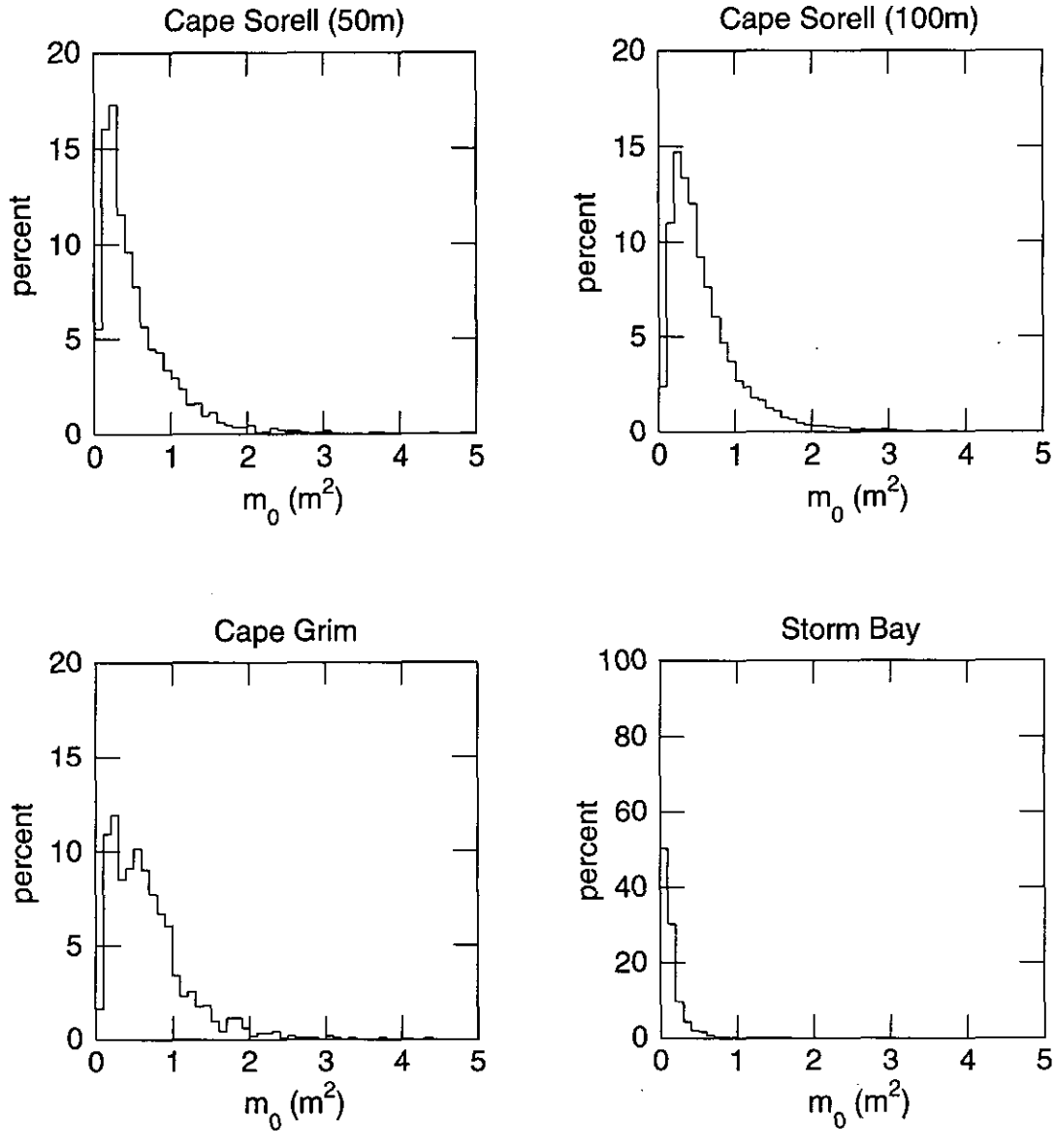


Figure 25: Histograms showing distribution of spectral moment, $m_0$.

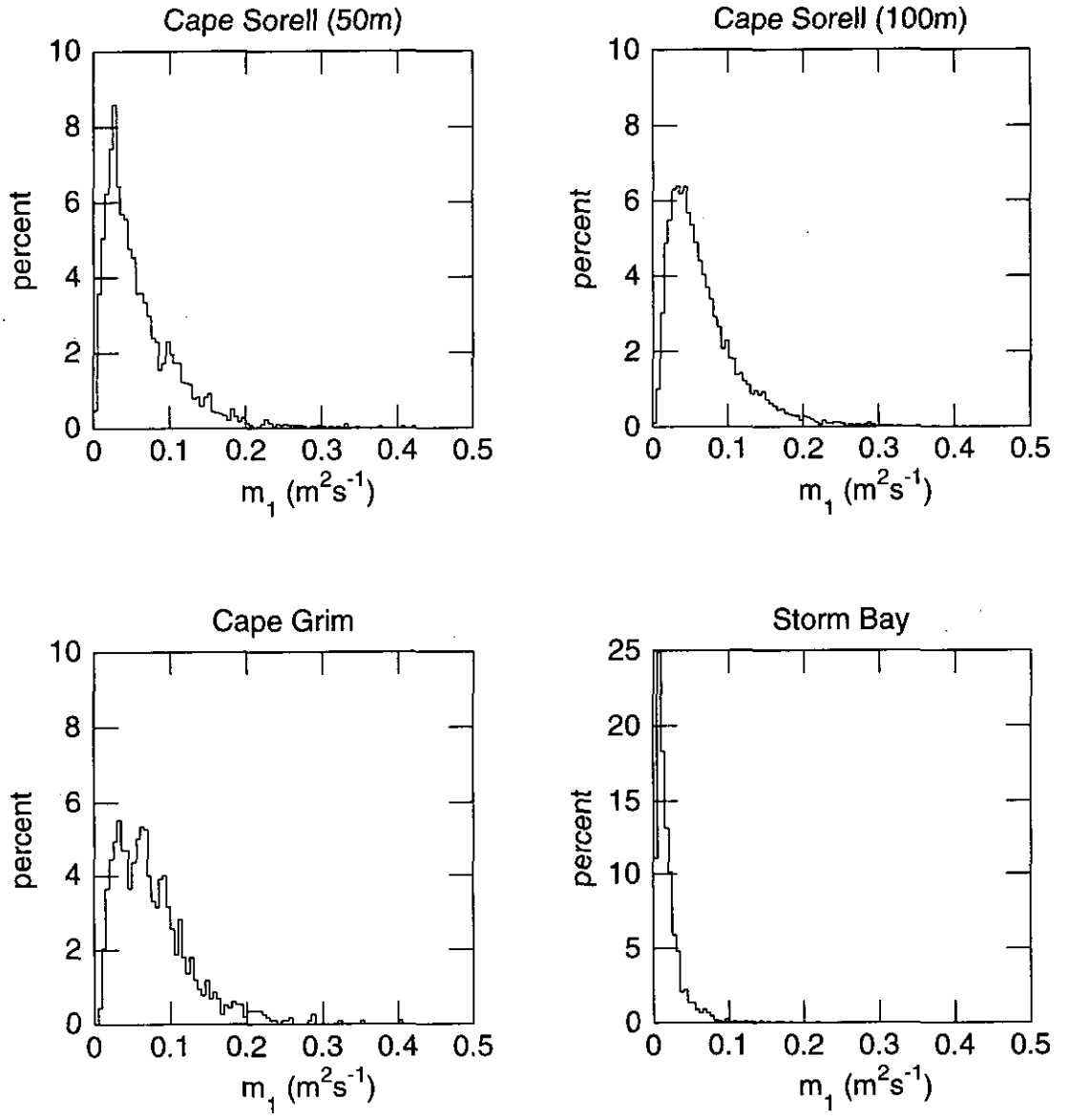


Figure 26: Histograms showing distribution of spectral moment, $m_1$.

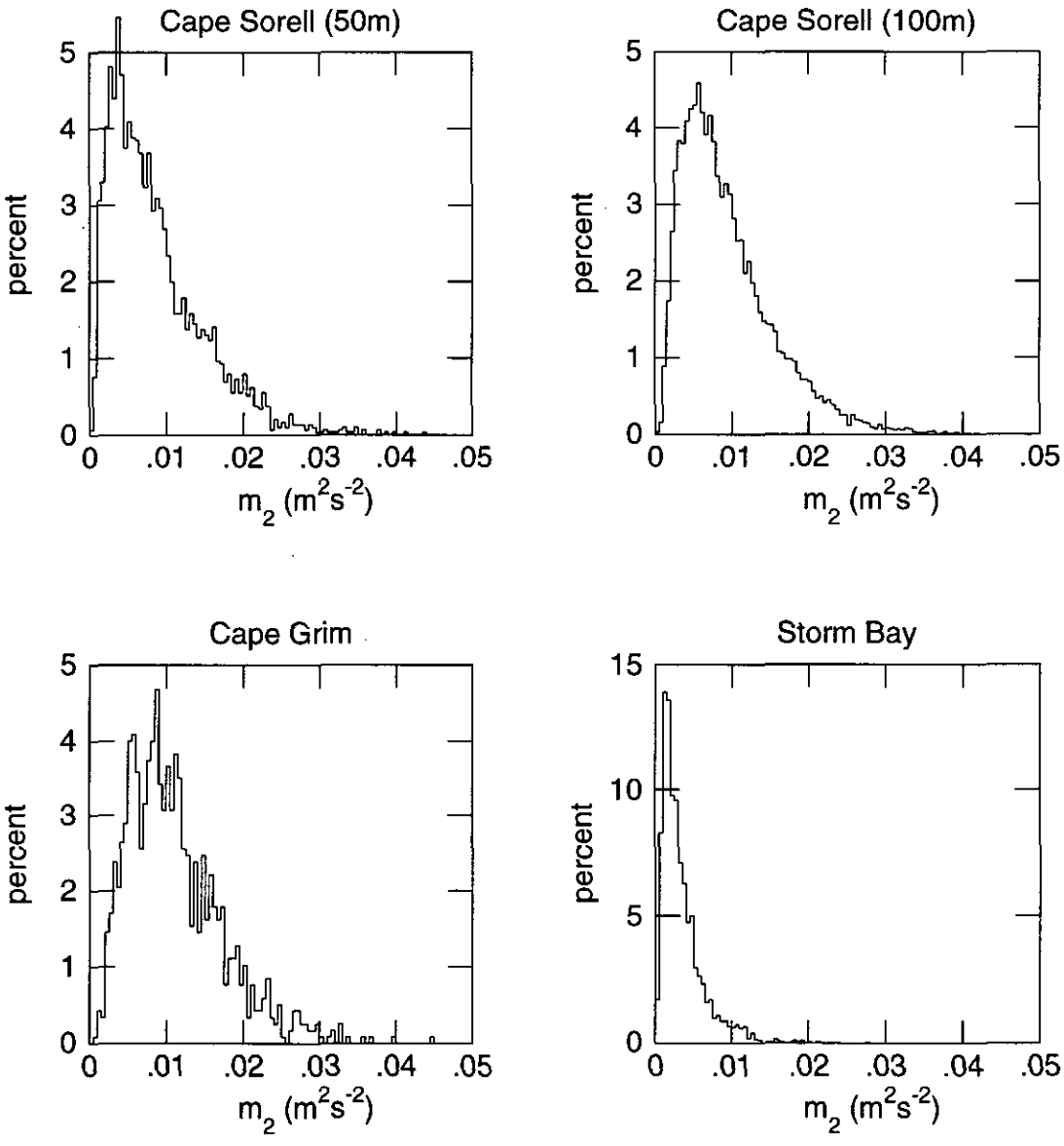


Figure 27: Histograms showing distribution of spectral moment, $m_2$.

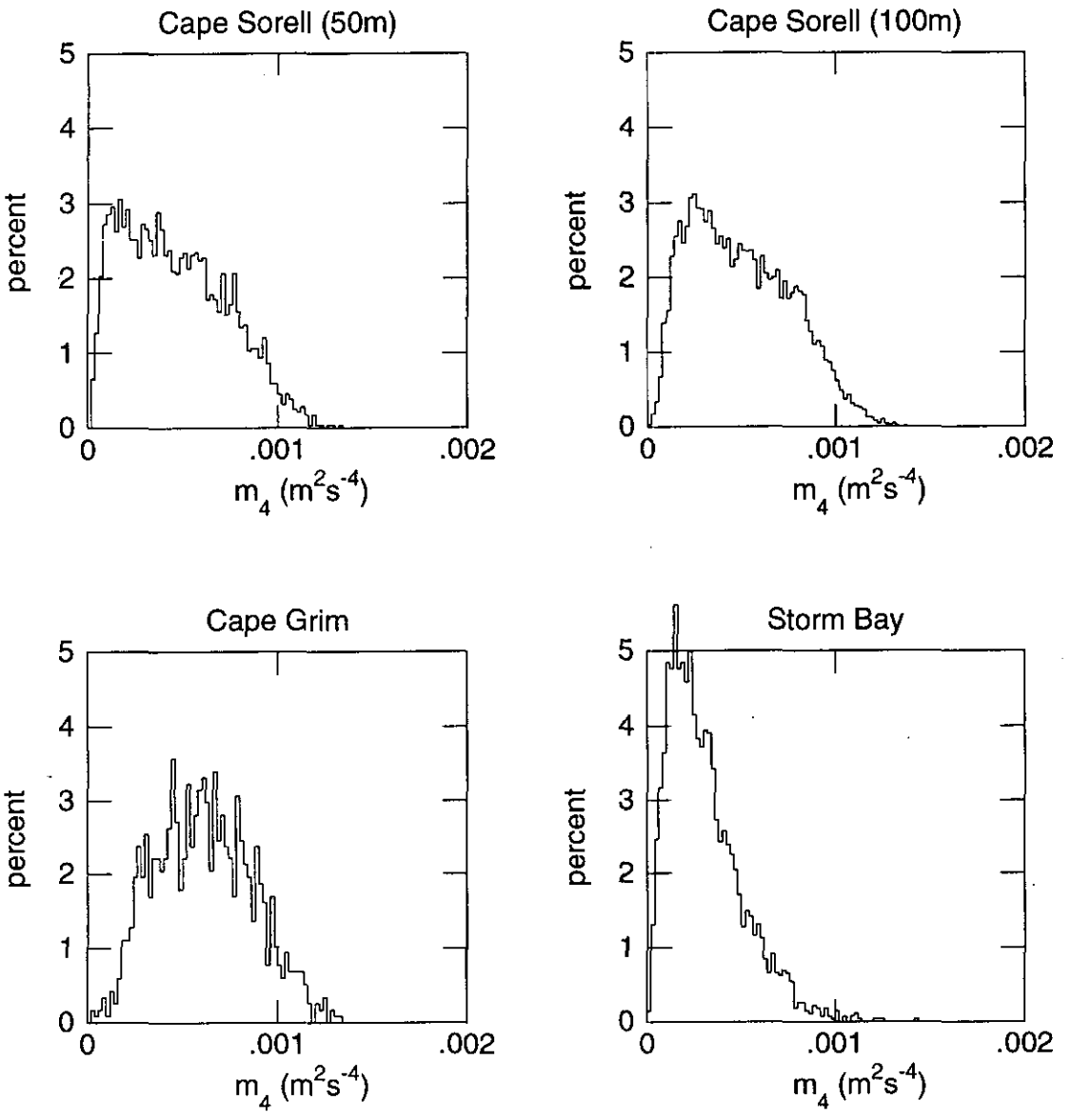


Figure 28: Histograms showing distribution of spectral moment, $m_4$.

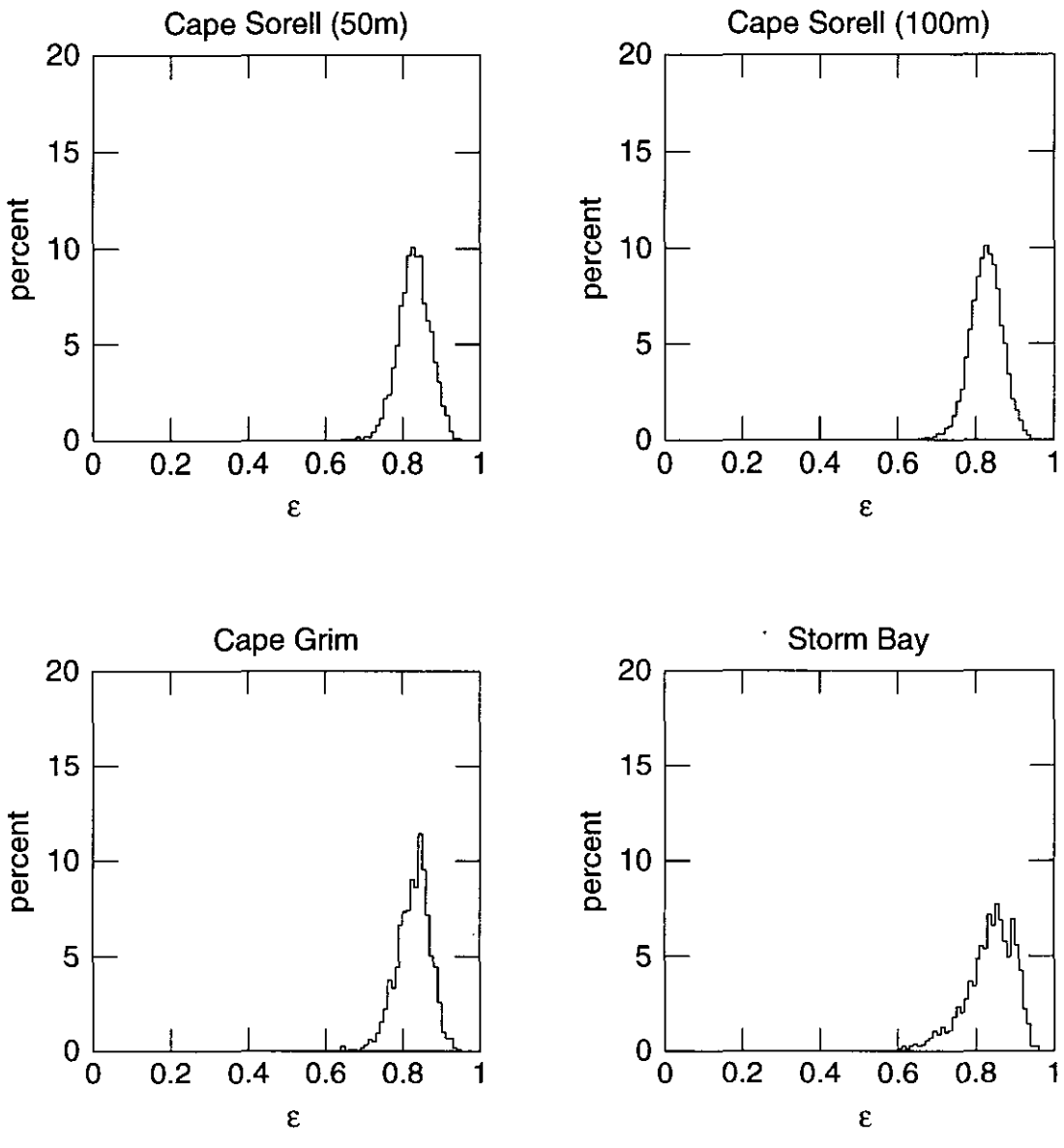


Figure 29: Histograms showing distribution of spectral width parameter.

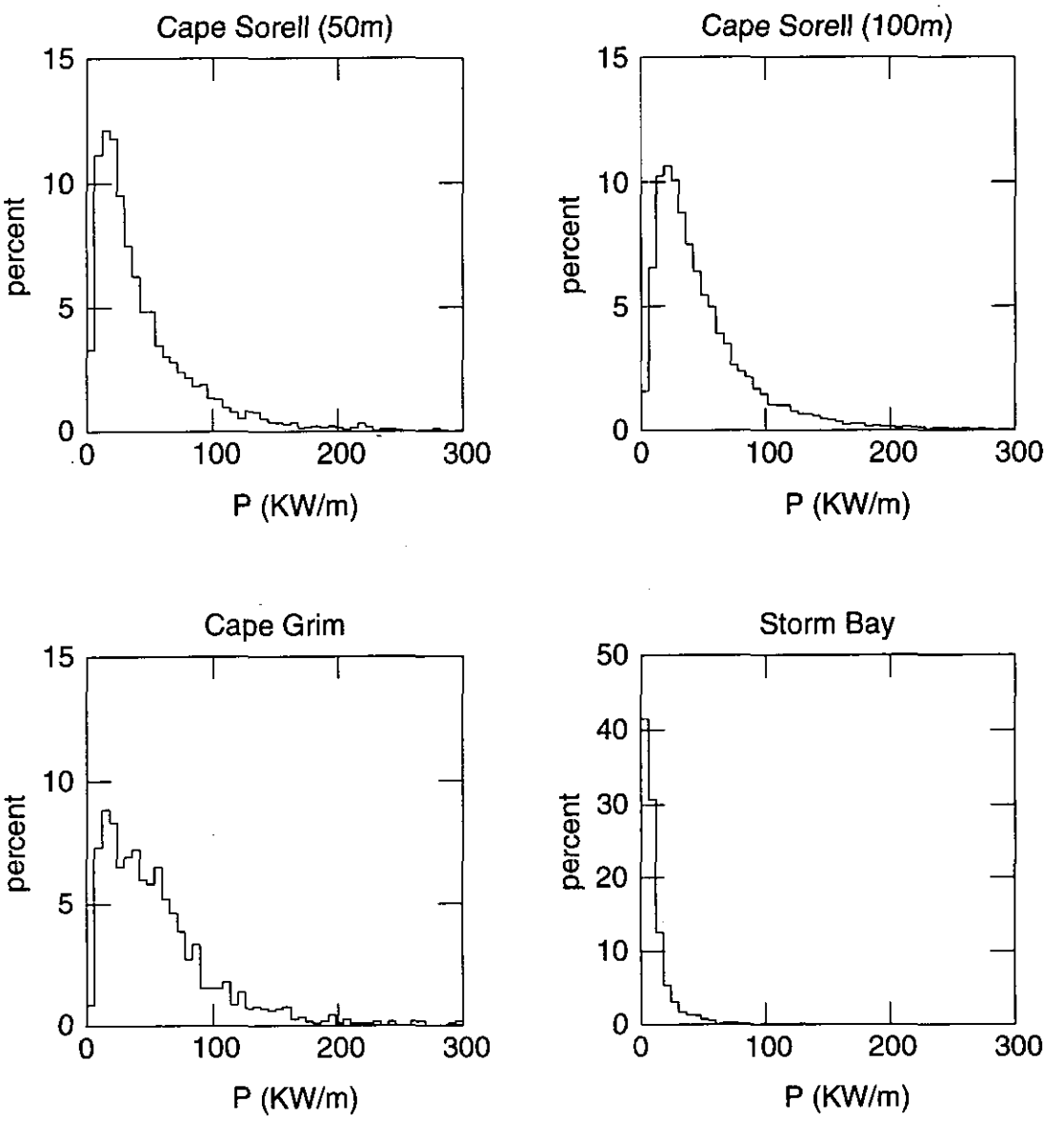


Figure 30: Histograms showing distribution of wave energy flux, P.

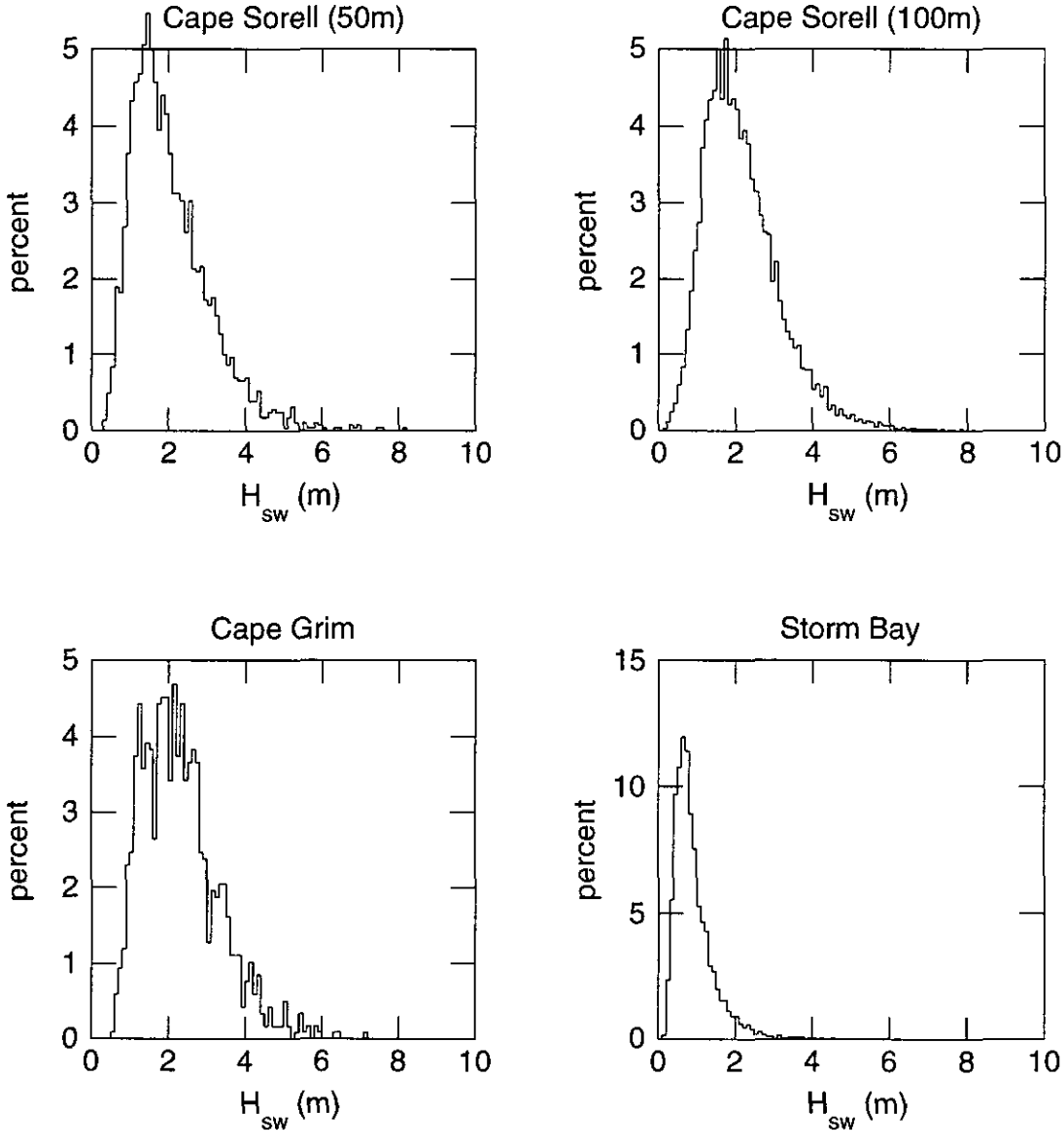


Figure 31: Histograms showing distribution of "swell height", $H_{sw}$.

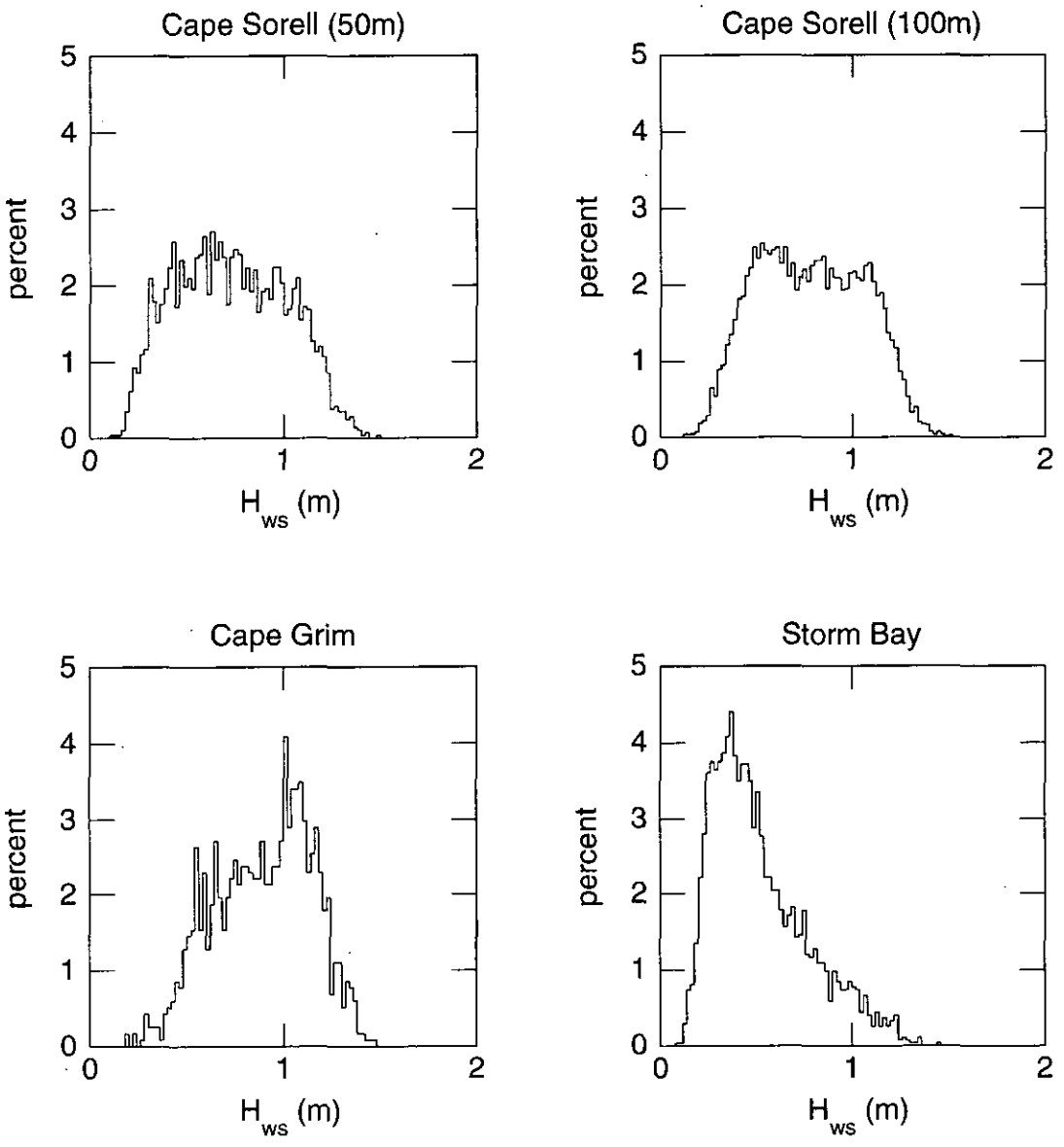


Figure 32: Histograms showing distribution of "wind sea height", $H_{ws}$.

| | min | max | mean | st.dev. | median | mode |
|---|---|---|---|---|---|---|
| $H_{mu}$ | 0.8803 | 16.0801 | 4.1798 | 1.8359 | 3.8393 | 3.3000 |
| $H_{md}$ | 0.9006 | 14.0203 | 4.0940 | 1.7867 | 3.7701 | 2.9000 |
| $H_{\sigma}$ | 0.6483 | 9.3140 | 2.8336 | 1.2131 | 2.6069 | 2.1000 |
| $H_m$ | 0.6231 | 8.9338 | 2.7371 | 1.1736 | 2.5119 | 2.0500 |
| $a_{cmax}$ | 0.4968 | 8.0692 | 2.2330 | 0.9777 | 2.0531 | 1.7000 |
| $a_{tmax}$ | 0.4760 | 8.8886 | 2.2757 | 1.0169 | 2.0706 | 1.7000 |
| $H_{\frac{1}{3}}$ | 0.5376 | 8.9295 | 2.6622 | 1.1488 | 2.4544 | 1.9500 |
| $T_{\frac{1}{3}}$ | 4.6929 | 16.7258 | 10.4596 | 1.5660 | 10.4631 | 10.6000 |
| $T_z$ | 3.6740 | 14.1962 | 7.9009 | 1.3379 | 7.9335 | 7.9000 |
| $T_c$ | 2.2207 | 7.6039 | 4.3634 | 0.7752 | 4.3939 | 4.4500 |
| $T_p$ | 3.8277 | 21.0526 | 12.5444 | 2.3259 | 12.5000 | 12.6250 |
| $T_{-1}$ | 5.4864 | 15.8612 | 10.3130 | 1.3623 | 10.2891 | 10.2999 |
| $T_1$ | 4.1208 | 14.6858 | 8.8050 | 1.3591 | 8.8538 | 8.9000 |
| $T_2$ | 3.5896 | 13.5722 | 7.8077 | 1.2901 | 7.8710 | 8.1000 |
| $T_4$ | 3.0294 | 9.2922 | 5.7906 | 0.9359 | 5.8330 | 5.9500 |
| $m_{-1}$ | 0.2136 | 69.1321 | 5.9470 | 6.1192 | 3.9611 | 2.5000 |
| $m_0$ | 0.0242 | 4.9882 | 0.5543 | 0.5072 | 0.3943 | 0.2500 |
| $m_1$ | 0.0030 | 0.4243 | 0.0609 | 0.0496 | 0.0461 | 0.0275 |
| $m_2$ | 0.0004 | 0.0438 | 0.0086 | 0.0062 | 0.0070 | 0.0037 |
| $m_4$ | 0.0000 | 0.0013 | 0.0004 | 0.0002 | 0.0004 | 0.0001 |
| $\epsilon$ | 0.6438 | 0.9549 | 0.8287 | 0.0415 | 0.8291 | 0.8250 |
| $P$ | 1.6888 | 546.4746 | 47.0099 | 48.3715 | 31.3120 | 15.0000 |
| $H_{sw}$ | 0.3561 | 8.1450 | 2.0287 | 1.0110 | 1.8194 | 1.4500 |
| $H_{ws}$ | 0.1069 | 1.4965 | 0.7274 | 0.2817 | 0.7164 | 0.6300 |

Table 8: Statistics - Cape Sorell (50m)

| | min | max | mean | st.dev. | median | mode |
|---|---|---|---|---|---|---|
| $H_{mu}$ | 0.8935 | 14.7695 | 4.4442 | 1.7469 | 4.1460 | 3.7000 |
| $H_{md}$ | 0.8625 | 13.5633 | 4.3668 | 1.6876 | 4.0819 | 3.7000 |
| $H_{\sigma}$ | 0.6720 | 9.4096 | 3.0198 | 1.1407 | 2.8378 | 2.7000 |
| $H_m$ | 0.6360 | 9.0521 | 2.9140 | 1.1048 | 2.7406 | 2.6500 |
| $a_{cmax}$ | 0.4523 | 7.7738 | 2.3751 | 0.9102 | 2.2197 | 1.9000 |
| $a_{tmax}$ | 0.4856 | 8.5803 | 2.4181 | 0.9635 | 2.2376 | 2.1000 |
| $H_{\frac{1}{3}}$ | 0.6118 | 8.7420 | 2.8402 | 1.0883 | 2.6647 | 2.4500 |
| $T_{\frac{1}{3}}$ | 4.0310 | 17.5611 | 10.4598 | 1.6262 | 10.4964 | 10.6000 |
| $T_z$ | 3.3727 | 14.0141 | 7.9491 | 1.3614 | 7.9375 | 8.1000 |
| $T_c$ | 2.5421 | 7.3452 | 4.4427 | 0.7122 | 4.4256 | 4.4500 |
| $T_p$ | 3.5555 | 21.0526 | 12.3341 | 2.2164 | 12.3076 | 12.6250 |
| $T_{-1}$ | 4.6044 | 16.5715 | 10.2492 | 1.4173 | 10.2517 | 10.2999 |
| $T_1$ | 3.7594 | 14.3311 | 8.8136 | 1.3937 | 8.8474 | 8.9000 |
| $T_2$ | 3.4263 | 13.1772 | 7.8425 | 1.2922 | 7.8743 | 7.9000 |
| $T_4$ | 3.0328 | 9.1560 | 5.8354 | 0.8782 | 5.8461 | 5.9500 |
| $m_{-1}$ | 0.1619 | 68.0626 | 6.4412 | 5.8316 | 4.7541 | 2.5000 |
| $m_0$ | 0.0252 | 5.1213 | 0.6070 | 0.4904 | 0.4694 | 0.2500 |
| $m_1$ | 0.0025 | 0.4661 | 0.0671 | 0.0484 | 0.0541 | 0.0325 |
| $m_2$ | 0.0003 | 0.0499 | 0.0094 | 0.0061 | 0.0080 | 0.0057 |
| $m_4$ | 0.0000 | 0.0013 | 0.0004 | 0.0002 | 0.0004 | 0.0002 |
| $\epsilon$ | 0.5354 | 0.9527 | 0.8249 | 0.0424 | 0.8263 | 0.8250 |
| $P$ | 1.2805 | 538.0214 | 50.9166 | 46.0979 | 37.5808 | 21.0000 |
| $H_{sw}$ | 0.1818 | 8.1521 | 2.1636 | 0.9913 | 1.9937 | 1.7500 |
| $H_{ws}$ | 0.1324 | 1.5100 | 0.7798 | 0.2737 | 0.7733 | 0.5300 |

Table 9: Statistics - Cape Sorell (100m)

| | min | max | mean | st.dev. | median | mode |
|---|---|---|---|---|---|---|
| $H_{mu}$ | 1.3521 | 15.4555 | 4.7456 | 1.7859 | 4.6101 | 4.7000 |
| $H_{md}$ | 1.4850 | 12.3895 | 4.6582 | 1.6860 | 4.5602 | 4.9000 |
| $H_{\sigma}$ | 1.0371 | 8.6714 | 3.2170 | 1.1615 | 3.1467 | 3.7000 |
| $H_{m}$ | 0.9966 | 8.3389 | 3.1072 | 1.1270 | 3.0224 | 2.8500 |
| $a_{cmax}$ | 0.7904 | 6.9766 | 2.5413 | 0.9172 | 2.4628 | 2.5000 |
| $a_{tmax}$ | 0.7777 | 8.4789 | 2.5877 | 0.9736 | 2.4949 | 2.9000 |
| $H_{\frac{1}{3}}$ | 0.9006 | 8.1405 | 3.0116 | 1.1120 | 2.9478 | 2.7500 |
| $T_{\frac{1}{3}}$ | 4.2855 | 15.1834 | 10.3574 | 1.7528 | 10.3811 | 10.2000 |
| $T_{z}$ | 3.8534 | 12.3001 | 7.6949 | 1.3634 | 7.6766 | 7.7000 |
| $T_{c}$ | 2.6445 | 6.3062 | 4.2666 | 0.6815 | 4.2509 | 4.1500 |
| $T_{p}$ | 3.7558 | 19.5121 | 12.4284 | 2.2194 | 12.5000 | 12.6250 |
| $T_{-1}$ | 5.8721 | 14.8113 | 10.2053 | 1.4631 | 10.1402 | 9.9000 |
| $T_{1}$ | 4.3096 | 13.3024 | 8.6219 | 1.4494 | 8.5673 | 7.9000 |
| $T_{2}$ | 3.8603 | 12.0510 | 7.5957 | 1.3286 | 7.5430 | 7.5000 |
| $T_{4}$ | 3.3446 | 8.5171 | 5.6298 | 0.8743 | 5.6058 | 5.5500 |
| $m_{-1}$ | 0.5143 | 52.4442 | 7.2346 | 6.0260 | 5.7671 | 2.5000 |
| $m_{0}$ | 0.0620 | 4.3461 | 0.6828 | 0.5065 | 0.5709 | 0.2500 |
| $m_{1}$ | 0.0076 | 0.4032 | 0.0765 | 0.0499 | 0.0662 | 0.0325 |
| $m_{2}$ | 0.0008 | 0.0447 | 0.0110 | 0.0062 | 0.0099 | 0.0087 |
| $m_{4}$ | 0.0000 | 0.0013 | 0.0006 | 0.0002 | 0.0006 | 0.0004 |
| $\epsilon$ | 0.6478 | 0.9406 | 0.8270 | 0.0428 | 0.8313 | 0.8450 |
| $P$ | 4.0658 | 414.5607 | 57.1884 | 47.6346 | 45.5884 | 15.0000 |
| $H_{sw}$ | 0.5849 | 7.1086 | 2.3086 | 0.9998 | 2.1644 | 2.1500 |
| $H_{ws}$ | 0.1882 | 1.4773 | 0.8938 | 0.2506 | 0.9178 | 1.0100 |

Table 10: Statistics - Cape Grim

| | min | max | mean | st.dev. | median | mode |
|---|---|---|---|---|---|---|
| $H_{mu}$ | 0.5007 | 8.7266 | 2.1254 | 1.0046 | 1.9235 | 1.5000 |
| $H_{md}$ | 0.5012 | 7.9186 | 2.0950 | 0.9707 | 1.9024 | 1.7000 |
| $H_{\sigma}$ | 0.3455 | 6.1329 | 1.4742 | 0.6796 | 1.3431 | 1.1000 |
| $H_m$ | 0.2644 | 5.7788 | 1.3830 | 0.6473 | 1.2623 | 1.1500 |
| $a_{cmax}$ | 0.2757 | 4.4298 | 1.1897 | 0.5604 | 1.0692 | 0.9000 |
| $a_{tmax}$ | 0.2805 | 4.6716 | 1.2001 | 0.5740 | 1.0741 | 1.1000 |
| $H_{\frac{1}{3}}$ | 0.2888 | 5.6035 | 1.3219 | 0.6311 | 1.2013 | 1.0500 |
| $T_{\frac{1}{3}}$ | 3.0222 | 31.5625 | 9.3470 | 2.2062 | 9.3750 | 9.8000 |
| $T_z$ | 2.7876 | 12.9802 | 6.5340 | 1.4302 | 6.5019 | 5.7000 |
| $T_c$ | 2.0919 | 5.4633 | 3.3358 | 0.5978 | 3.3081 | 3.3500 |
| $T_p$ | 2.4539 | 20.5128 | 12.1695 | 2.8555 | 12.5000 | 12.6250 |
| $T_{-1}$ | 4.1991 | 16.2126 | 9.4445 | 1.7650 | 9.4558 | 9.2999 |
| $T_1$ | 2.9984 | 12.9378 | 7.4413 | 1.6238 | 7.4637 | 7.3000 |
| $T_2$ | 2.7195 | 10.7101 | 6.2935 | 1.3746 | 6.2674 | 6.5000 |
| $T_4$ | 2.4763 | 7.0452 | 4.5488 | 0.8161 | 4.4905 | 4.2500 |
| $m_{-1}$ | 0.0397 | 22.3259 | 1.4277 | 1.7750 | 0.9054 | 2.5000 |
| $m_0$ | 0.0043 | 2.0871 | 0.1457 | 0.1630 | 0.0996 | 0.2500 |
| $m_1$ | 0.0006 | 0.2196 | 0.0190 | 0.0187 | 0.0136 | 0.0075 |
| $m_2$ | 0.0001 | 0.0279 | 0.0035 | 0.0029 | 0.0026 | 0.0012 |
| $m_4$ | 0.0000 | 0.0014 | 0.0003 | 0.0001 | 0.0002 | 0.0001 |
| $\epsilon$ | 0.5019 | 0.9572 | 0.8345 | 0.0637 | 0.8437 | 0.8550 |
| $P$ | 0.3141 | 176.4821 | 11.2861 | 14.0310 | 7.1571 | 15.0000 |
| $H_{sw}$ | 0.1656 | 4.5151 | 0.9179 | 0.5219 | 0.7803 | 0.6500 |
| $H_{ws}$ | 0.0938 | 1.4400 | 0.5190 | 0.2483 | 0.4597 | 0.3700 |

Table 11: Statistics - Storm Bay

| | min | max | mean | st.dev. | median | mode |
|---|---|---|---|---|---|---|
| $H_{mu}$ | 0.5007 | 16.0801 | 4.0798 | 1.8671 | - | - |
| $H_{md}$ | 0.5012 | 14.0203 | 4.0074 | 1.8082 | - | - |
| $H_{\sigma}$ | 0.3455 | 9.4096 | 2.7751 | 1.2278 | - | - |
| $H_{m}$ | 0.2644 | 9.0521 | 2.6727 | 1.1936 | - | - |
| $a_{cmax}$ | 0.2757 | 8.0692 | 2.1885 | 0.9750 | - | - |
| $a_{tmax}$ | 0.2805 | 8.8886 | 2.2268 | 1.0223 | - | - |
| $H_{\frac{1}{3}}$ | 0.2888 | 8.9295 | 2.5992 | 1.1754 | - | - |
| $T_{\frac{1}{3}}$ | 3.0222 | 31.5625 | 10.2891 | 1.7674 | - | - |
| $T_{z}$ | 2.7876 | 14.1962 | 7.7168 | 1.4554 | - | - |
| $T_{c}$ | 2.0919 | 7.6039 | 4.2559 | 0.8037 | - | - |
| $T_{p}$ | 2.4539 | 21.0526 | 12.3486 | 2.3411 | - | - |
| $T_{-1}$ | 4.1991 | 16.5715 | 10.1377 | 1.4968 | - | - |
| $T_{1}$ | 2.9984 | 14.6858 | 8.5977 | 1.5078 | - | - |
| $T_{2}$ | 2.7195 | 13.5722 | 7.5930 | 1.4153 | - | - |
| $T_{4}$ | 2.4763 | 9.2922 | 5.6256 | 0.9873 | - | - |
| $m_{-1}$ | 0.0397 | 69.1321 | 5.6745 | 5.7738 | - | - |
| $m_{0}$ | 0.0043 | 5.1213 | 0.5355 | 0.4895 | - | - |
| $m_{1}$ | 0.0006 | 0.4661 | 0.0596 | 0.0487 | - | - |
| $m_{2}$ | 0.0001 | 0.0499 | 0.0085 | 0.0061 | - | - |
| $m_{4}$ | 0.0000 | 0.0014 | 0.0004 | 0.0002 | - | - |
| $\epsilon$ | 0.5019 | 0.9572 | 0.8271 | 0.0462 | - | - |
| $P$ | 0.3141 | 546.4746 | 44.8558 | 45.6407 | - | - |
| $H_{sw}$ | 0.1656 | 8.1521 | 1.9679 | 1.0392 | - | - |
| $H_{ws}$ | 0.0938 | 1.5100 | 0.7403 | 0.2875 | - | - |

Table 12: Statistics - all sites

## 3.3 Joint distributions of sample statistics

### 3.3.1 Scatter diagrams

Since the advent of systematic observations of waves a wide variety of statistics have come into being to define sea state and wave climate. Frequently these statistics are strongly dependent on one another and theoretical arguments are used to define this interdependence. However such arguments often depend on prior assumptions about the spectrum (for example, that it is narrow band) and may not be very useful in practice (see, for example Reid (1989)). A better approach might be to uncover inter-relationships empirically using the methods of experimental statistics. The disadvantage of this is that it lacks universality; the relationships revealed may only apply to the location under investigation and have little relevance elsewhere. In a sense the relations which are determined between various statistics in this way are as much a part of the description of the wave climate of the location as are the statistics themselves.

Nevertheless the investigation of such inter-relationships are worth pursuing. A marine engineer may require a wave climate statistic for design purposes which is not itself available but which can be estimated from other statistics which are known for a particular locality. He will need to know not only the regression coefficient for numerical conversion but also how good the correlation is between the two quantities.

In this section the interrelationships between the sample statistics listed in Table 7 are discussed. The degree to which they were correlated was assessed by plotting scatter diagrams and carrying out regression analysis of paired samples derived from the same burst.

Typical scatter diagrams are shown in Figures 33 to 37. Individual points are not shown in these figures. Rather the density of points is shown via filled contours in which the area containing the densest five percent of points is coloured black.

In general height parameters are well correlated with other height parameters as in Figures 33 and 34, while time parameters are less well correlated with other time parameters as in Figure 35. The correlation between time parameters $T_p$ and $T_z$ is very poor in Figure 36. This is because of the dominant roll played by swell and wind enhanced swell at each site. In general in these waters $T_p$ is controlled by the position of the swell peak at the low frequency end of the spectrum whereas $T_z$ depends more on the high frequency end of the spectrum and is affected more by wind sea particularly

when the wind is offshore. As a consequence these two parameters are almost independent. Only in the absence of swell when the spectral peak is at the high frequency end of the spectrum are the two quantities related. This is the reason for the "tails" at short periods in Figure 36.

The relationship between height parameters and time parameters is of some interest because it reflects the underlying physics of waves. It has been known for many years that waves have a limiting steepness; as a rule of thumb $H/L$ does not exceed $1/7$ where $H$ is the wave height and $L$ is the wavelength (Kinsman, 1965). Since $L = gT^2/2\pi$ , for monochromatic waves , that is

$$\frac{H}{gT^2} < \frac{1}{14\pi} \tag{14}$$

i.e.

$$\frac{H}{gT^2} < 0.023 \tag{15}$$

It is reasonable to assume that similar limiting behaviour will be observed even when waves are not monochromatic.

Joint distributions of $H_\sigma$ and $gT_z^2$ are shown in Figure 37. $gT_z^2$ is plotted rather than $T_z$ and as a consequence there is a linear upper bound to each distribution. The slopes of the linear part of the upper bounds in Figure 37 are, clockwise from top left, .0090, .0094, .0098 and .0094 $ms^{-2}$. The slopes are similar because they reflect a fundamental property of waves which is independent of the site of the observations. They differ from the value based on the $1/7$ rule because the quantities $H_\sigma$ and $T_z$ are averages for all the waves in a burst whereas the $1/7$ rule relates only to the extreme waves; the linear upper bound to the distributions shown in Figure 37 is the locus of extreme bursts rather than extreme waves.

It is often necessary in field work involving ocean waves to exercise quality control over data from remote observing sites (for example, Palao, 1994). Plotting scatter diagrams in the form shown in Figure 37 provides a convenient check on data validity; the existence of points above the maximum slope locus indicates invalid or improperly scaled data.

### 3.3.2 Regression relationships

Relationships expressed in the form of plots of joint distributions can often be expressed more succinctly using regression methods. When two variables such as $H_m$ and $H_\sigma$ are closely related as is shown in Fig. 34 their correlation coefficient will be close to unity. In effect the correlation coefficient describes

the ratio of the major and minor axis of the "ellipse of concentration" of the distribution and when the correlation coefficient is close to unity in magnitude the regression coefficients approximate the slope of the major axis.

The correlation coefficients calculated for various pairs of wave height statistics for the four sites are shown in Tables 13 to 16. The corresponding regression coefficients are shown in Tables 17 to 20. The correlation coefficients for various time statistics are shown in Tables 21 to 24 and their slopes in Tables 25 to 28. Tables 29 to 32 show the slopes and correlations when all the data are grouped into a single set.

### 3.3.3 Estimation

Tables 8 through 32 can be used to estimate the value of an unknown statistic in terms of a known statistic. For example if the mean zero-crossing period, $T_z$, is known then the significant wave period, $T_{1/3}$ can be estimated as follows. The two dimensional regression equation is

$$\hat{y} - \bar{y} = \hat{\beta}_{yx}(x - \bar{x}) \tag{16}$$

where $x$ is a known value of the independent variable, $\bar{x}$ and $\bar{y}$ are the means, $\hat{y}$ is the quantity to be estimated and $\hat{\beta}_{yx}$ is the regression coefficient of y on x. An estimate of $T_{1/3}$, $\hat{T}_{1/3}$ can be found in terms of $T_z$ by

$$\hat{T}_{1/3} = \hat{\beta}_{yx}(T_z - \bar{T}_z) + \bar{T}_{1/3} \tag{17}$$

The quantities $\bar{T}_z$ and $\bar{T}_{1/3}$ can be found in Table 12. They are 7.7168 and 10.2891 respectively. The slope of the regression line, $\hat{\beta}_{yx}$, is found from Table 32. It is 1.082. Substituting in (17) gives the equation

$$\hat{T}_{1/3} = 1.082T_z - 1.9395 \tag{18}$$

which may be used to estimate $T_{1/3}$ from a known value of $T_z$.

The correlation coefficient, $\rho$, given in Table 31 for these two quantities is 0.8917. This is relatively high and suggests that the estimate will be reasonably accurate. In fact the standard deviation of the estimate of $T_{1/3}$, $\sigma_e$ is given by

$$\sigma_e = \sigma\sqrt{1 - \rho^2} \tag{19}$$

where $\sigma$ is the standard deviation of the dependent variable. In this case, from Table 12, $\sigma = 1.7674$. Hence $\sigma_e = 0.80$.

The best correlation between any two statistics is that measured between $H_\sigma$ and $H_m$. An overall value of 0.9984 was found for the correlation coefficient

(Table 29). Hence $H_\sigma$ predicts 99.7 percent of the variance in $H_m$ and *vice versa*. The variance in $H_\sigma$ which is not accounted for by $H_m$ is largely that due to the twisted suspension error discussed in Section 2.4. The high value of the correlation coefficient is an encouraging indication that the twisted suspension error had little effect on the data.

An unexpected feature of the satistics listed in the tables is the fact that at each site the mean maximum upcrossing wave height, $H_{mu}$, was consistently larger than the mean maximum downcrossing wave height, $H_{md}$. This was also true of the medians, standard deviations and regression coefficients. No explanation can be offered for this effect.

Data recorded prior to 18 November 1985 was considered of too poor quality to included in the statistical analysis which lead to Tables 8 to 32. The maximum wave heights observed during the entire program were recorded prior to this on 29 July 1985 at 2020 EST and are listed in Table 41. The maximum upcrossing wave height was 19.83 m and the maximum downcrossing wave height was 17.05 m for this burst. Once again the upcrossing maximum was higher than the downcrossing maximum.

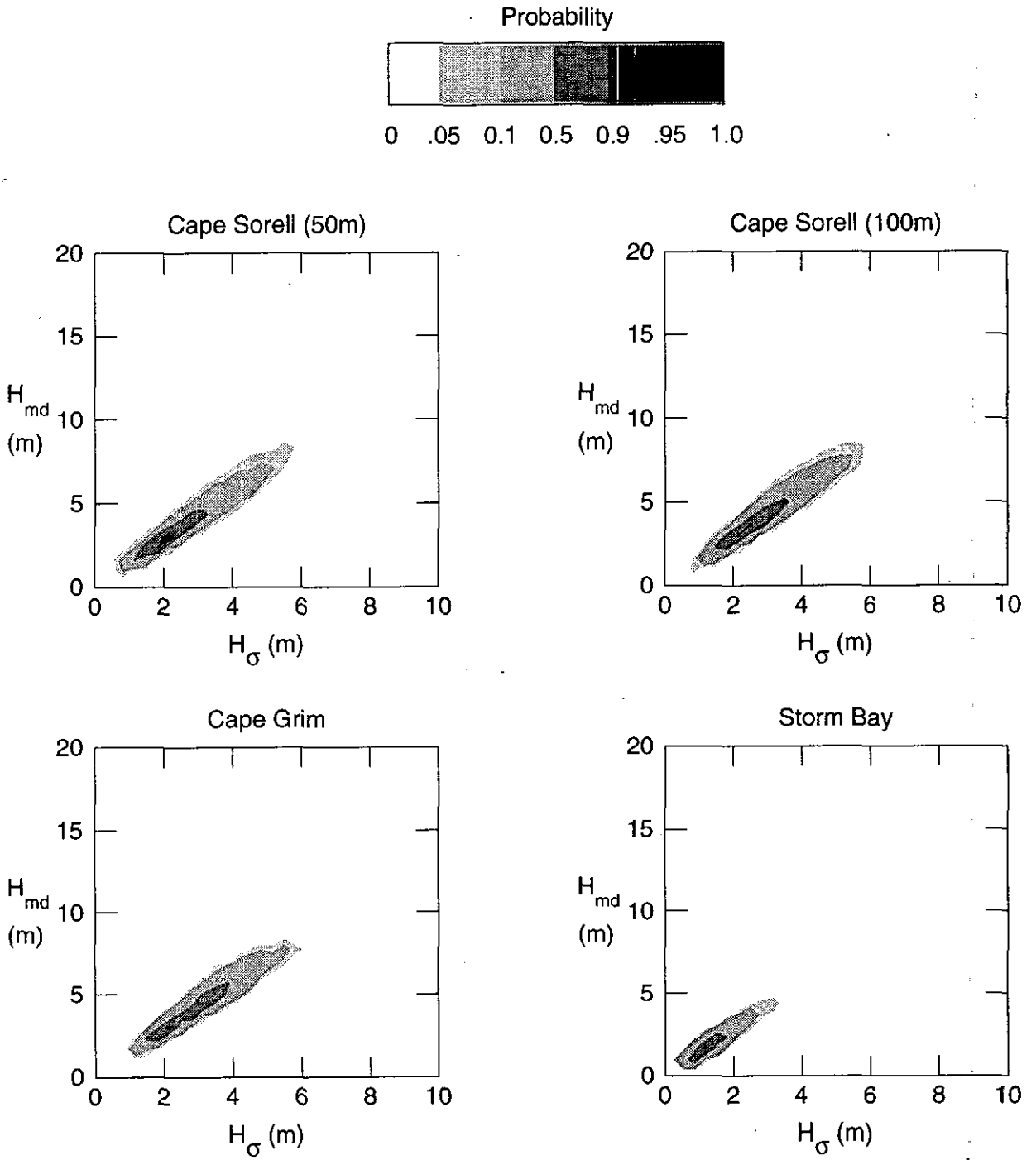


Figure 33: Scatter diagram of joint distribution of maximum down-crossing wave height, $H_{md}$, with significant wave height, $H_\sigma$.

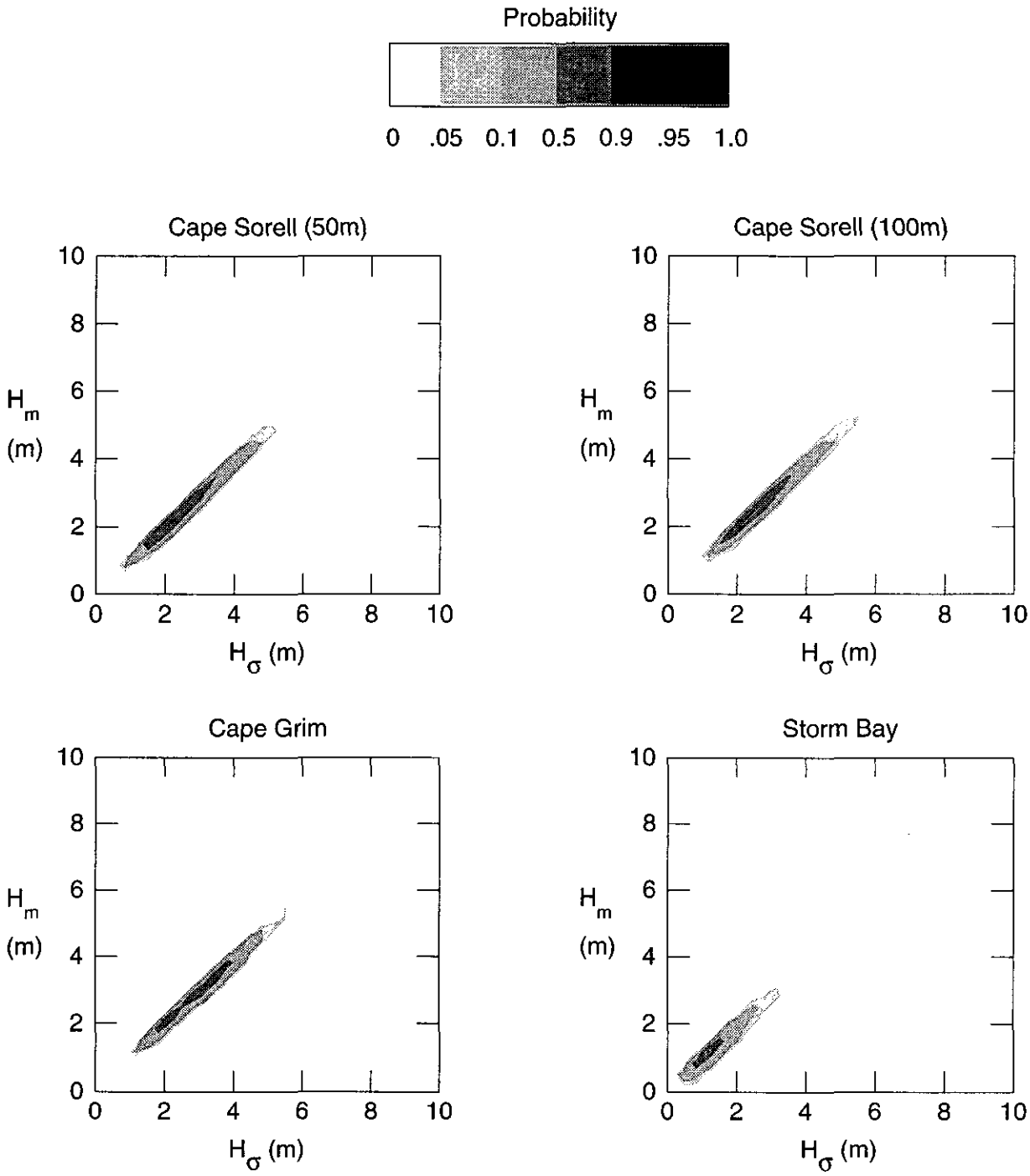


Figure 34: Scatter diagram of joint distribution of spectral moment wave height, $H_m$, with significant wave height, $H_\sigma$.

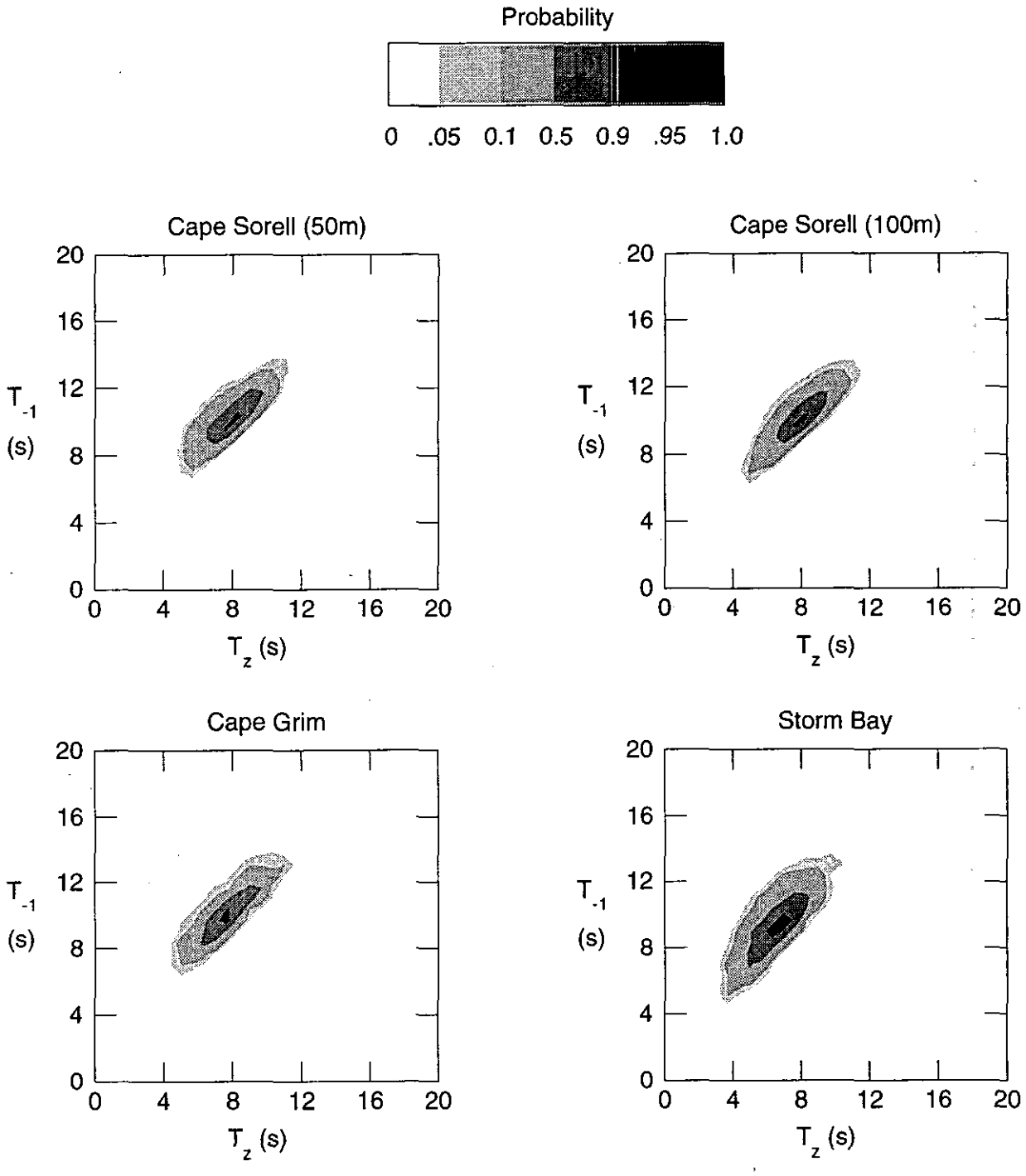


Figure 35: Scatter diagram of joint distribution of spectral mean period, $T_1$, with mean zero crossing period, $T_z$.

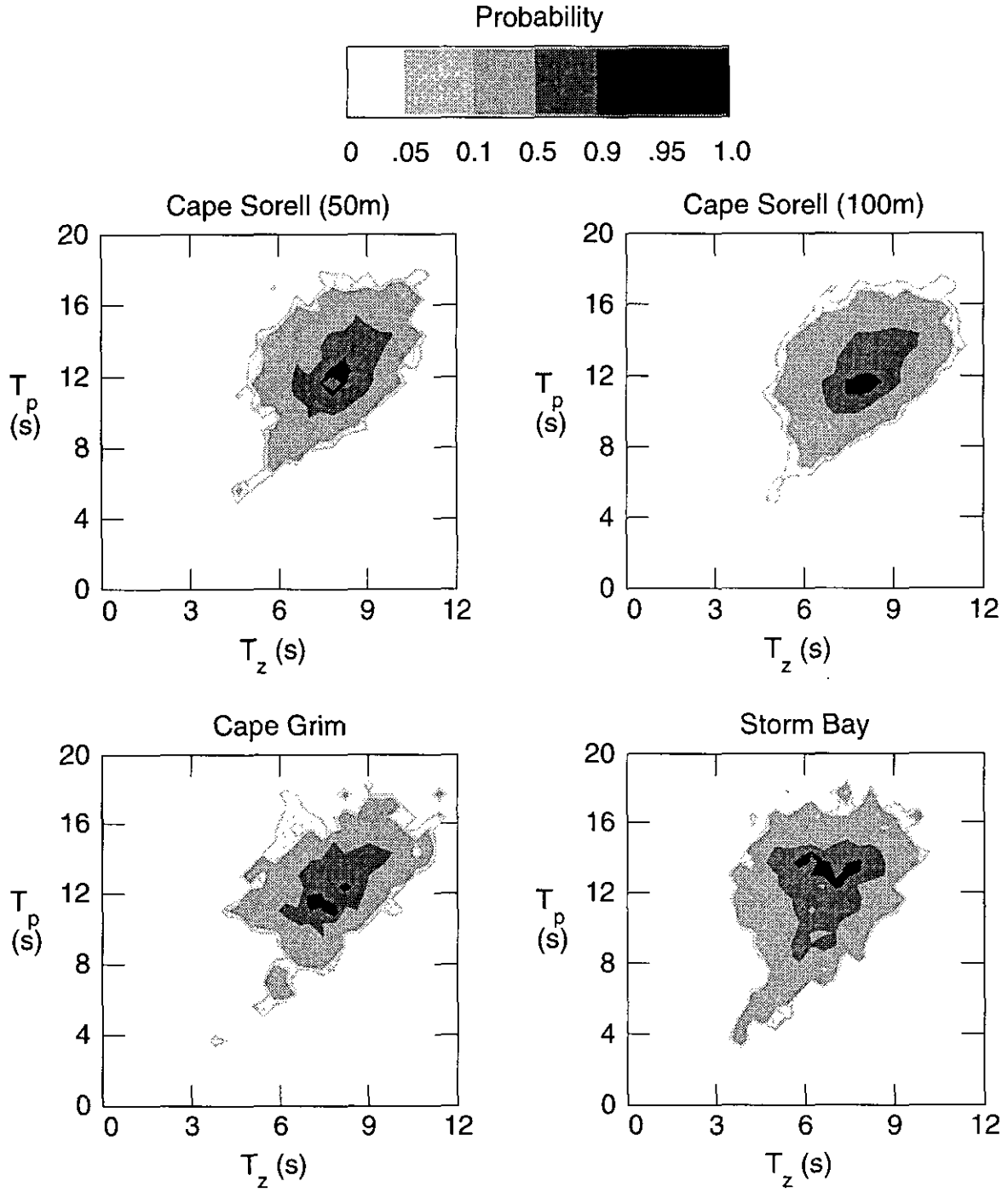


Figure 36: Scatter diagram of joint distribution of spectral peak period, $T_p$, with mean zero crossing period, $T_z$.

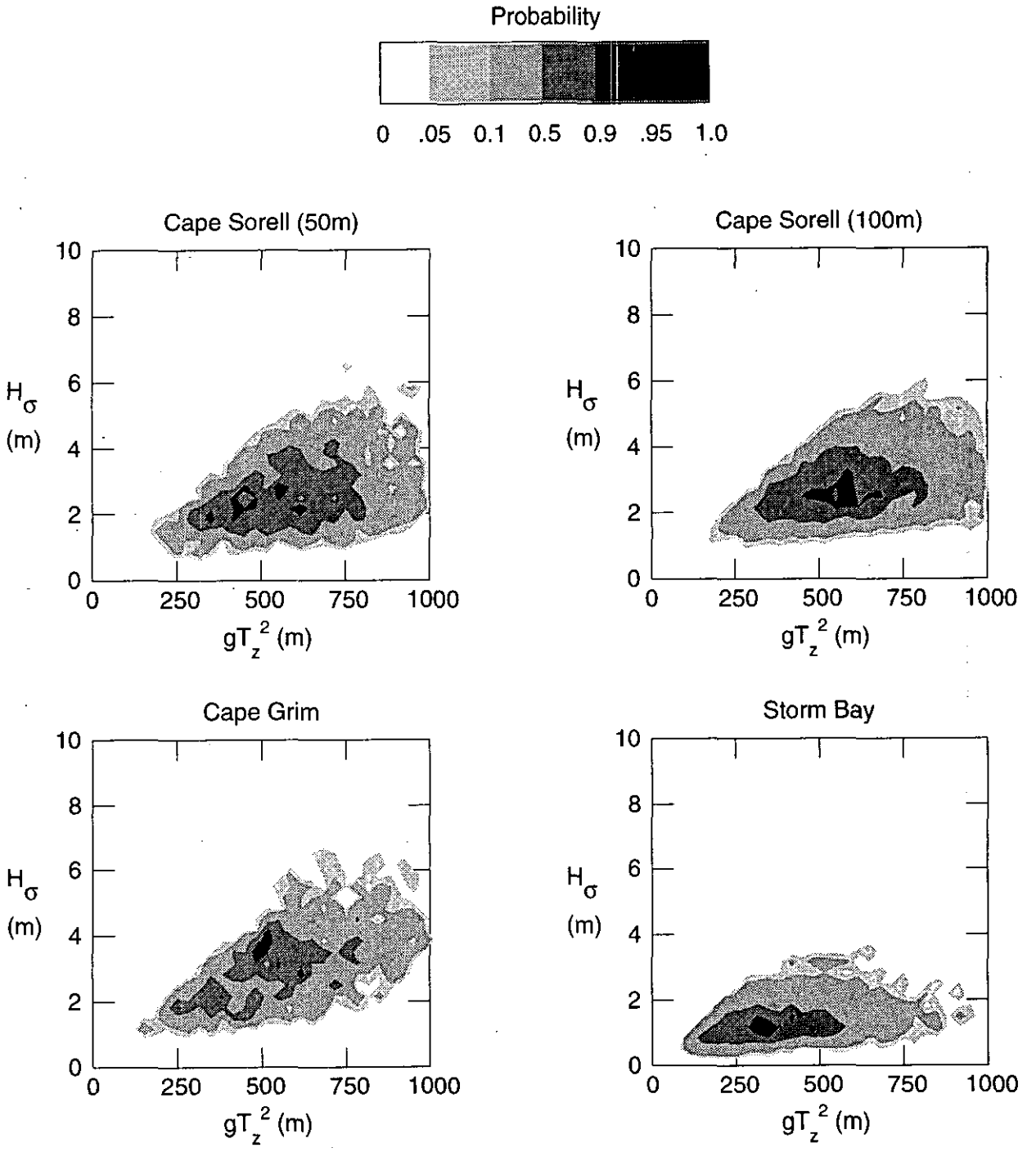


Figure 37: Scatter diagram of joint distribution of g times the squared mean zero crossing period, $gT_z^2$, with significant wave height, $H_\sigma$.

| | $H_{mu}$ | $H_{md}$ | $a_{cmax}$ | $a_{tmax}$ | $H_{\sigma}$ | $H_m$ | $H_{\frac{1}{3}}$ |
|---|---|---|---|---|---|---|---|
| $H_{mu}$ | 1.0000 | 0.9690 | 0.9687 | 0.9707 | 0.9647 | 0.9645 | 0.9622 |
| $H_{md}$ | 0.9690 | 1.0000 | 0.9648 | 0.9689 | 0.9685 | 0.9683 | 0.9666 |
| $a_{cmax}$ | 0.9687 | 0.9648 | 1.0000 | 0.9353 | 0.9624 | 0.9610 | 0.9583 |
| $a_{tmax}$ | 0.9707 | 0.9689 | 0.9353 | 1.0000 | 0.9610 | 0.9597 | 0.9573 |
| $H_{\sigma}$ | 0.9647 | 0.9685 | 0.9624 | 0.9610 | 1.0000 | 0.9988 | 0.9970 |
| $H_m$ | 0.9645 | 0.9683 | 0.9610 | 0.9597 | 0.9988 | 1.0000 | 0.9970 |
| $H_{\frac{1}{3}}$ | 0.9622 | 0.9666 | 0.9583 | 0.9573 | 0.9970 | 0.9970 | 1.0000 |

Table 13: Wave height correlation coefficients - Cape Sorell (50m).

| | $H_{mu}$ | $H_{md}$ | $a_{cmax}$ | $a_{tmax}$ | $H_{\sigma}$ | $H_m$ | $H_{\frac{1}{3}}$ |
|---|---|---|---|---|---|---|---|
| $H_{mu}$ | 1.0000 | 0.9634 | 0.9656 | 0.9658 | 0.9582 | 0.9580 | 0.9565 |
| $H_{md}$ | 0.9634 | 1.0000 | 0.9601 | 0.9629 | 0.9607 | 0.9606 | 0.9593 |
| $a_{cmax}$ | 0.9656 | 0.9601 | 1.0000 | 0.9243 | 0.9535 | 0.9530 | 0.9506 |
| $a_{tmax}$ | 0.9658 | 0.9629 | 0.9243 | 1.0000 | 0.9514 | 0.9506 | 0.9483 |
| $H_{\sigma}$ | 0.9582 | 0.9607 | 0.9535 | 0.9514 | 1.0000 | 0.9989 | 0.9975 |
| $H_m$ | 0.9580 | 0.9606 | 0.9530 | 0.9506 | 0.9989 | 1.0000 | 0.9972 |
| $H_{\frac{1}{3}}$ | 0.9565 | 0.9593 | 0.9506 | 0.9483 | 0.9975 | 0.9972 | 1.0000 |

Table 14: Wave height correlation coefficients - Cape Sorell (100m).

| | $H_{mu}$ | $H_{md}$ | $a_{cmax}$ | $a_{tmax}$ | $H_{\sigma}$ | $H_m$ | $H_{\frac{1}{3}}$ |
|---|---|---|---|---|---|---|---|
| $H_{mu}$ | 1.0000 | 0.9564 | 0.9616 | 0.9659 | 0.9583 | 0.9577 | 0.9545 |
| $H_{md}$ | 0.9564 | 1.0000 | 0.9546 | 0.9572 | 0.9579 | 0.9572 | 0.9560 |
| $a_{cmax}$ | 0.9616 | 0.9546 | 1.0000 | 0.9213 | 0.9498 | 0.9496 | 0.9454 |
| $a_{tmax}$ | 0.9659 | 0.9572 | 0.9213 | 1.0000 | 0.9520 | 0.9511 | 0.9468 |
| $H_{\sigma}$ | 0.9583 | 0.9579 | 0.9498 | 0.9520 | 1.0000 | 0.9992 | 0.9975 |
| $H_m$ | 0.9577 | 0.9572 | 0.9496 | 0.9511 | 0.9992 | 1.0000 | 0.9972 |
| $H_{\frac{1}{3}}$ | 0.9545 | 0.9560 | 0.9454 | 0.9468 | 0.9975 | 0.9972 | 1.0000 |

Table 15: Wave height correlation coefficients - Cape Grim

| | $H_{mu}$ | $H_{md}$ | $a_{cmax}$ | $a_{tmax}$ | $H_{\sigma}$ | $H_m$ | $H_{\frac{1}{3}}$ |
|---|---|---|---|---|---|---|---|
| $H_{mu}$ | 1.0000 | 0.9687 | 0.9557 | 0.9469 | 0.9664 | 0.9668 | 0.9652 |
| $H_{md}$ | 0.9687 | 1.0000 | 0.9567 | 0.9443 | 0.9676 | 0.9660 | 0.9653 |
| $a_{cmax}$ | 0.9557 | 0.9567 | 1.0000 | 0.9153 | 0.9594 | 0.9436 | 0.9440 |
| $a_{tmax}$ | 0.9469 | 0.9443 | 0.9153 | 1.0000 | 0.9577 | 0.9239 | 0.9269 |
| $H_{\sigma}$ | 0.9664 | 0.9676 | 0.9594 | 0.9577 | 1.0000 | 0.9833 | 0.9855 |
| $H_m$ | 0.9668 | 0.9660 | 0.9436 | 0.9239 | 0.9833 | 1.0000 | 0.9967 |
| $H_{\frac{1}{3}}$ | 0.9652 | 0.9653 | 0.9440 | 0.9269 | 0.9855 | 0.9967 | 1.0000 |

Table 16: Wave height correlation coefficients - Storm Bay

| | $H_{mu}$ | $H_{md}$ | $a_{cmax}$ | $a_{tmax}$ | $H_{\sigma}$ | $H_m$ | $H_{\frac{1}{3}}$ |
|---|---|---|---|---|---|---|---|
| $H_{mu}$ | 1.000 | 0.943 | 0.515 | 0.537 | 0.637 | 0.616 | 0.602 |
| $H_{md}$ | 0.995 | 1.000 | 0.528 | 0.551 | 0.657 | 0.636 | 0.621 |
| $a_{cmax}$ | 1.819 | 1.763 | 1.000 | 0.972 | 1.194 | 1.153 | 1.126 |
| $a_{tmax}$ | 1.752 | 1.702 | 0.899 | 1.000 | 1.146 | 1.107 | 1.081 |
| $H_{\sigma}$ | 1.460 | 1.426 | 0.775 | 0.805 | 1.000 | 0.966 | 0.944 |
| $H_m$ | 1.508 | 1.474 | 0.800 | 0.831 | 1.032 | 1.000 | 0.976 |
| $H_{\frac{1}{3}}$ | 1.537 | 1.503 | 0.815 | 0.847 | 1.052 | 1.018 | 1.000 |

Table 17: Wave height regression coefficients - Cape Sorell (50m)

| | $H_{mu}$ | $H_{md}$ | $a_{cmax}$ | $a_{tmax}$ | $H_{\sigma}$ | $H_m$ | $H_{\frac{1}{3}}$ |
|---|---|---|---|---|---|---|---|
| $H_{mu}$ | 1.000 | 0.930 | 0.503 | 0.532 | 0.625 | 0.605 | 0.595 |
| $H_{md}$ | 0.997 | 1.000 | 0.517 | 0.549 | 0.649 | 0.628 | 0.618 |
| $a_{cmax}$ | 1.853 | 1.780 | 1.000 | 0.978 | 1.195 | 1.156 | 1.136 |
| $a_{tmax}$ | 1.751 | 1.686 | 0.873 | 1.000 | 1.126 | 1.089 | 1.071 |
| $H_{\sigma}$ | 1.467 | 1.421 | 0.760 | 0.803 | 1.000 | 0.967 | 0.951 |
| $H_m$ | 1.514 | 1.467 | 0.785 | 0.829 | 1.031 | 1.000 | 0.982 |
| $H_{\frac{1}{3}}$ | 1.535 | 1.487 | 0.795 | 0.839 | 1.045 | 1.012 | 1.000 |

Table 18: Wave height regression coefficients - Cape Sorell (100m)

| | $H_{mu}$ | $H_{md}$ | $a_{cmax}$ | $a_{tmax}$ | $H_\sigma$ | $H_m$ | $H_{\frac{1}{3}}$ |
|---|---|---|---|---|---|---|---|
| $H_{mu}$ | 1.000 | 0.902 | 0.493 | 0.526 | 0.623 | 0.604 | 0.594 |
| $H_{md}$ | 1.013 | 1.000 | 0.519 | 0.552 | 0.659 | 0.639 | 0.630 |
| $a_{cmax}$ | 1.872 | 1.754 | 1.000 | 0.977 | 1.202 | 1.166 | 1.146 |
| $a_{tmax}$ | 1.771 | 1.657 | 0.867 | 1.000 | 1.135 | 1.101 | 1.081 |
| $H_\sigma$ | 1.473 | 1.390 | 0.750 | 0.798 | 1.000 | 0.969 | 0.955 |
| $H_m$ | 1.517 | 1.432 | 0.772 | 0.821 | 1.029 | 1.000 | 0.984 |
| $H_{\frac{1}{3}}$ | 1.532 | 1.449 | 0.779 | 0.828 | 1.041 | 1.010 | 1.000 |

Table 19: Wave height regression coefficients - Cape Grim

| | $H_{mu}$ | $H_{md}$ | $a_{cmax}$ | $a_{tmax}$ | $H_\sigma$ | $H_m$ | $H_{\frac{1}{3}}$ |
|---|---|---|---|---|---|---|---|
| $H_{mu}$ | 1.000 | 0.936 | 0.533 | 0.541 | 0.653 | 0.623 | 0.606 |
| $H_{md}$ | 1.002 | 1.000 | 0.552 | 0.558 | 0.677 | 0.644 | 0.627 |
| $a_{cmax}$ | 1.713 | 1.656 | 1.000 | 0.937 | 1.163 | 1.089 | 1.062 |
| $a_{tmax}$ | 1.657 | 1.596 | 0.893 | 1.000 | 1.133 | 1.041 | 1.019 |
| $H_\sigma$ | 1.428 | 1.382 | 0.791 | 0.808 | 1.000 | 0.936 | 0.915 |
| $H_m$ | 1.500 | 1.448 | 0.817 | 0.819 | 1.032 | 1.000 | 0.971 |
| $H_{\frac{1}{3}}$ | 1.536 | 1.484 | 0.838 | 0.843 | 1.061 | 1.022 | 1.000 |

Table 20: Wave height regression coefficients - Storm Bay

| | $T_{\frac{1}{3}}$ | $T_z$ | $T_p$ | $T_{-1}$ | $T_1$ | $T_2$ | $T_4$ |
|---|---|---|---|---|---|---|---|
| $T_{\frac{1}{3}}$ | 1.0000 | 0.8875 | 0.6210 | 0.9534 | 0.9488 | 0.8851 | 0.7182 |
| $T_z$ | 0.8875 | 1.0000 | 0.4521 | 0.8241 | 0.9464 | 0.9646 | 0.8984 |
| $T_p$ | 0.6210 | 0.4521 | 1.0000 | 0.7042 | 0.5531 | 0.4590 | 0.3236 |
| $T_{-1}$ | 0.9534 | 0.8241 | 0.7042 | 1.0000 | 0.9334 | 0.8463 | 0.6625 |
| $T_1$ | 0.9488 | 0.9464 | 0.5531 | 0.9334 | 1.0000 | 0.9775 | 0.8530 |
| $T_2$ | 0.8851 | 0.9646 | 0.4590 | 0.8463 | 0.9775 | 1.0000 | 0.9372 |
| $T_4$ | 0.7182 | 0.8984 | 0.3236 | 0.6625 | 0.8530 | 0.9372 | 1.0000 |

Table 21: Wave period correlation coefficients - Cape Sorell (50m)

| | $T_{\frac{1}{3}}$ | $T_z$ | $T_p$ | $T_{-1}$ | $T_1$ | $T_2$ | $T_4$ |
|---|---|---|---|---|---|---|---|
| $T_{\frac{1}{3}}$ | 1.0000 | 0.8958 | 0.6357 | 0.9651 | 0.9540 | 0.8941 | 0.7301 |
| $T_z$ | 0.8958 | 1.0000 | 0.4753 | 0.8537 | 0.9516 | 0.9653 | 0.8974 |
| $T_p$ | 0.6357 | 0.4753 | 1.0000 | 0.7077 | 0.5691 | 0.4814 | 0.3413 |
| $T_{-1}$ | 0.9651 | 0.8537 | 0.7077 | 1.0000 | 0.9473 | 0.8730 | 0.6971 |
| $T_1$ | 0.9540 | 0.9516 | 0.5691 | 0.9473 | 1.0000 | 0.9803 | 0.8614 |
| $T_2$ | 0.8941 | 0.9653 | 0.4814 | 0.8730 | 0.9803 | 1.0000 | 0.9389 |
| $T_4$ | 0.7301 | 0.8974 | 0.3413 | 0.6971 | 0.8614 | 0.9389 | 1.0000 |

Table 22: Wave period correlation coefficients - Cape Sorell (100m)

| | $T_{\frac{1}{3}}$ | $T_z$ | $T_p$ | $T_{-1}$ | $T_1$ | $T_2$ | $T_4$ |
|---|---|---|---|---|---|---|---|
| $T_{\frac{1}{3}}$ | 1.0000 | 0.9053 | 0.6039 | 0.9610 | 0.9574 | 0.8952 | 0.7444 |
| $T_z$ | 0.9053 | 1.0000 | 0.4656 | 0.8524 | 0.9565 | 0.9693 | 0.9121 |
| $T_p$ | 0.6039 | 0.4656 | 1.0000 | 0.6888 | 0.5474 | 0.4627 | 0.3394 |
| $T_{-1}$ | 0.9610 | 0.8524 | 0.6888 | 1.0000 | 0.9410 | 0.8607 | 0.6962 |
| $T_1$ | 0.9574 | 0.9565 | 0.5474 | 0.9410 | 1.0000 | 0.9788 | 0.8725 |
| $T_2$ | 0.8952 | 0.9693 | 0.4627 | 0.8607 | 0.9788 | 1.0000 | 0.9499 |
| $T_4$ | 0.7444 | 0.9121 | 0.3394 | 0.6962 | 0.8725 | 0.9499 | 1.0000 |

Table 23: Wave period correlation coefficients - Cape Grim

| | $T_{\frac{1}{3}}$ | $T_z$ | $T_p$ | $T_{-1}$ | $T_1$ | $T_2$ | $T_4$ |
|---|---|---|---|---|---|---|---|
| $T_{\frac{1}{3}}$ | 1.0000 | 0.8950 | 0.5155 | 0.8764 | 0.8780 | 0.7930 | 0.5935 |
| $T_z$ | 0.8950 | 1.0000 | 0.3768 | 0.7732 | 0.9257 | 0.9391 | 0.8457 |
| $T_p$ | 0.5155 | 0.3768 | 1.0000 | 0.6884 | 0.4811 | 0.3587 | 0.1898 |
| $T_{-1}$ | 0.8764 | 0.7732 | 0.6884 | 1.0000 | 0.9024 | 0.7743 | 0.5352 |
| $T_1$ | 0.8780 | 0.9257 | 0.4811 | 0.9024 | 1.0000 | 0.9655 | 0.8074 |
| $T_2$ | 0.7930 | 0.9391 | 0.3587 | 0.7743 | 0.9655 | 1.0000 | 0.9269 |
| $T_4$ | 0.5935 | 0.8457 | 0.1898 | 0.5352 | 0.8074 | 0.9269 | 1.0000 |

Table 24: Wave period correlation coefficients - Storm Bay

| | $T_{\frac{1}{3}}$ | $T_z$ | $T_p$ | $T_{-1}$ | $T_1$ | $T_2$ | $T_4$ |
|---|---|---|---|---|---|---|---|
| $T_{\frac{1}{3}}$ | 1.000 | 0.758 | 0.922 | 0.829 | 0.823 | 0.729 | 0.429 |
| $T_z$ | 1.038 | 1.000 | 0.785 | 0.839 | 0.961 | 0.930 | 0.628 |
| $T_p$ | 0.418 | 0.260 | 1.000 | 0.412 | 0.323 | 0.254 | 0.130 |
| $T_{-1}$ | 1.096 | 0.809 | 1.202 | 1.000 | 0.931 | 0.801 | 0.455 |
| $T_1$ | 1.093 | 0.931 | 0.946 | 0.935 | 1.000 | 0.927 | 0.587 |
| $T_2$ | 1.074 | 1.000 | 0.827 | 0.893 | 1.029 | 1.000 | 0.679 |
| $T_4$ | 1.201 | 1.284 | 0.804 | 0.964 | 1.238 | 1.291 | 1.000 |

Table 25: Wave period regression coefficients - Cape Sorell (50m)

| | $T_{\frac{1}{3}}$ | $T_z$ | $T_p$ | $T_{-1}$ | $T_1$ | $T_2$ | $T_4$ |
|---|---|---|---|---|---|---|---|
| $T_{\frac{1}{3}}$ | 1.000 | 0.749 | 0.866 | 0.841 | 0.817 | 0.710 | 0.394 |
| $T_z$ | 1.070 | 1.000 | 0.773 | 0.888 | 0.974 | 0.916 | 0.578 |
| $T_p$ | 0.466 | 0.292 | 1.000 | 0.452 | 0.357 | 0.280 | 0.135 |
| $T_{-1}$ | 1.107 | 0.820 | 1.106 | 1.000 | 0.931 | 0.796 | 0.431 |
| $T_1$ | 1.113 | 0.929 | 0.905 | 0.963 | 1.000 | 0.908 | 0.542 |
| $T_2$ | 1.125 | 1.017 | 0.825 | 0.957 | 1.057 | 1.000 | 0.638 |
| $T_4$ | 1.351 | 1.391 | 0.861 | 1.125 | 1.367 | 1.381 | 1.000 |

Table 26: Wave period regression coefficients - Cape Sorell (100m)

| | $T_{\frac{1}{3}}$ | $T_z$ | $T_p$ | $T_{-1}$ | $T_1$ | $T_2$ | $T_4$ |
|---|---|---|---|---|---|---|---|
| $T_{\frac{1}{3}}$ | 1.000 | 0.704 | 0.764 | 0.802 | 0.791 | 0.678 | 0.371 |
| $T_z$ | 1.163 | 1.000 | 0.757 | 0.914 | 1.016 | 0.944 | 0.584 |
| $T_p$ | 0.476 | 0.286 | 1.000 | 0.454 | 0.357 | 0.277 | 0.133 |
| $T_{-1}$ | 1.151 | 0.794 | 1.044 | 1.000 | 0.932 | 0.781 | 0.416 |
| $T_1$ | 1.157 | 0.899 | 0.838 | 0.949 | 1.000 | 0.897 | 0.526 |
| $T_2$ | 1.181 | 0.994 | 0.773 | 0.947 | 1.067 | 1.000 | 0.625 |
| $T_4$ | 1.492 | 1.422 | 0.861 | 1.165 | 1.446 | 1.443 | 1.000 |

Table 27: Wave period regression coefficients - Cape Grim

| | $T_{\frac{1}{3}}$ | $T_z$ | $T_p$ | $T_{-1}$ | $T_1$ | $T_2$ | $T_4$ |
|---|---|---|---|---|---|---|---|
| $T_{\frac{1}{3}}$ | 1.000 | 0.580 | 0.667 | 0.701 | 0.646 | 0.494 | 0.219 |
| $T_z$ | 1.380 | 1.000 | 0.752 | 0.954 | 1.051 | 0.902 | 0.482 |
| $T_p$ | 0.398 | 0.188 | 1.000 | 0.425 | 0.273 | 0.172 | 0.054 |
| $T_{-1}$ | 1.095 | 0.626 | 1.113 | 1.000 | 0.830 | 0.603 | 0.247 |
| $T_1$ | 1.192 | 0.815 | 0.846 | 0.980 | 1.000 | 0.817 | 0.405 |
| $T_2$ | 1.272 | 0.977 | 0.745 | 0.994 | 1.140 | 1.000 | 0.550 |
| $T_4$ | 1.604 | 1.482 | 0.664 | 1.157 | 1.606 | 1.561 | 1.000 |

Table 28: Wave period regression coefficients - Storm Bay

| | $H_{mu}$ | $H_{md}$ | $a_{cmax}$ | $a_{tmax}$ | $H_\sigma$ | $H_m$ | $H_{\frac{1}{3}}$ |
|---|---|---|---|---|---|---|---|
| $H_{mu}$ | 1.0000 | 0.9712 | 0.9718 | 0.9719 | 0.9677 | 0.9676 | 0.9662 |
| $H_{md}$ | 0.9712 | 1.0000 | 0.9678 | 0.9693 | 0.9698 | 0.9697 | 0.9686 |
| $a_{cmax}$ | 0.9718 | 0.9678 | 1.0000 | 0.9392 | 0.9637 | 0.9624 | 0.9604 |
| $a_{tmax}$ | 0.9719 | 0.9693 | 0.9392 | 1.0000 | 0.9620 | 0.9597 | 0.9579 |
| $H_\sigma$ | 0.9677 | 0.9698 | 0.9637 | 0.9620 | 1.0000 | 0.9984 | 0.9973 |
| $H_m$ | 0.9676 | 0.9697 | 0.9624 | 0.9597 | 0.9984 | 1.0000 | 0.9977 |
| $H_{\frac{1}{3}}$ | 0.9662 | 0.9686 | 0.9604 | 0.9579 | 0.9973 | 0.9977 | 1.0000 |

Table 29: Wave height correlation coefficients - all data

| | $H_{mu}$ | $H_{md}$ | $a_{cmax}$ | $a_{tmax}$ | $H_\sigma$ | $H_m$ | $H_{\frac{1}{3}}$ |
|---|---|---|---|---|---|---|---|
| $H_{mu}$ | 1.000 | 0.940 | 0.507 | 0.532 | 0.636 | 0.618 | 0.608 |
| $H_{md}$ | 1.002 | 1.000 | 0.521 | 0.548 | 0.658 | 0.640 | 0.629 |
| $a_{cmax}$ | 1.860 | 1.794 | 1.000 | 0.984 | 1.213 | 1.178 | 1.157 |
| $a_{tmax}$ | 1.775 | 1.714 | 0.895 | 1.000 | 1.155 | 1.120 | 1.101 |
| $H_\sigma$ | 1.471 | 1.428 | 0.765 | 0.801 | 1.000 | 0.970 | 0.954 |
| $H_m$ | 1.513 | 1.469 | 0.786 | 0.822 | 1.027 | 1.000 | 0.982 |
| $H_{\frac{1}{3}}$ | 1.534 | 1.490 | 0.796 | 0.833 | 1.041 | 1.013 | 1.000 |

Table 30: Wave height regression coefficients - all data

| | $T_{\frac{1}{3}}$ | $T_z$ | $T_p$ | $T_{-1}$ | $T_1$ | $T_2$ | $T_4$ |
|---|---|---|---|---|---|---|---|
| $T_{\frac{1}{3}}$ | 1.0000 | 0.8917 | 0.5946 | 0.9445 | 0.9350 | 0.8669 | 0.7054 |
| $T_z$ | 0.8917 | 1.0000 | 0.4339 | 0.8333 | 0.9514 | 0.9652 | 0.8997 |
| $T_p$ | 0.5946 | 0.4339 | 1.0000 | 0.6941 | 0.5274 | 0.4287 | 0.2895 |
| $T_{-1}$ | 0.9444 | 0.8333 | 0.6941 | 1.0000 | 0.9311 | 0.8420 | 0.6636 |
| $T_1$ | 0.9350 | 0.9514 | 0.5274 | 0.9311 | 1.0000 | 0.9771 | 0.8614 |
| $T_2$ | 0.8669 | 0.9652 | 0.4287 | 0.8420 | 0.9771 | 1.0000 | 0.9443 |
| $T_4$ | 0.7054 | 0.8997 | 0.2895 | 0.6636 | 0.8614 | 0.9443 | 1.0000 |

Table 31: Wave period correlation coefficients - all data

| | $T_{\frac{1}{3}}$ | $T_z$ | $T_p$ | $T_{-1}$ | $T_1$ | $T_2$ | $T_4$ |
|---|---|---|---|---|---|---|---|
| $T_{\frac{1}{3}}$ | 1.000 | 0.734 | 0.787 | 0.799 | 0.797 | 0.694 | 0.394 |
| $T_z$ | 1.082 | 1.000 | 0.698 | 0.857 | 0.985 | 0.938 | 0.610 |
| $T_p$ | 0.448 | 0.269 | 1.000 | 0.443 | 0.339 | 0.259 | 0.122 |
| $T_{-1}$ | 1.115 | 0.810 | 1.085 | 1.000 | 0.938 | 0.796 | 0.437 |
| $T_1$ | 1.095 | 0.918 | 0.818 | 0.924 | 1.000 | 0.917 | 0.564 |
| $T_2$ | 1.082 | 0.992 | 0.709 | 0.890 | 1.041 | 1.000 | 0.658 |
| $T_4$ | 1.262 | 1.326 | 0.686 | 1.006 | 1.315 | 1.353 | 1.000 |

Table 32: Wave period regression coefficients - all data

## 3.4 Relationships between sites

During the course of these observations there were two intervals when buoys were deployed at two different locations. These were from 11/7/85 to 18/11/85 when buoys were deployed at Cape Sorell at the 50m depth and 100m depth contours, and from 28/3/91 to 20/4/92 when buoys were (intermittently) deployed off Cape Grim and off Cape Sorell (100m). There were two subsets of data from which information about sea states occuring simultaneously at different locations could be obtained. There were 1064 good simultaneous data bursts in the first set and 793 in the second. The buoys were separated by distances of 10 Km and 150 Km respectively.

In the first case the data bursts were saved by the same onshore receiver system. Bursts lasting 400 seconds were saved from the inshore buoy first then from the offshore buoy twenty minutes later so that the bursts were not strictly simultaneous. In the second case separate shore bases recorded 800 second bursts simultaneously within the accuracy of the computer clocks (about a minute or so).

The regression statistics for the Cape Sorell 50m/100m pair are shown in Table 33 for the twenty-four burst statistics listed in Table 7. The regression statistics for the Cape Grim - Cape Sorell pair are listed in Table 34. The statistics listed in the columns are the sample means of the x and y values, $\bar{x}$, $\bar{y}$, the sample correlation coefficient $\hat{\rho}$, the two regression coefficients, $\hat{\beta}_{yx}$ and $\hat{\beta}_{xy}$ and the slope of the principal component axis or "line of best fit" , $m$. In each case the value from the Cape Sorell buoy at the 100m contour was taken as the $x$ value.

Some of the highest correlations in Tables 33 and 34 are between the various spectral moments. The corresponding behaviour of the slope, $m$, suggests that it might be worth examining the spectra in more detail. For example, consider the relationship between $V_{18}$ measured at Cape Grim and at Cape Sorell. The quantity $V_{18}$ is defined as the variance in the frequency range 0.16 Hz to 0.18 Hz as defined by (4) above. A scatter diagram is shown in Figure 38 showing the two regression lines (dashed) and the line-of-best-fit.

| | $\bar{x}$ | $\bar{y}$ | $\hat{\rho}$ | $\hat{\beta}_{yx}$ | $\hat{\beta}_{xy}$ | $m$ |
|---|---|---|---|---|---|---|
| $H_{mu}$ | 4.1056 | 3.5582 | 0.8327 | 0.7225 | 0.9598 | 0.8434 |
| $H_{md}$ | 4.0478 | 3.5198 | 0.8320 | 0.7188 | 0.9629 | 0.8391 |
| $H_\sigma$ | 3.0394 | 2.6134 | 0.9199 | 0.8375 | 1.0103 | 0.9031 |
| $H_m$ | 2.8889 | 2.5237 | 0.9169 | 0.8192 | 1.0264 | 0.8843 |
| $a_{cmax}$ | 2.2136 | 1.9051 | 0.8227 | 0.7134 | 0.9489 | 0.8410 |
| $a_{tmax}$ | 2.2592 | 1.9361 | 0.8230 | 0.7235 | 0.9363 | 0.8552 |
| $H_{\frac{1}{3}}$ | 2.8240 | 2.4576 | 0.9005 | 0.8087 | 1.0026 | 0.8875 |
| $T_{\frac{1}{3}}$ | 10.8978 | 10.5423 | 0.7668 | 0.7786 | 0.7552 | 1.0201 |
| $T_z$ | 8.2617 | 7.8895 | 0.7387 | 0.7510 | 0.7267 | 1.0225 |
| $T_c$ | 4.4204 | 4.2099 | 0.7933 | 0.8707 | 0.7228 | 1.1244 |
| $T_p$ | 12.6127 | 12.5217 | 0.4905 | 0.5186 | 0.4640 | 1.1197 |
| $T_{-1}$ | 10.4850 | 10.3397 | 0.8600 | 0.8994 | 0.8224 | 1.0534 |
| $T_1$ | 8.9558 | 8.7951 | 0.8466 | 0.8786 | 0.8157 | 1.0448 |
| $T_2$ | 7.9200 | 7.7495 | 0.8499 | 0.8882 | 0.8132 | 1.0532 |
| $T_4$ | 5.8449 | 5.6828 | 0.8571 | 0.9336 | 0.7869 | 1.1048 |
| $m_{-1}$ | 6.3309 | 4.7827 | 0.9050 | 0.7139 | 1.1473 | 0.7698 |
| $m_0$ | 0.5893 | 0.4521 | 0.9156 | 0.7228 | 1.1598 | 0.7728 |
| $m_1$ | 0.0646 | 0.0507 | 0.9273 | 0.7433 | 1.1568 | 0.7881 |
| $m_2$ | 0.0091 | 0.0074 | 0.9360 | 0.7801 | 1.1230 | 0.8232 |
| $m_4$ | 0.0004 | 0.0004 | 0.9272 | 0.8956 | 0.9600 | 0.9632 |
| $\epsilon$ | 0.8324 | 0.8362 | 0.7548 | 0.8444 | 0.6747 | 1.1599 |
| $P$ | 50.0451 | 37.8069 | 0.9050 | 0.7139 | 1.1473 | 0.7698 |
| $H_{sw}$ | 2.1960 | 1.8686 | 0.8719 | 0.7682 | 0.9896 | 0.8649 |
| $H_{ws}$ | 0.7750 | 0.6918 | 0.9116 | 0.8989 | 0.9246 | 0.9846 |

Table 33: Regression of Cape Sorell (50m) on Cape Sorell (100m) - burst statistics

| | $\bar{x}$ | $\bar{y}$ | $\hat{\rho}$ | $\hat{\beta}_{yx}$ | $\hat{\beta}_{xy}$ | $m$ |
|---|---|---|---|---|---|---|
| $H_{mu}$ | 4.7174 | 4.5557 | 0.8511 | 0.9078 | 0.7978 | 1.0788 |
| $H_{md}$ | 4.6393 | 4.4836 | 0.8487 | 0.8688 | 0.8290 | 1.0279 |
| $H_{\sigma}$ | 3.2128 | 3.0785 | 0.9241 | 0.9681 | 0.8821 | 1.0516 |
| $H_m$ | 3.0890 | 2.9695 | 0.9207 | 0.9773 | 0.8674 | 1.0669 |
| $a_{cmax}$ | 2.5145 | 2.4317 | 0.8344 | 0.8631 | 0.8067 | 1.0413 |
| $a_{tmax}$ | 2.5634 | 2.4838 | 0.8441 | 0.8716 | 0.8174 | 1.0388 |
| $H_{\frac{1}{3}}$ | 3.0205 | 2.8766 | 0.9161 | 0.9631 | 0.8714 | 1.0561 |
| $T_{\frac{1}{3}}$ | 10.7628 | 10.3739 | 0.7493 | 0.8375 | 0.6704 | 1.1598 |
| $T_z$ | 8.1990 | 7.6484 | 0.6188 | 0.6316 | 0.6062 | 1.0337 |
| $T_c$ | 4.5620 | 4.1842 | 0.5080 | 0.4900 | 0.5267 | 0.9314 |
| $T_p$ | 12.4701 | 12.4746 | 0.5670 | 0.6159 | 0.5219 | 1.1568 |
| $T_{-1}$ | 10.4963 | 10.2387 | 0.8272 | 0.8846 | 0.7735 | 1.0844 |
| $T_1$ | 9.0718 | 8.6088 | 0.7206 | 0.7644 | 0.6793 | 1.0852 |
| $T_2$ | 8.0789 | 7.5512 | 0.6646 | 0.6969 | 0.6338 | 1.0739 |
| $T_4$ | 5.9961 | 5.5670 | 0.5985 | 0.6066 | 0.5905 | 1.0226 |
| $m_{-1}$ | 7.1003 | 6.6090 | 0.8941 | 0.9519 | 0.8399 | 1.0725 |
| $m_0$ | 0.6627 | 0.6258 | 0.9005 | 0.9610 | 0.8438 | 1.0748 |
| $m_1$ | 0.0720 | 0.0704 | 0.9088 | 0.9735 | 0.8483 | 1.0786 |
| $m_2$ | 0.0099 | 0.0103 | 0.8997 | 0.9529 | 0.8496 | 1.0658 |
| $m_4$ | 0.0005 | 0.0005 | 0.7411 | 0.7217 | 0.7611 | 0.9648 |
| $\epsilon$ | 0.8280 | 0.8311 | 0.5691 | 0.6416 | 0.5049 | 1.2330 |
| $P$ | 56.1268 | 52.2433 | 0.8941 | 0.9519 | 0.8399 | 1.0725 |
| $H_{sw}$ | 2.3642 | 2.2218 | 0.8913 | 0.9212 | 0.8624 | 1.0376 |
| $H_{ws}$ | 0.7971 | 0.8666 | 0.6776 | 0.6451 | 0.7117 | 0.9301 |

Table 34: Regression of Cape Grim on Cape Sorell (100m) - burst statistics

| | $\bar{x}$ | $\bar{y}$ | $\hat{\rho}$ | $\hat{\beta}_{yx}$ | $\hat{\beta}_{xy}$ | $m$ |
|---|---|---|---|---|---|---|
| $V_{04}$ | 0.0455 | 0.0964 | -0.4289 | -0.7902 | -0.2328 | -3.3293 |
| $V_{05}$ | 0.0015 | 0.0008 | 0.5926 | 0.5347 | 0.6568 | 0.8411 |
| $V_{06}$ | 0.0141 | 0.0111 | 0.8210 | 0.7593 | 0.8876 | 0.9094 |
| $V_{07}$ | 0.0717 | 0.0536 | 0.7716 | 0.6203 | 0.9599 | 0.7546 |
| $V_{08}$ | 0.1054 | 0.0772 | 0.6632 | 0.4954 | 0.8877 | 0.6490 |
| $V_{10}$ | 0.1610 | 0.1162 | 0.7511 | 0.5413 | 1.0421 | 0.6502 |
| $V_{12}$ | 0.0834 | 0.0665 | 0.7611 | 0.5993 | 0.9665 | 0.7320 |
| $V_{14}$ | 0.0459 | 0.0397 | 0.7349 | 0.7063 | 0.7647 | 0.9474 |
| $V_{16}$ | 0.0302 | 0.0249 | 0.7142 | 0.5547 | 0.9195 | 0.7044 |
| $V_{18}$ | 0.0199 | 0.0162 | 0.6933 | 0.5708 | 0.8420 | 0.7569 |
| $V_{20}$ | 0.0136 | 0.0111 | 0.7317 | 0.5869 | 0.9122 | 0.7413 |
| $V_{25}$ | 0.0121 | 0.0097 | 0.7295 | 0.6222 | 0.8552 | 0.8047 |
| $V_{30}$ | 0.0183 | 0.0145 | 0.8218 | 0.7269 | 0.9291 | 0.8614 |
| $V_{40}$ | 0.0081 | 0.0067 | 0.8029 | 0.7842 | 0.8219 | 0.9711 |
| $V_{50}$ | 0.0025 | 0.0023 | 0.7879 | 0.8546 | 0.7263 | 1.1086 |
| $V_{60}$ | 0.0007 | 0.0008 | 0.7107 | 0.9186 | 0.5498 | 1.4297 |

Table 35: Regression of Cape Sorell (50m) on Cape Sorell (100m) - frequency band variances

| | $\bar{x}$ | $\bar{y}$ | $\hat{\rho}$ | $\hat{\beta}_{yx}$ | $\hat{\beta}_{xy}$ | $m$ |
|---|---|---|---|---|---|---|
| $V_{04}$ | 0.0096 | 0.0029 | 0.1446 | 0.0344 | 0.6072 | 0.0364 |
| $V_{05}$ | 0.0010 | 0.0010 | 0.5672 | 0.4265 | 0.7542 | 0.6129 |
| $V_{06}$ | 0.0152 | 0.0182 | 0.8445 | 1.0951 | 0.6513 | 1.3582 |
| $V_{07}$ | 0.0710 | 0.0653 | 0.7981 | 0.7155 | 0.8902 | 0.8722 |
| $V_{08}$ | 0.1202 | 0.1090 | 0.7400 | 0.7310 | 0.7490 | 0.9837 |
| $V_{10}$ | 0.1931 | 0.1697 | 0.7520 | 0.7211 | 0.7842 | 0.9458 |
| $V_{12}$ | 0.0970 | 0.0890 | 0.7647 | 0.8954 | 0.6531 | 1.2283 |
| $V_{14}$ | 0.0530 | 0.0516 | 0.7744 | 0.9547 | 0.6282 | 1.3085 |
| $V_{16}$ | 0.0318 | 0.0327 | 0.7545 | 0.9125 | 0.6238 | 1.2851 |
| $V_{18}$ | 0.0208 | 0.0222 | 0.7405 | 0.8946 | 0.6130 | 1.2891 |
| $V_{20}$ | 0.0147 | 0.0156 | 0.6758 | 0.7715 | 0.5919 | 1.2157 |
| $V_{25}$ | 0.0130 | 0.0141 | 0.6414 | 0.7024 | 0.5857 | 1.1517 |
| $V_{30}$ | 0.0195 | 0.0229 | 0.5703 | 0.6261 | 0.5194 | 1.1772 |
| $V_{40}$ | 0.0082 | 0.0097 | 0.5419 | 0.5223 | 0.5623 | 0.9342 |
| $V_{50}$ | 0.0026 | 0.0031 | 0.5105 | 0.4659 | 0.5592 | 0.8368 |
| $V_{60}$ | 0.0007 | 0.0009 | 0.3846 | 0.3690 | 0.4008 | 0.8982 |

Table 36: Regression of Cape Grim on Cape Sorell (100m) - frequency band variances

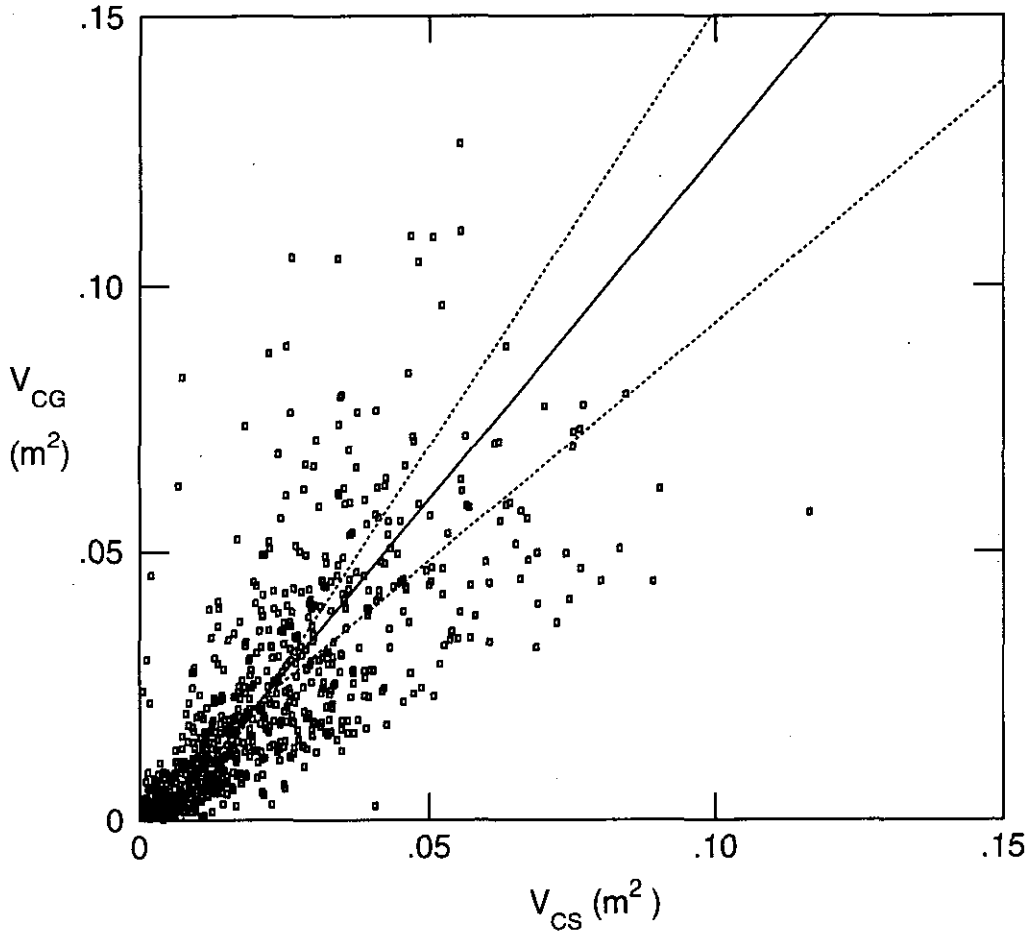


Figure 38: Scatter diagram showing the correlation between the variance in the frequency band 0.16 Hz $< f <$ 0.18 Hz, at Cape Grim, $V_{CG}$ and that at Cape Sorell, $V_{CS}$. The dashed lines are the two regression lines and the solid line is the principle axis of the ellipse of concentration of the distribution. There were 793 points in the sample.

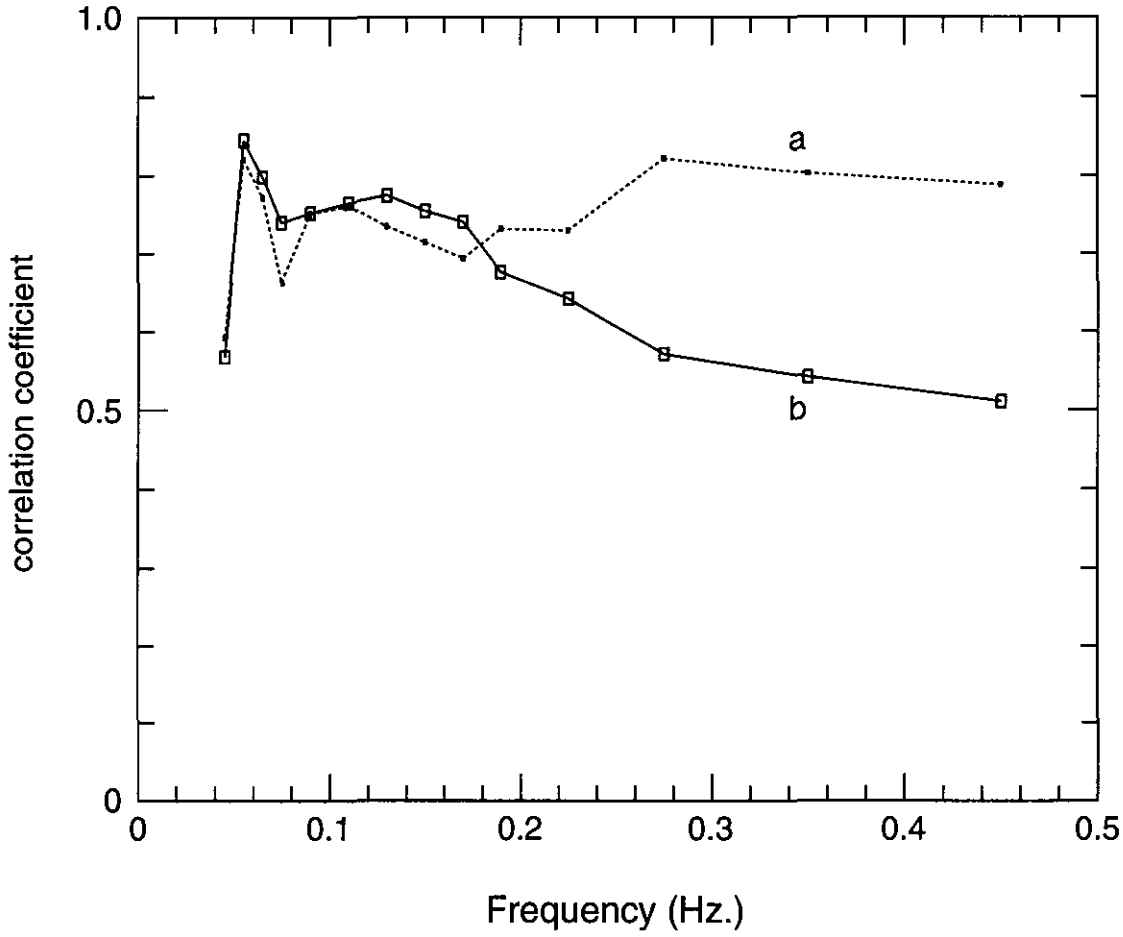


Figure 39: Correlation between frequency band variances. Correlation coefficient vs frequency - (a) Cape Sorell (50m) vs Cape Sorell (100m), (b) Cape Grim vs Cape Sorell (100m).

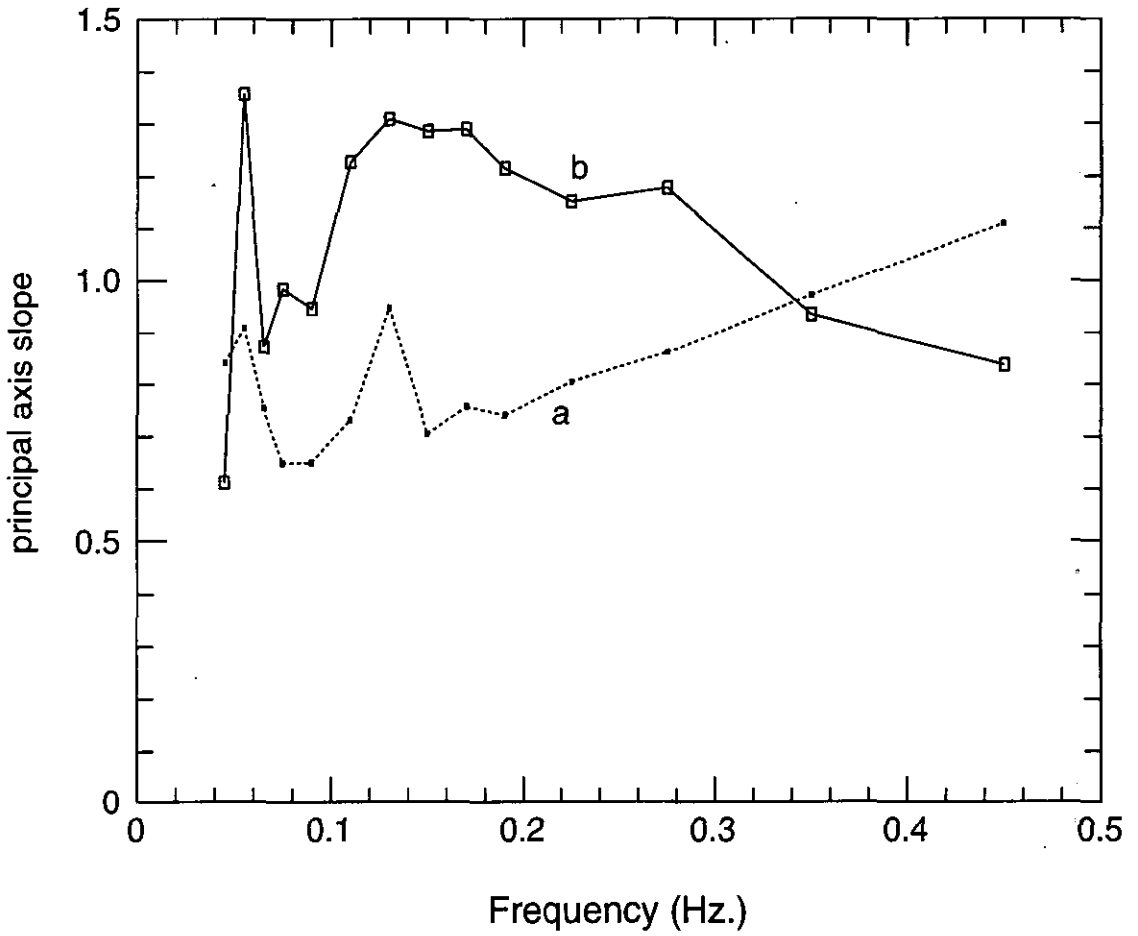


Figure 40: Correlation between frequency band variances. Slope of principal axes of joint distributions vs frequency - (a) Cape Sorell (50m) vs Cape Sorell (100m), (b) Cape Grim vs Cape Sorell (100m).

The correlation coefficients for fourteen such frequency band variances are shown plotted as a function of the centre frequency in Figure 39 and the corresponding line-of-best-fit slopes are shown in Figure 40. The regression statistics for the frequency band variances are also listed in Tables 35 and 36.

Figures 39 and 40 show some interesting features. The correlations for both pairs of sites are fairly high and quite similar in the range 0.05 Hz to .2 Hz but at higher frequencies the correlation falls off for the Cape Grim - Cape Sorell pair. No doubt this fall off is due to differences in local wind velocity between the distant sites which do not occur for sites only 10 Km apart. The close resemblance of the two curves at lower frequencies suggests that the lack of perfect correlation is due only to the inherent noisiness of the burst statistics rather than any physical process involving the swell. The sudden drop in correlation for the range 0.04 Hz to 0.05 Hz ($V_{05}$) is most likely due to the twisted suspension problem discussed earlier.

The principal axis (line-of-best-fit) slope in Figure 40 indicate that the inshore buoy of the 50m - 100m pair experienced significantly less wave energy than the outer buoy in the low frequency range. On the other hand the Cape Grim buoy experienced more energetic wave action than the 100m Cape Sorell buoy in the mid-range of frequencies from 0.1 to 0.3 Hz.

It is tempting to explain the lower variances of the inshore buoy at Cape Sorell in terms of bottom friction acting on the longer wavelengths but other factors may be at work. The two curves in Figure 40 show a strong similarity in the range 0.05 to 0.12 Hz. There are two peaks at .055 and 0.13 Hz in both cases and the intervening troughs both have a minimum near .07 Hz. The resemblance is more remarkable when it is considered that the data sets do not overlap in time and were gathered several years apart. A possible explanation is that the swells coming predominantly from one direction, the south west, are refracted by features in the bottom topography as they cross the continental shelf. Such refraction would be a function of velocity and would therefore be frequency dependent. At some frequencies focussing would occur causing an average increase in energy density over a small range of frequencies at one particular location. A buoy located at a focus would experience a higher average wave energy over a small range of frequencies. and other buoys outside the focus would show a comparitive energy deficit over the same range of frequencies.

Therefore a possible explanation of the resemblence of the two curves in Figure 40 is that the 100m Cape Sorell buoy lay at a focus for swells coming from the predominant swell direction with frequencies near 0.08 Hz leading to an apparent trough at this frequency when the other two buoys were compared with it. Possibly the other buoys also experienced this focussing effect, for example near 0.13 Hz in the case of the Cape Sorell (50m) buoy.

## 3.5 Efficiency of sample statistics

The correlations of frequency band variances recorded at the inner and outer Cape Sorell sites, curve "a" in Figure 39 are almost independent of frequency. The various burst statistics listed in Table 7 are all in some way dependent on spectral shape and might be expected to exhibit similar correlations to the frequency band variances and to one another. Examination of the values of the correlation coefficients listed in Table 33 reveals that this is not the case; they range from 0.4905 to 0.9360 whereas the frequency band variances listed in Table 35 have correlations ranging from 0.6632 to 0.8218.

In this analysis there are two scales of statistics. The statistics defined above and listed in Table 7 are sample statistics and can be regarded as estimators of population parameters describing the sea state which is assumed constant for the duration of each burst. In examining the distributions of burst statistics in Section 3.2 and their regression relationships in Section 3.3.2 and Section 3.4 an underlying assumption has been made that these population parameters are not constant and can be regarded as random variables on a longer time scale.

Hence the variability of a burst statistic such as the fourth spectral moment, $m_4$, has two components, the variability of the population parameter in the long term and the variability associated with estimating the parameter from a given burst. For some statistics the second variability can be estimated theoretically; for example $m_4$ is distributed as a $\chi^2$ variable with approximately 2048 degrees of freedom and its variance is known but in general this is not the case.

The high and almost constant correlations of frequency band variances in Figure 39 (a) indicate that the long term variability of sea state is statistically similar at the two Cape Sorell sites. Hence the observed variations in the correlation coefficient among the burst statistics must be attributed to the second form of variability. The correlation coefficients listed in Table 33 amount to "figures of merit" for the various statistics, that is they indicate how well a sample statistic estimates the underlying population value.

As an example consider the correlation coefficients listed in Table 33 for $H_{sw}$ and $H_{ws}$. These are higher than the correlations listed in Table 35 for any of the frequency band variances and less than the values for $H_\sigma$ and $H_m$. This is as expected. The variance of a statistical estimator depends inversely on the number of degrees of freedom it has. Hence those estimators which incorporate more of the spectrum have smaller variances and higher correlation coefficients in Tables 33 and 35.

These results indicate that the spectral peak period, $T_p$, with a correlation coefficient of only 0.4905 is a poor statistic compared to the other wave periods.

## 3.6 Seasonal variation of sample statistics

Monthly means of significant wave height, mean zero crossing period and spectral peak period are shown for each site in Figures 41, 42 and 43. The overall average for each month is plotted as a heavy black line. Only in the case of the Cape Sorell (100m) site can any meaningful conclusions be drawn. Data were not collected for sufficient time at the other sites to be useful but results are shown for completeness.

It can be seen from the Cape Sorell (100m) average that the average seasonal dependence for this site is quite small in all three cases. Only the significant wave height shows much variation being slightly larger at 3.4 metres from July to October than in the summer and autumn months when it averages 2.9 metres.

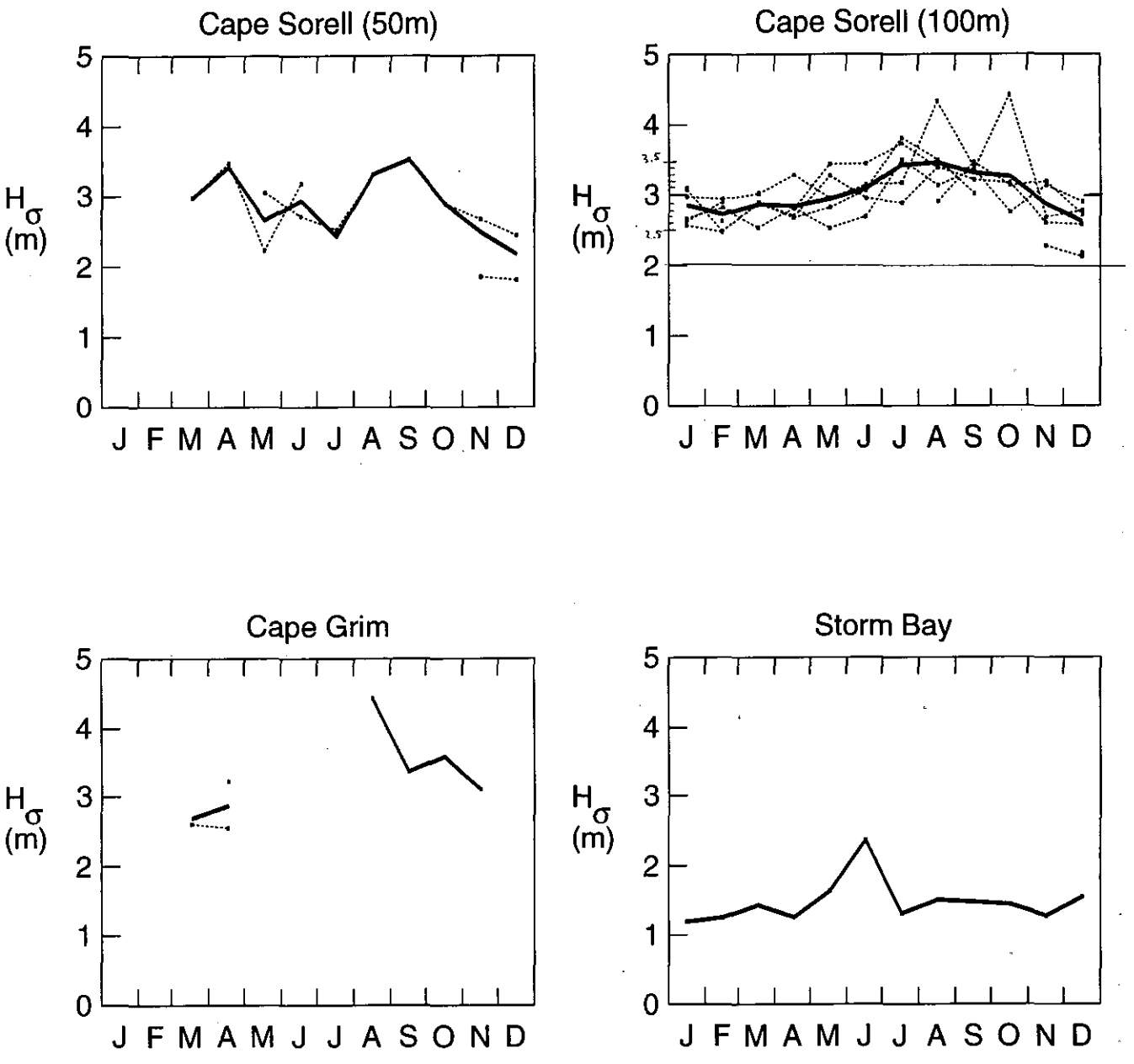


Figure 41: Monthly means of Significant Wave Height.

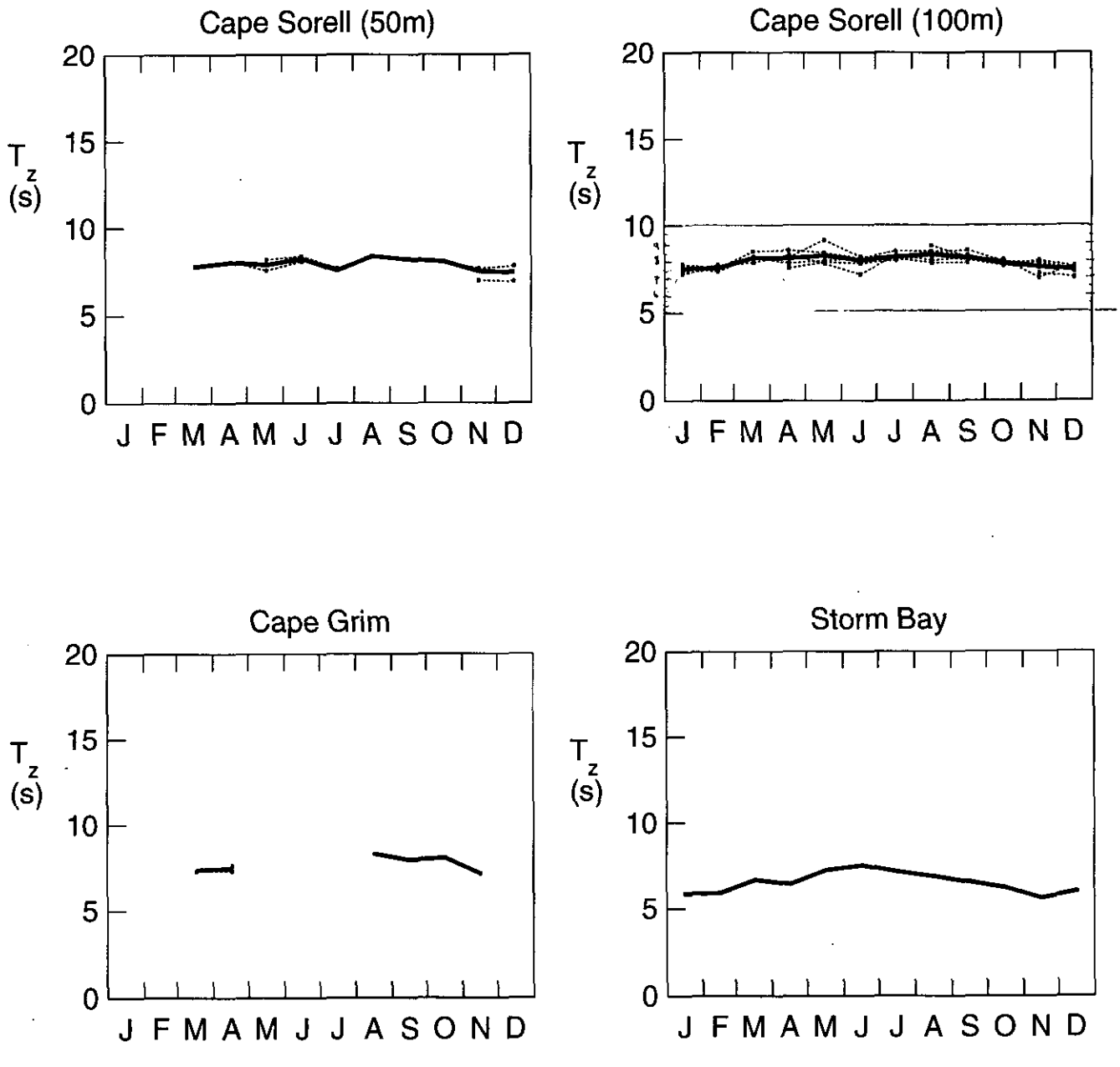


Figure 42: Monthly means of Mean Zero Crossing Period.

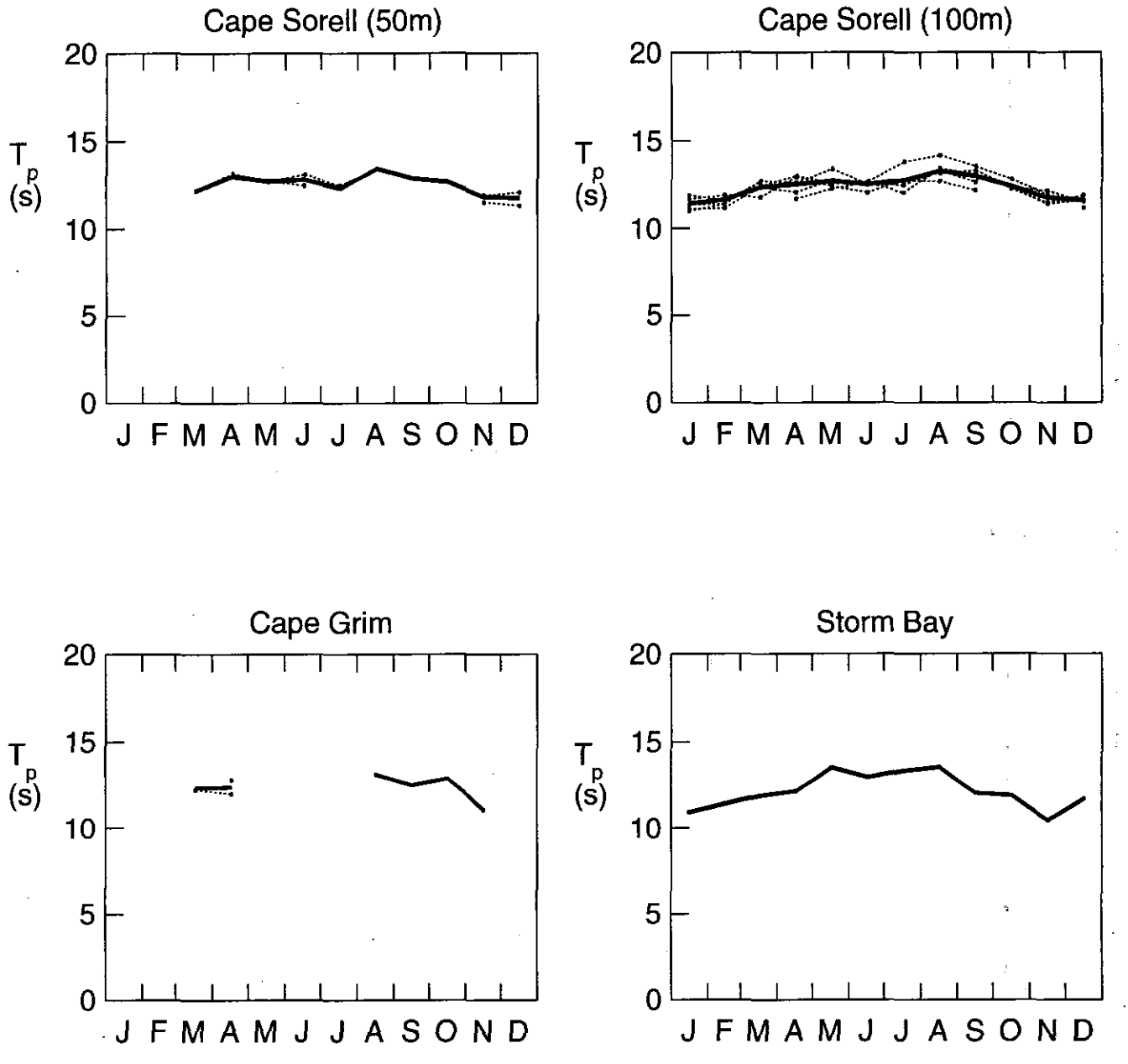


Figure 43: Monthly means of Spectral Peak Period.

# 4 Relationship between waves and wind velocity

## 4.1 Winds

At Granville Harbour, 30 Km to the north of the wave measurement site, wind speed and direction were routinely logged. The wind measurement site is 1 km inland and 40 m above mean sea level. Wind measurements from 10 m altitude at this site in the form of hourly records of 10 minute vector averaged speed, U and direction, $\phi$, were saved for comparison with the wave measurements for the period 18 November 1985 to 24 September 1992.

The coast and continental shelf are roughly parallel with azimuth 343° . In order to avoid coastal effects and to ensure that the wind was unambiguously either onshore or offshore the spectra chosen for study were confined to those for which the wind vector azimuth, $\phi$, lay within 45° of the normal to the coast in one of the ranges

$$\begin{aligned} 28^o &< \phi < 118^o \quad \text{(onshore set)} \\ 208^o &< \phi < 298^o \quad \text{(offshore set)} \end{aligned}$$

There were 1896 spectra in the onshore set and 2742 in the offshore set.

A wind-sea takes a finite time to become "developed". For this reason the data were further restricted to "persistent" winds i.e. those for which:

(i) valid wind data was available for the given time and for 3 hours and 6 hours previously,

(ii) the wind was consistently either onshore or offshore for the three 3-hourly periods according to the above definitions, and

(iii) the wind speed differed by no more than 2 m/s from that measured 3 hours and 6 hours previously.

## 4.2 Relationship between wind speed and wave statistics

The correlations holding between wind speed and various wave sample statistics are shown in Table 37. Correlation coefficients were computed for

| | onshore | | offshore | |
|---|---|---|---|---|
| statistic | inst. | pers. | inst. | pers. |
| $H_\sigma$ | 0.579 | 0.610 | -0.170 | -0.229 |
| $T_z$ | -0.157 | -0.043 | -0.567 | -0.664 |
| $H_\sigma/T_z^2$ | 0.819 | 0.809 | 0.567 | 0.686 |
| $m_4$ | 0.883 | 0.900 | 0.603 | 0.692 |
| number | 1094 | 713 | 2744 | 1020 |

Table 37: Correlation coefficients calculated for wind speed vs. various sample statistics for "instantaneous" and "persistent" winds

four cases, viz: onshore instantaneous winds, onshore persistent winds, offshore instantaneous winds and offshore persistent winds. By "instantaneous" is meant the ten minute vector averaged mean wind at the time of the wave sample.

In Table 37 the quantity $H_\sigma/T_z^2$ is a mean vertical acceleration or mean steepness for the sample (since wavelength is proportional to the square of the period). The quantity $m_4$ is the fourth moment of the displacement spectrum defined by

$$m_4 = \int_0^\infty S(f) f^4 df \tag{20}$$

From (30)

$$m_4 = (2\pi)^{-4} \int_0^\infty S_a(f) df \tag{21}$$

that is, $m_4$ is proportional to the area enclosed by the acceleration spectrum.

In practice wave buoys do not respond to displacements and accelerations much above 0.5 Hz while accelerations at frequencies much greater than this contribute to the integral in (21). Consequently the statistic $m_4$ is defined in practice by (6).

The correlation coefficients listed in Table 37 show that commonly used time domain statistics, $H_\sigma$ and $T_z$ are not well correlated with wind speed. In fact $H_\sigma$ shows a slight negative correlation with offshore winds as a consequence of the erosion of the swell peak mentioned earlier.

On the other hand those quantities which are related to the mean vertical acceleration generally show a much better correlation with the wind, particularly in the onshore case. The value of 0.9 for the correlation coefficient relating $m_4$ to persistent onshore winds is remarkably high considering the distance between the wave buoys and the wind tower

(30 Km). The regression relationship between measured mean square acceleration and onshore wind speed was found to be

$$m_4 = a_0 + a_1 U \tag{22}$$

where

$$\begin{aligned} a_0 &= 1.34 \times 10^{-4} \quad m^2 s^{-4} \\ a_1 &= .36 \times 10^{-5} \quad m s^{-3} \end{aligned}$$

A corresponding relationship between wind speed and mean square slope was noted by Cox and Munk (1954).

Cox and Munk used photogrammetric measurements of sun glitter to estimate the distribution of slopes, viz:

$$\sigma_x^2 + \sigma_y^2 = 0.003 + 5.12 \times 10^{-3} U \tag{23}$$

where $\sigma_x^2$ and $\sigma_y^2$ are the mean square slopes in the upwind and crosswind directions and U is the wind speed (at 19.5 m altitude) in m/s. The mean square slope is given in terms of the two dimensional wave number spectrum $S(k_x, k_y)$ as follows

$$\sigma_x^2 + \sigma_y^2 = \int_{-\infty}^{\infty} \int_{-\infty}^{\infty} S(k_x, k_y)(k_x^2 + k_y^2) dk_x dk_y \tag{24}$$

$$\sigma_x^2 + \sigma_y^2 = \int_0^{\infty} \int_0^{2\pi} S(k, \theta) d\theta k^3 dk \tag{25}$$

where $k_x = k \cos\theta$ and $k_y = k \sin\theta$. It follows from the dispersion relation, $k = \omega^2/g$, that

$$\int_0^{2\pi} S(k, \theta) d\theta k dk = S(\omega) 2\omega d\omega \tag{26}$$

Hence

$$\sigma_x^2 + \sigma_y^2 = 2 \int_0^{\infty} S(\omega) \omega^4 d\omega / g^2 \tag{27}$$

Thus

$$\sigma_x^2 + \sigma_y^2 = 2(2\pi)^5 m_4 / g^2 \tag{28}$$

Substituting (22) in (28) yields $7.26 \times 10^{-4}\ m^{-1}s$ for the regression coefficient, a value considerably smaller than that of $5.12 \times 10^{-3}\ m^{-1}s$ in (23)

above. This discrepancy can be attributed to the approximation made by limiting the domain of integration of the integral in (20). The mean square slopes found by Cox and Munk were larger than those derived here because their optical technique was sensitive to slopes covering a wider range of spatial frequencies than is taken into account by the integration.

The lower values of the correlation between the slope/acceleration statistics and the wind in the offshore cases may be due to differences in wind speed between the wind tower and the open ocean. Measured offshore winds are less likely to be representative of the open sea owing to topographic effects. The west coast of Tasmania is mountainous with elevations of 1000m being common within 40 Km of the sea. Nevertheless even in this case the correlation is still as good as would be expected between two sets of wind measurements from localities 30 Km apart in a coastal environment.

## 4.3 Relation between wind speed and the variance density of sea surface elevation

The relationship between frequency band variances and instantaneous onshore and offshore wind speeds was found by computing the correlation coefficient, r, for windspeed versus frequency band variance defined by (4) for various frequency bands in the range .04 to .5 Hz. The results for the two classes are shown graphically as the solid curves in Figure 44. The maximum value of the correlation coefficient was r = 0.85 for the frequency range 0.25 to 0.30 Hz for the onshore data set. The correlation was negative at frequencies below 0.16 Hz with a minumum of -.235 for the frequency range 0.10 to 0.12 Hz for the offshore data set. Because of the large number of points in the sample this negative correlation coefficient is significantly different from zero to better than one part in $10^{20}$ .

The results for persistent winds are shown as the dashed lines in Figure 44. There were 492 cases in the upper, onshore sample and 723 cases in the lower, offshore sample.

The correlation between variance density and wind speed shown by the solid curves in Figure 44 is certainly remarkably good at frequencies greater than about 0.25 Hz, particularly in the onshore case. At lower frequencies the curves are quite different; the variance density being negatively correlated with wind speeed for the offshore case at frequencies below 0.2 Hz.

The persistence of the wind appears to make little difference in the onshore case although it does have a small but significant effect on the offshore

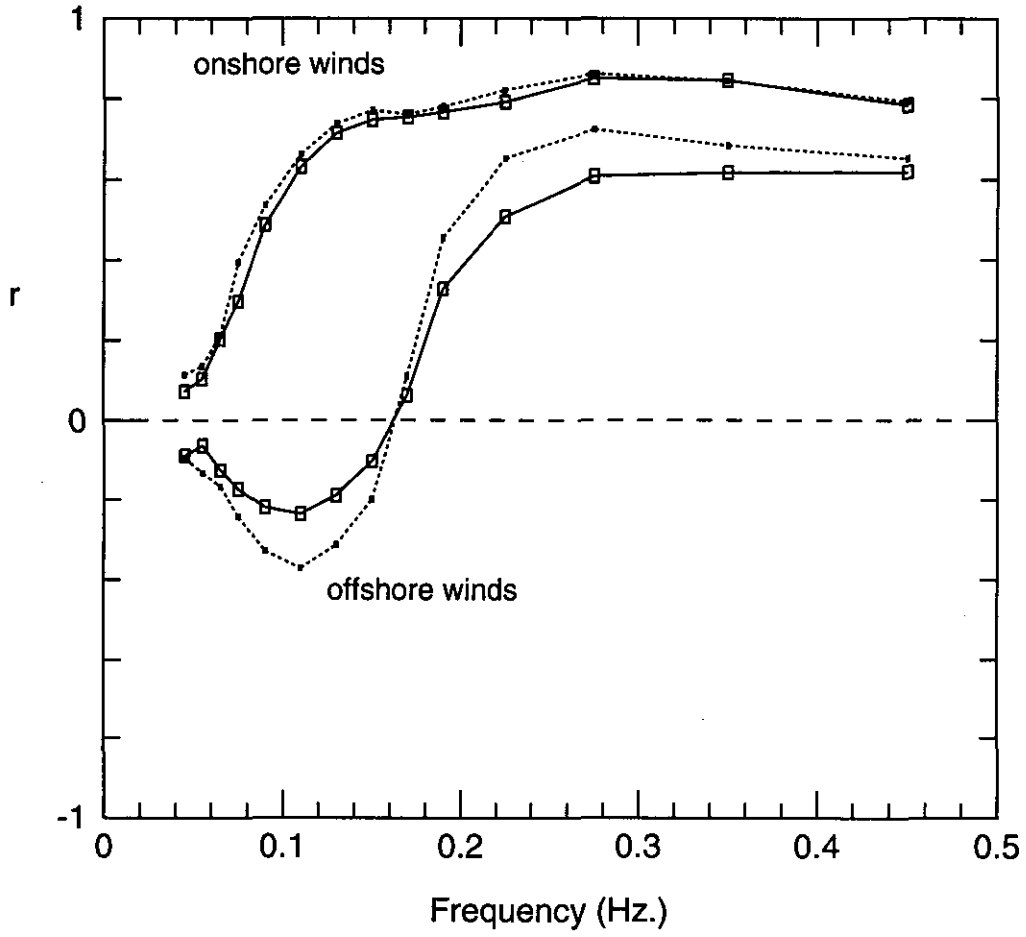


Figure 44: Sample correlation coefficient, r, of sea surface displacement variance density vs wind speed as a function of frequency. Upper curves - onshore winds, lower curves - offshore winds. The dotted curves show the values for "persistent" winds (see text).

| group | range m/s | number onshore | offshore |
|---|---|---|---|
| 1 | $0 \leq U < 2$ | 138 | 278 |
| 2 | $2 \leq U < 4$ | 351 | 764 |
| 3 | $4 \leq U < 6$ | 369 | 747 |
| 4 | $6 \leq U < 8$ | 344 | 433 |
| 5 | $8 \leq U < 10$ | 390 | 277 |
| 6 | $10 \leq U < 12$ | 194 | 169 |
| 7 | $12 \leq U < 14$ | 75 | 51 |
| 8 | $14 \leq U < 16$ | 35 | 23 |

Table 38: Numbers of spectra averaged in each wind group

correlations. Evidently in the open ocean the waves are generally close to equilibrium with the wind in terms of the three hour sampling time of this study.

## 4.4 Average spectra

The variance density spectral estimate of sea surface displacement $S(f)$ is found by averaging $P_n$ over a range of frequencies, viz:

$$S(f) = \sum_{n=n_1}^{n_2} P_n/(n_2 - n_1)\delta f \tag{29}$$

It is often more informative with ocean wave spectra to plot the variance density of the vertical component of sea surface acceleration, $S_a(f)$, rather than of sea surface displacement. Thus

$$S_a(f) = \sum_{n=n_1}^{n_2} (2\pi f)^4 P_n/(n_2 - n_1)\delta f \tag{30}$$

where $f = (n-1)\delta f$.

In practice owing to the transfer function of the buoy telemetry system, the variance density falls off very rapidly with frequency above 0.5 Hz. This is well below the Nyquist frequency implying that the spectra were free from aliasing effects.

The onshore and offshore sets were divided into eight groups according to the absolute magnitude of the wind speed. The ranges and the number of spectra in each group are shown in Table 38. The periodograms for each group were averaged to produce a mean periodogram from which a mean spectral

estimates were derived by (29) and (30) above. The resulting smoothed mean displacement and acceleration spectra are shown in Figures 45 and 46. The spectra of Figures 45 and 46 were averaged over 21 neighbouring values of $P_n$ giving a frequency resolution of 0.02625 Hz. This is about half the width of the narrower peaks in Figure 46 (b).

All of the mean displacement spectra in Figures Figures 45 (a) and 46 (a) are dominated by a single peak at 0.08 Hz. Only the mean spectra for high offshore wind speeds show a separate wind-sea peak. Apart from this the only major difference between displacement spectra for the different wind speed groups lies in the size of this peak; for onshore winds the peak increases in size with increasing wind speed while for offshore winds it generally decreases with increasing wind speed.

More detail can be seen in the acceleration spectra Figures 45 (b) and 46 (b) the density spectra have been multiplied by the function $(2\pi f)^4$. The differences between the two sets of mean acceleration spectra are more striking. In the onshore case there are no sharp peaks while in the offshore case the spectra are sharply peaked for the high wind speed groups. This is the "overshoot effect" of Barnett and Wilkerson (1967) which is characteristic of short fetch spectra.

The onshore and offshore acceleration spectra for winds of less than 2 metres per second (Group 1) are almost identical and are flat in both cases with a low frequency cut-off near 0.07 Hz. This indicates that the high frequency tail of the corresponding displacement spectra have a fourth power decay with frequency. These spectra describe an average "swell background" for this site since negligable wind-sea would be generated in such light winds. Effectively this is the shape of the average spectrum at the site in the absence of local wind.

This swell background appears to control the shape of spectra at higher wind speeds in the onshore case in that all the mean displacement spectra have a similar shape and peak frequency to the Group 1 spectrum. Even in the offshore case the shapes of the displacement spectra are dominated by this peak even though the spectra of the higher wind speed groups exhibit a second or "wind-sea" peak. The offshore acceleration spectra on the other hand are dominated by this "enhanced" wind-sea peak similar to that observed at higher wind speeds in swell free conditions, for example by Donelan *et al* (1985) .

Thus an onshore wind or wind-sea enhances the pre-existing swell background without changing its frequency whereas an offshore wind or wind-sea diminishes the swell background and superimposes a wind-sea on top of it.

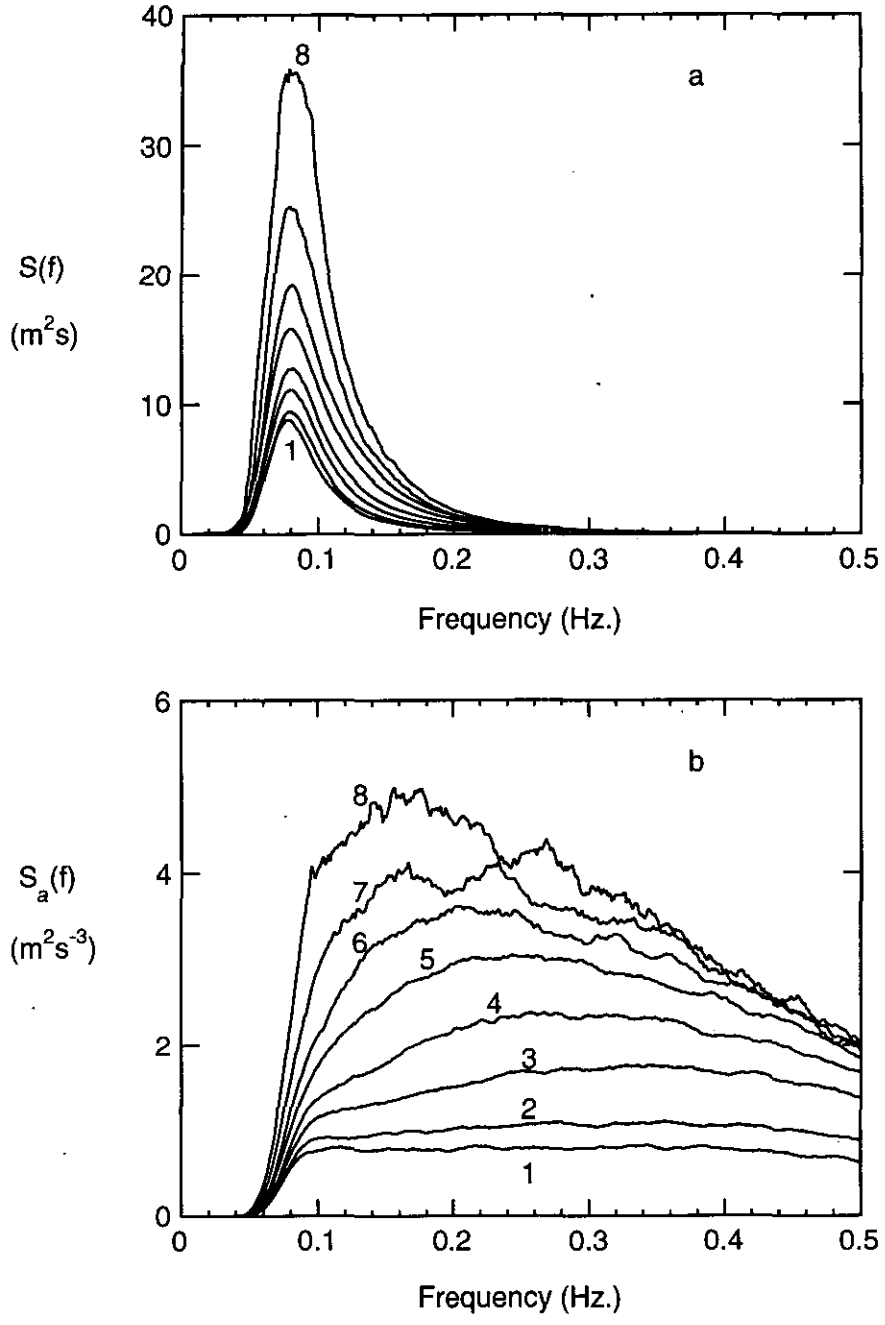


Figure 45: (a) Mean sea surface displacement variance density spectra and (b) mean sea surface acceleration variance density spectra for eight onshore wind speeds. The spectra are labelled according to the wind speed groups shown in Table 38. The spectra are smoothed with a 21 point running mean.

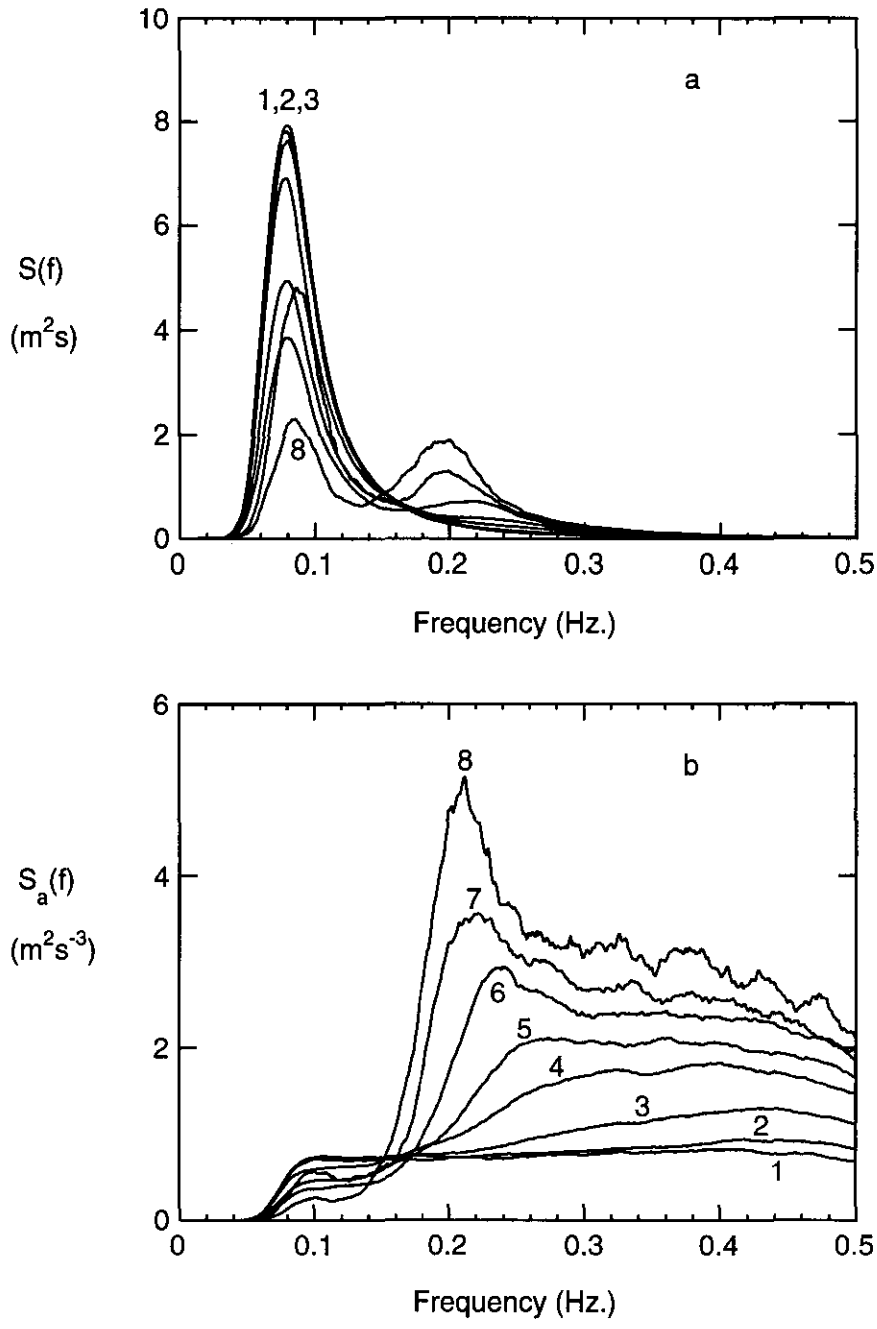


Figure 46: (a) Mean sea surface displacement variance density spectra and (b) mean sea surface acceleration variance density spectra for eight offshore wind speeds. The spectra are labelled according to the wind speed groups shown in Table 38. The spectra are smoothed with a 21 point running mean.

## 4.5 Conclusions

Mean wave spectra observed in this open ocean regime where swell was almost always present differed from self-similar wave spectra observed previously by other workers in the absence of swell. These include for example Pierson and Moskowitz (1964), Hasselmann *et al* (1973) and Donelan *et al* (1985).

Mean displacement spectra were dominated by a single peak at a frequency which was independent of wind speed and equal to the peak frequency of the background swell observed in light winds. Increasing wind speeds caused the peak to be enhanced or diminished according to whether the wind was onshore or offshore but did not alter its frequency. These observations suggest that in the open ocean the development of wind-sea is conditioned by the pre-existing swell and that energy input from the wind is ultimately transferred to frequencies at which energy was already present in the spectrum.

Fetch limited wind-seas generated by offshore winds developed in a similar way to those in described for swell-free conditions (Donelan *et al* 1987) and showed strong peak enhancement at higher wind speeds. During offshore winds wave energy at the low frequency end of the spectrum was found to be negatively correlated with the wind speed in accordance with the nautical maxim:"an opposing wind flattens a swell".

The significant wave height, $H_\sigma$ , and mean zero crossing period, $T_z$ , did not correlate well with wind speed. However "surface slope" parameters such as $H_\sigma/T_z^2$ were much better correlated with the wind and the sample acceleration variance, $m_4$ , showed an exceptionally high correlation with onshore winds. This is consistent with Cox and Munk's (1954) relationship between wind speed and the mean square slope of the sea surface.

# 5 Estimating the return period of significant wave height

## 5.1 Introduction

Estimating such return period values is problematic. Ideally the physical quantity in question should be monitored for many lifetimes of a structure in order to gain a proper statistical assessment. In practice this luxury is denied us and estimates must be made on the basis of observations which endure for only a small fraction of the lifetime in question. As a result we are forced to make *a priori* assumptions about the underlying statistics of the physical quantity being assessed. In particular we must assume a distribution function for the quantity.

Nevertheless there are some mitigating aspects. Because we are only interested in extreme values only certain distributions are possible. For example, Fisher and Tippett (1926) have shown that there are only three limiting forms of the frequency distribution function of the largest or smallest member of a sample. Their work has been followed by others, notably Gumbel (1954, 1958). The subject is reviewed by Isaacson et al (1981) and is discussed in many engineering texts.

Much of the work in this field has been concerned with observations of extreme events, often made visually. In recent times changing technology has enabled the automatic recording of natural physical quantities such as wave height, wind speed and so on. Generally such recordings are made by sampling at regular intervals of time. Such discretely recorded data are fundamentally different from extreme data recorded previously. This is so for two reasons -

(i) the data are no longer comprised solely of extremes so that the assumptions and hence the distributions of Fisher and Tippett may no longer apply, and

(ii) because of the discrete sampling, extreme events which are shorter than the sampling period may be missed altogether by the sampling process.

This fundamental distinction between event based or continuously recorded data on the one hand and discretely sampled data on the other has received little attention in the literature but it has some important consequences.

Return periods based on the two approaches can be related to one another via the mean duration of events

## 5.2 Relationship Between Return Periods

An attempt to reconcile the two approaches has been attempted by Carter (1987) who fitted a Gumbel (Fisher-Tippett type I) distribution to discretely sampled significant wave height data. Certainly the fit is remarkably good considering that the Fisher-Tippett conditions no longer apply. He defines the $N$-year return value $x_N$ as that value which is exceeded on average once in $N$ years and gives the following formula for $x_N$

$$\Pr(H_\sigma < x_N) = 1 - \frac{1}{Nn} \tag{31}$$

i.e.

$$\Pr(H_\sigma \geq x_N) = \frac{1}{Nn} \tag{32}$$

where $n$ is the number of samples per year. It is certainly true that this formula gives the probability of sampling a value of $x_N$ or greater in $Nn$ samples this is not the same thing as a the probability of the value $x_N$ or greater occurring in $N$ years because it may occur at a time when no sample is being taken.

This distinction between occurring and merely being observed or sampled is an important one. After all marine structures do not exist for only seventeen minutes every three hours; they must survive wave conditions continuously. Furthermore sampling is often carried out with long periods between samples. For example satellite altimeters sample a given area of ocean with the return period of the satellite which may be many days. In this case value of $n$ in (31) would be much less than that used by Carter and the return period $N$ in (31) would need to be much larger to give the same number of samples and the same encounter probability. The return period, $N$, in Carter's formula depends on the sampling rate - it should be called the "discrete sampling return period", $T_d$ . For practical purposes what is required is the "occurrence return period", $T_c$ . The two are different; one depends on the sampling rate and the other does not. The occurrence period, $T_c$ , is required for engineering purposes while $T_d$ is derived from the observations.

The two periods may be related by the following simple argument. A quantity such as significant wave height can be considered a continuous function of time. Consider some threshold level, $x$, which the continuous function, $H_\sigma(t)$, crosses from time to time. Let the interval between an

upcrossing of the threshold level and the succeeding downcrossing be termed an "event" and the time between the upcrossing and downcrossing be termed the "event duration", $D$. The "event rate", $R$, is the average number of events expected in unit time, i.e.

$$R = \frac{N_e}{T} \tag{33}$$

where $N_e$ is the number of events occurring in time $T$. The return period of the continuous process is $T_c$ , the occurrence return period, and is defined as

$$T_c = 1/R \tag{34}$$

The mean event duration, $\bar{D}$, is given by

$$\bar{D} = \sum_{i=1}^{N_e} \frac{D_i}{N_e} \tag{35}$$

where $D_i$ is the duration of the $i$ th event. The proportion of time for which the process, $H_\sigma(t)$, is above the threshold is $\bar{D}.N_e/T$. Hence the probability, $p$, of an event being in progress at a random instant is

$$p = \frac{N_e.\bar{D}}{T} \tag{36}$$

i.e.

$$p = \frac{\bar{D}}{T_c} \tag{37}$$

It follows that the probability, $P_n$ , of observing at least one event in progress in $n$ randomly selected instants is

$$P_n = 1 - (1 - p)^n \tag{38}$$

i.e.

$$P_n = np \tag{39}$$

if $p$ is small. Since event occurrences are assumed to be random (39) also applies to $n$ equally spaced sampling times. If the process $H_\sigma(t)$ is sampled at the rate of $n$ samples per year, this probability, $P_n$ , is the probability of observing at least one event in one year by discrete sampling. That is, $P_n$ is the number of events expected per year at a sampling rate of $n$ samples per year; it is the discrete sampling event rate. By analogy with (34), the discrete sampling return period, $T_d$ , is given by

$$T_d = 1/P_n \tag{40}$$

i.e.

$$T_d = \frac{T_c}{n.\bar{D}} \tag{41}$$

and the distribution function for discrete sampling, $F(x)$ , is given by

$$F(x) = \Pr(H_\sigma < x) = 1 - p \tag{42}$$

i.e.

$$F(x) = 1 - \frac{\bar{D}}{T_c} \tag{43}$$

where $\bar{D}$ and $T_c$ are both functions of the threshold value $x$.

It is $F(x)$ which is determined experimentally by fitting a distribution to the observations. Equation (43) implies that in order to determine the return period of events, $T_c$, from the fitted distribution the mean duration of events, $\bar{D}$, must be known or estimated in some way. The transition from sampling probability to occurrence probability involves a property of the events themselves, it does not depend solely on the sampling interval.

## 5.3 The High Density Data Set

Of the statistics discussed the one of most interest is the significant wave height, $H_\sigma$, defined as four times the sample standard deviation of sea surface height. Figure 47 shows the autocorrelation function for this statistic computed from the 11,788 samples in the database. The half width of the autocorrelation function, i.e. twice the lag for which the autocorrelation function has the value of 0.5, is 54 hours.

It may be argued that the width of the autocorrelation function gives an indication of the mean duration of events but this is not the case. The shape of the autocorrelation function is dominated by a very large number of moderately sized events whereas we are interested in a few extreme events which may have an altogether different temporal structure. Furthermore a cursory examination of the data indicated that large events tended to have durations which were small compared with the three hour sampling time. Ideally, to estimate the mean duration a continuous record of the statistic as a function of time would be required.

Although continuous data were not available, fortuitously a high density data set was saved. From 24 January 1987 until 8 September 1992 summary

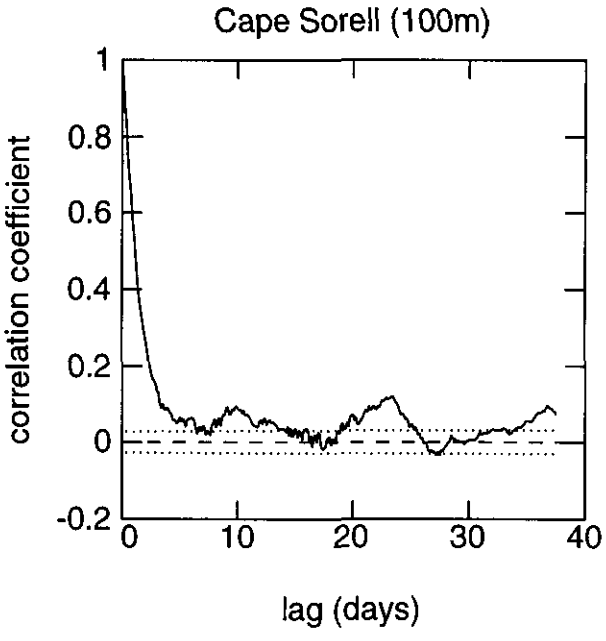


Figure 47: Autocorrelation function of significant wave height.

statistics were computed and saved every 20 minutes. These were originally calculated to allow real time monitoring of sea state at the remotely located shore base by the Bureau of Meteorology. These statistics included the standard deviation of sea surface height from which significant wave height can be computed. Thus, for this period of five and a half years significant wave height data were saved at nine times the rate of the routinely archived data. This data set was suitable for estimating mean event duration as a function of threshold significant wave height.

## 5.4 Estimation of Mean Event Duration

Unfortunately large data gaps occurred from time to time because of equipment failures. In all only 3.75 years of good data were available. The existence of data gaps had to be taken into account in devising a scheme for estimating mean event duration. It was assumed that data gaps were random and not related to sea state. In fact most data losses were due to radio interference from distant broadcast stations.

Data thresholds in $H_\sigma$ from 5.0 m to 10.0 m in steps of 0.1 m were used. The time series of twenty minute values of $H_\sigma$ was scanned. The time of

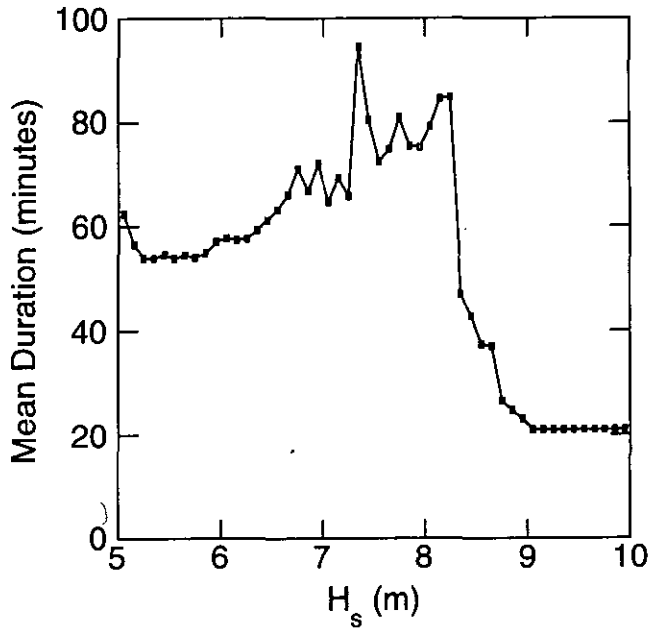


Figure 48: Mean duration as a function of significant wave height.

upcrossing of the 5.0 m threshold was noted and an "event" flag set. The event flag was cancelled at the first downcrossing of the 5.0 m level. During each these event intervals the total time spent above each of the thresholds was summed and the number of upcrossings of each threshold was counted. At the end of the event, providing there were no data gaps in the event interval, the counts and times for each threshold were added to the grand totals of counts and times for that threshold. If on the other hand a data gap of greater than 50 minutes was encountered the event was aborted and the grand totals were not updated. This was done to prevent data gaps from biasing the statistics. When a data gap resulted in an event being rejected all the events at all thresholds were rejected otherwise thresholds giving rise to short events would have been favoured over those giving rise to long events. The results are shown graphically in Figure 48.

In Figure 48 the mean duration for thresholds above 9.0 m is 20 minutes. Obviously these are not real. These values were generated by a single event and reflect the 20 minute time resolution of the method. The mean duration of events rises from around 60 minutes to around 80 minutes as the threshold increases from 5.0 m to 8.2 m. However the most striking feature of Figure 48 is the sudden drop in mean duration of events for threshold values above 8.2 m; its value falls rapidly from 80 minutes to 20 minutes as the threshold

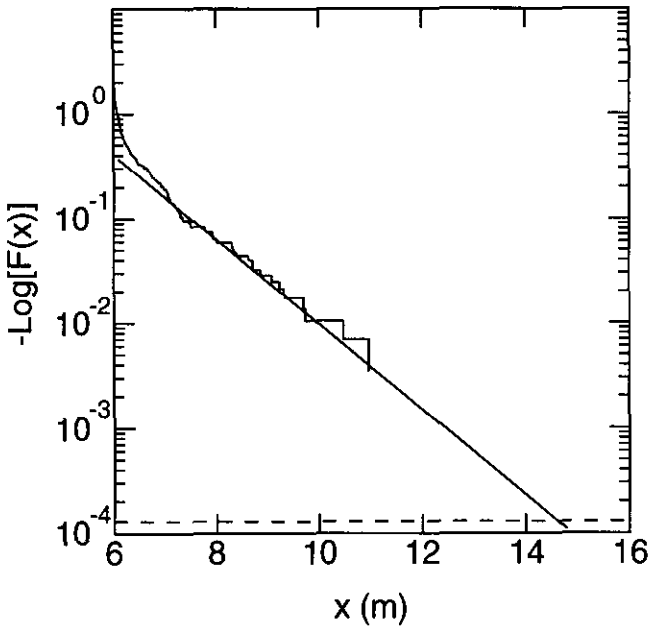


Figure 49: Event data fitted to a Gumbel distribution.

increases from 8.0 m to 9.0 m. Since the method cannot resolve durations shorter than 20 minutes, this rapidly decreasing trend suggests that mean durations for thresholds above 9.0 m may be even less than this resolution limit.

## 5.5 Event based computation of 100 year return period

The high density data set was also used to compute return periods based on the distribution of extreme events. All the events with thresholds greater than 6 m were saved for analysis. No attempt was made to allow for data gaps. An observed cumulative distribution, $G_e(x)$, was defined by

$$G_e(x) = \frac{N_e(x)}{N} \tag{44}$$

where $N_e(x)$ is the number of events for which $H_\sigma < x$ and $N$ is the total number of events.

The three Fisher-Tippett distributions, also known as the Gumbel, Fréchet and Weibull distributions, were fitted to $G_e(x)$. The observed and fitted

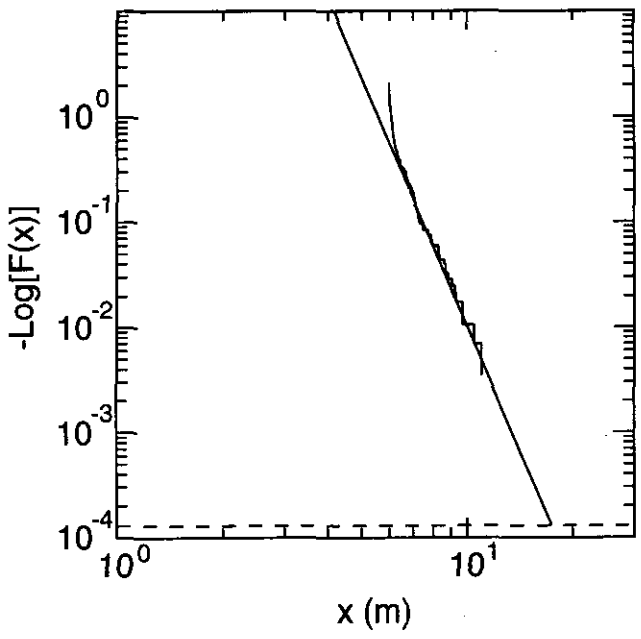


Figure 50: Event data fitted to a Fréchet distribution.

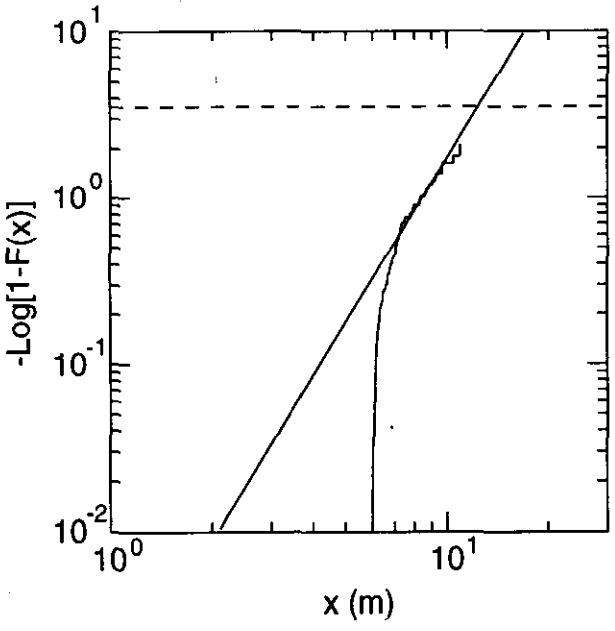


Figure 51: Event data fitted to a Weibull distribution.

| Figure | Distribution | $x_{100}$ |
|---|---|---|
| 3 | Gumbel | 14.62m |
| 4 | Fréchet | 17.42m |
| 5 | Weibull | 12.40m |

Table 39: Hundred year significant wave heights estimated from storms

distributions are shown in Figures 49, 50 and 51. The axes were chosen so that fitted distributions would be straight lines in each case and could be fitted by the method of linear regression. The value of the fitted distribution function, $\hat{F}_e(x)$, corresponding to the 100 year return period is shown plotted as the dashed line in each of these figures. This value, $\hat{F}_e(x_{100})$, was computed as follows: Let $R$ be the rate of storms of a given maximum significant wave height per year. Now $R$ is the rate of events per storm multiplied by the number of storms per year, $S$. Hence

$$R = [1 - \hat{F}_e(x)].S \tag{45}$$

where $S = n/T$ where $n$ is the number of storms and $T$ is the length of time of the observations not including data gaps. Thus

$$\hat{F}_e(x) = 1 - \frac{R}{S} \tag{46}$$

The value of $x_{100}$ is found by setting $R = 0.01$ and solving (46) for $x$. Estimated values of $x_{100}$ are shown in Table 39. Despite the apparently good fit to each of the possible distributions there is a spread of thirty percent in the three estimates of hundred year significant wave height.

## 5.6 Sample based estimation of 100 year return period

The above calculations were based on data from a high density data set in which samples were taken every twenty minutes. Significant wave height is not usually sampled this frequently; three hourly sampling is more common. Carter (1987) has described a method for estimation of return period from discretely sampled data of this sort.

Three hourly data bursts from the Cape Sorell 50m and 100m sites were saved along with the high density set described above. Only those bursts recorded in the same time interval as the high density data were used in this analysis to allow comparison of the results with results from the other data set. Significant wave height values in the range 0 to 20 m from this set were

sorted into 100 bins or range sets each 0.2 m wide. In all 10086 values were sorted. Plots of this binned data are shown in Figure 52.

In Figure 52 the upper graph shows the cumulative distribution of the binned data while the lower graph shows a histogram of the percentage of the significant wave height values lying in each range set.

A Gumbel distribution was fitted to the binned data, viz:

$$F(x) = e^{-e^{-\frac{x-A}{B}}} \tag{47}$$

i.e.

$$y = -\frac{x - A}{B} \tag{48}$$

where

$$y = \ln[-\ln F(x)] \tag{49}$$

Two methods were used to estimate the parameters, $A$ and $B$, of the Gumbel distribution. The upper solid line shows the fit obtained using the method of moments whereby the mean, $\bar{x}$, and standard deviation, $\sigma$, of the sample were equated to those of the Gumbel distribution giving the following relations to be solved for $\hat{A}$ and $\hat{B}$ -

$$\bar{x} = \hat{A} + \gamma\hat{B} \tag{50}$$

and

$$\sigma = \frac{\pi\hat{B}}{\sqrt{6}} \tag{51}$$

The lower solid line shows the fit obtained by fitting the linearised form (48) to the plotted points by the method of linear regression. For example the parameter, $\hat{B}$, was found as the reciprocal of the regression coefficient of $y = \ln[-\ln G(x_i)]$ on $x_i$, where $G(x_i)$ is the proportion of observed significant wave height values, $H_\sigma$, which lie in the range $x_i - \Delta x/2 < H_\sigma < x_i + \Delta x/2$ where $\Delta x$ is the width of each bin.

The density function, $\hat{f}(x)$, the derivative of the fitted distribution function, $\hat{F}(x)$ in (47), is shown superimposed on the histogram of the binned values in the lower graph of Figure 52. The values of $\hat{A}$ and $\hat{B}$ derived by the method of moments were used.

Having determined a distribution function, $\hat{F}(x)$, which fits the data, all that is required to estimate the 100 year significant wave height is to extrapolate the function using (43) above to find the value of $x$ which corresponds to a return period, $T_c$, of 100 years. Firstly a value of $\bar{D}$ must be chosen. In effect

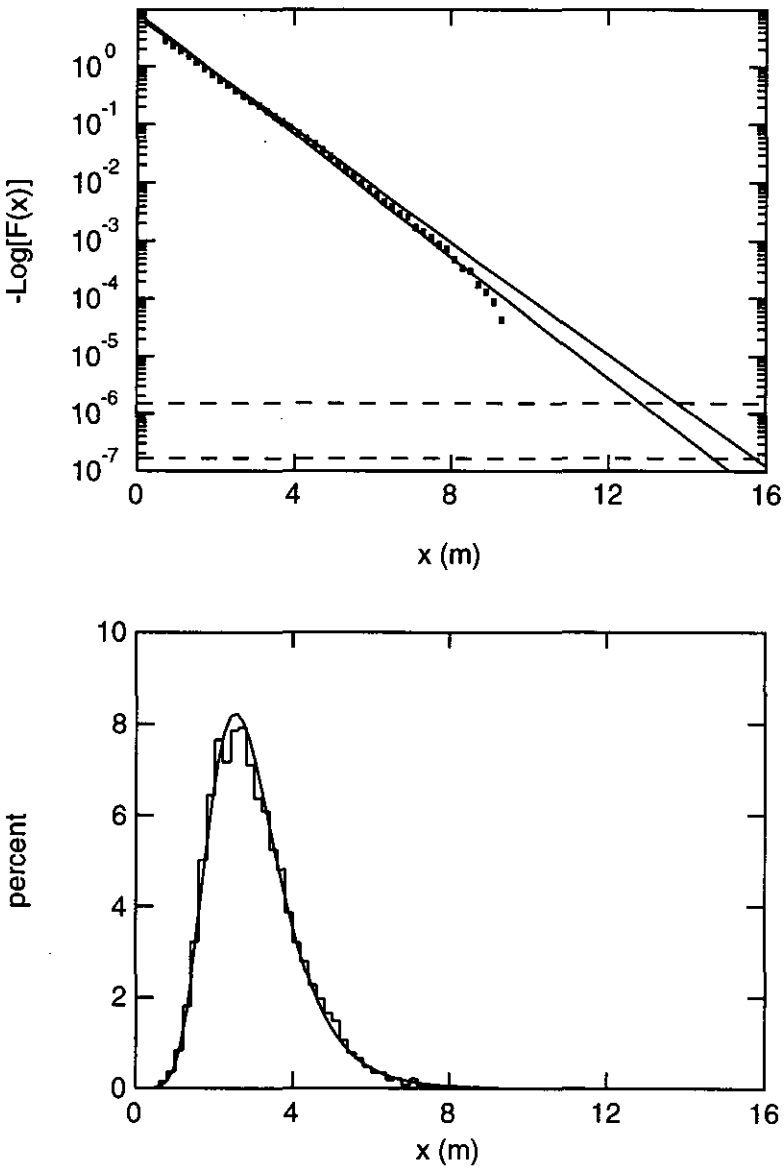


Figure 52: Sample data fitted to a Gumbel distribution. The upper graph shows cumulative data, the lower graph binned data. The solid lines show the fitted distributions. The dashed lines show the hundred year event probabilities based on assumed durations of 3 hours (upper) and 20 minutes (lower) respectively.

| Type of Fit | Gumbel Parameters | | $H_{\sigma 100}$ | |
|---|---|---|---|---|
| | $\hat{A}$ | $\hat{B}$ | $\bar{D}$ = 3 hrs | $\bar{D}$ = 20 min |
| regression | 2.464 | 0.8244 | 12.84 m | 14.65 m |
| moments | 2.517 | 0.8937 | 13.76 m | 15.72 m |

Table 40: Hundred year significant wave heights estimated by sampling

Carter (1987) uses the 3 hour sampling period for $\bar{D}$ whereas Figure 48 suggests that a much shorter time than this should be used, say 20 minutes.

The upper dashed line in Figure 52 show the values of $F(x)$ corresponding to $T_c = 100$ years and $\bar{D} = 3$ hours. The lower dashed line shows the probability for $\bar{D} = 20$ minutes.

The values of significant wave height corresponding to the four intersections of the two fitted distributions in Figure 52 with the two probability levels are shown in Table 40.

Setting $\bar{D}$ equal to the sampling interval of 3 hours in (43) is equivalent to using Carter's (1987) formula, (31). It can be seen from Table 40 that the predicted 100 year maxima of significant wave height are considerably less than those predicted using a more realistic estimate of extreme event duration of 20 minutes. Assuming for the moment that the method of moments gives the better estimate, then 13.76 metres is the maximum significant wave height expected in data sampled every three hours for 100 years while the expected maximum for continuous sampling is 15.72 metres under the assumption that such events only last for about twenty minutes.

Carter noted that points at the upper end of his plot lay below the fitted distribution and that such "dropping away" seemed to be a common experience. The same effect can be seen in the upper graph of Figure 52. It is interesting to note that in both Carter's plot and in Figure 52, this dropping away occurs at a similar significant wave height to that at which the mean event duration in Figure 48 begins to decrease rapidly. Presumably fewer events are observed in the sampled data because the events are shorter rather than less frequent. The fact that this height of just over 8 metres is the same for both data sets suggests that there may be something fundamental in the physics of ocean waves which causes wave energy to dissipate more rapidly when the significant wave height exceeds this threshold.

This dropping away of the frequency of higher significant wave heights is important in another sense. Two methods of estimating the Gumbel parameters A and B were used, viz; the method of moments and the regression method. Under the latter method the best least squares fit of a

straight line was made to the log-log plot of the observed cumulative distribution of the binned data. Under this method all of the data points were given equal weight despite the fact that there were considerably fewer data points determining the location of the points at the outer end of the plot. This method was therefore biased in favour of these extreme points. The fact that these points tended to lie below the trend line reveals why the regression line was steeper than the moment-fitted line and predicted lower 100 year wave heights. For these reasons the moment fitted estimates of the parameters are considered to be better estimates.

Using the moment-fitted estimate of the Gumbel parameters and assuming a mean event duration of 20 minutes gives an estimated value of the significant wave height with 100 year return period of 15.72 m, the largest of the four values in Table 40.

## 5.7 The Extreme Event of 29 July 1985

In the context of extreme value estimation, the storm which took place on 29 July 1985 will now be examined. The storm was remarkable in that significant wave heights and maximum wave heights were recorded which were considerably larger than any others recorded during the seven year span of the program. It occurred outside the period of high density data collection and so was not included in the statistics discussed above.

The main surface wave statistics for the most intense part of the storm are listed in Table 42. Two buoys were in operation, moored in 100m and 50m of water at sites A and B in Figure 4 at distances of 17 Km and 7 Km off-shore respectively. The onshore data logging system was programmed to commence saving a burst of data from site B at every even hour and then to switch receiver channels and commence saving a burst from site A 20 minutes later. Each burst comprised 1024 sea surface height records sampled at a rate of 2.56 samples per second to give 400 seconds of data per burst. Data bursts containing even one "unlocked" bit were usually rejected for analysis purposes. However in this case all the available bursts have been listed including those with a non-zero "unlocked" count. The unlocked count, U, is included in Table 41. Also included are the significant wave heights, $H_\sigma$ and $H_{\frac{1}{3}}$, the maximum upcrossing wave height for each burst, $H_{mu}$, the maximum downcrossing wave height for each burst, $H_{md}$, the mean zero crossing period, $T_z$, and the spectral peak period, $T_p$.

The storm occurred only eighteen days after the commencement of the wave program and some faults in the data logging system were still to be

| buoy | date July 1985 | time EST | U | $H_\sigma$ m | $H_{\frac{1}{3}}$ m | $H_{mu}$ m | $H_{md}$ m | $T_z$ s | $T_p$ s |
|---|---|---|---|---|---|---|---|---|---|
| B | 29 | 1400 | 0 | 8.68 | 8.08 | 12.21 | 12.87 | 9.53 | 15.38 |
| A | 29 | 1420 | 0 | 7.99 | 7.69 | 10.77 | 11.12 | 9.14 | 10.00 |
| B | 29 | 1600 | 0 | 8.74 | 8.24 | 11.59 | 12.18 | 9.92 | 12.50 |
| B | 29 | 1800 | 0 | 7.93 | 7.68 | 10.36 | 12.07 | 9.92 | 16.67 |
| B | 29 | 2000 | 7 | 13.59 | 12.80 | 18.87 | 16.98 | 12.09 | 14.81 |
| A | 29 | 2020 | 0 | 13.15 | 12.64 | 19.83 | 17.05 | 12.78 | 17.39 |
| B | 30 | 0200 | 127 | 8.15 | 7.33 | 11.52 | 11.69 | 9.48 | 16.00 |
| A | 30 | 0220 | 3 | 8.86 | 8.20 | 10.51 | 9.85 | 10.31 | 18.18 |
| B | 30 | 0400 | 0 | 8.01 | 7.83 | 10.62 | 10.87 | 9.96 | 12.90 |
| A | 30 | 0420 | 292 | 7.13 | 7.78 | 10.26 | 9.21 | 10.76 | 17.39 |
| B | 30 | 0600 | 0 | 8.02 | 7.13 | 10.33 | 9.75 | 11.08 | 18.18 |

Table 41: Burst statistics for the event of 29 July 1985

remedied. In particular from time to time bursts of data were not saved as they should have been leaving gaps in the record. The bursts from buoy A at 2220 and 0020 and from buoy B at midnight are missing for this reason.

If the peak value of $H_\sigma$ of 13.15 m had been recorded by buoy A alone some spurious origin or instrumental failure would have been suspected, particularly as the values before and after were not particularly large. However a similar significant wave height was recorded twenty minutes later by the other buoy situated 10 Km away. This is a compelling argument for the validity of the data. Furthermore the other height statistics $H_{md}$ and $H_{mu}$ varied in proportion with $H_\sigma$, an unlikely outcome if the data had been corrupted in some way.

The fact that the ratios $H_{mu}/H_\sigma$ and $H_{md}/H_\sigma$ remained close to their usual value of about 1.5 indicates that the high values of $H_\sigma$ and $H_{\frac{1}{3}}$ were not due to a small number of very large waves; this was an extreme storm not an extreme wave. The shift in $T_z$ to greater than 12 seconds during the storm peak indicates that the extra energy lay in the swell end of the spectrum around periods of 17 seconds or so according to the value of $T_p$.

How does the observation of such an extreme event relate to methods of prediction of extreme events discussed above?

Several methods of predicting 100 year significant wave heights for the site have been described. The fortuitous observation of this event provides a benchmark against which to test these methods. The inverse problem is easily solved, that is, given a wave height and a distribution, what is the probability of the wave height being exceeded at least once in a given period

of time. In the calculations discussed below the value of the significant wave height of 13.15m recorded at 2020 EST by buoy A is used (see Table 41). This is done for two reasons, firstly the higher value of 13.59 m at 2000 EST was calculated from a data burst which exhibited "unlocked" data indicating the possibility that this burst was corrupted in some way, and secondly, buoy A was located at the mooring site from which the high density data set was collected.

Using the event based distributions shown in Figures 49, 50 and 51 the return period was calculated in each case by evaluating the fitted distribution, $\hat{F}(x)$ at $x = 13.15$ and substituting in (45) to find $R$. The return period, $T_c$, for this significant wave height is then given by

$$T_c = \frac{1}{R} \tag{52}$$

The probability of occurrence of this wave height at least once during the seven year period of the wave program, $P_7$, is given by

$$P_7 = 1 - (1 - p)^7 \tag{53}$$

where $p = R$ is the probability of an occurrence in any single year. The results are shown in Table 43. Note that the probability of occurrence, $p$, is not the same thing in general as the expected rate of occurrence, $R$. The two quantities are numerically equal only when $R$ is very small and the occurrence probability for the interval has a Poisson distribution as in this case. If, for example, $R$ were to be expressed in units of events per century this would not be the case.

Using the sample based distribution shown in Figure 52 the return period, $T_c$, may be calculated by substituting $x = 13.15$ in (43). Only the upper, moment-fitted distribution, $F(x)$, in Figure 52 is used for reasons discussed above. The event duration, $\bar{D}$, was assumed to be 20 minutes. The probability of occurrence in 7 years is found using (53). The results are shown in Table 43. For comparison the discrete sampling return period and the probability of observing a significant wave height this large in seven years of three hourly sampling is also shown in Table 43. These were calculated using (41), which with (43) is equivalent to Carter's (1987) formula quoted here as (31).

| Distribution | return period (years) | $P_7$ |
|---|---|---|
| Gumbel | 25.46 | .245 |
| Fréchet | 19.96 | .488 |
| Weibull | 562.8 | .012 |

Table 42: Event-based return period and probability of $H_\sigma = 13.15$ m

| | return period (years) | $P_7$ |
|---|---|---|
| occurring | 5.62 | 0.746 |
| observable | 50.6 | 0.130 |

Table 43: Sampling-based return period and probability of $H_\sigma = 13.15$ m

## 5.8 Summary

Various methods of extreme analysis have been used to estimate the significant wave height with a hundred year return period from data acquired from Tasmania's west coast.

The three Fisher-Tippett type distributions were fitted to event data from a high density data set in which observations were recorded every twenty minutes for a nett period of 3.75 years. The hundred year significant wave height predictions estimated in this way varied from 12.4m to 17.2m depending on the distribution used.

The same data set was used to estimate the mean duration of events as a function of the threshold significant wave height. This quantity was found to decline rapidly for events with thresholds exceeding 8.3 m at this site. Events with thresholds of 9 m or more were found to have durations of the order of twenty minutes or less. This event duration was used to estimate the hundred year return period from data which had been discretely sampled over the same period at three hourly intervals. The sample-based prediction of 15.72 m is consistent with the event-based predictions but is dependent on the mean event duration assumed for the population.

The high density data set was part of a longer set which had been sampled two hourly or, more commonly, three hourly for an interval of seven years. During this longer interval a single extreme event with a significant wave height of 13.15 m was recorded. The probability of occurrence of an event of this magnitude in seven years was estimated using each of the fitted distribution functions. Only the event- fitted Weibull distribution resulted in

a small probability. In all other cases the probabilities of such an event occurring in a seven year interval were found to be unremarkable. Under the assumption that the average duration of an event of this magnitude is twenty minutes, the sample- fitted Gumbel distribution yielded a value of 0.746 for the probability of such an event occurring in a seven year period, i.e. such an event is likely to occur in this time interval. Note however that the same distribution yielded only 0.13 for the probability that such an event would actually be observed during a three hourly sampling regime. There are three chances in four that such an event will occur at least once but only one chance in eight that it will be observed.

## 5.9 Conclusion

In order to predict the probability of occurrence of an event from sampled data it is essential that the mean duration of the event be known or estimated. This is particularly true of extremes of significant wave height because the durations of events in excess of 8m or so appear to be shorter than those for more moderate wave heights.

Traditionally wave data has been sampled at three hourly intervals. With the advent of high capacity disk storage it is now possible to sample and store wave data continuously and to estimate the average duration of events as well as their frequency of occurrence. This needs to be done if adequate predictions of extreme events are to be made.

# 6 Acknowledgements

This work was supported financially by grants from Steedman Science and Engineering of Perth Western Australia, from the Fisheries Industry Research Trust Account and by CSIRO appropriation funding. The authors wish to thank the Tasmanian Hydro-Electric Commission for provision of the Granville Harbour wind data, the Forestry Commission for housing the shore base facility at Strahan and the Officer in Charge and staff of the Cape Grim Baseline Air Pollution Station for looking after the shore base at Cape Grim. We would also like to thank Professor Ian Young of the Australian Defence Forces Academy for his helpful review of the manuscript.

# 7 References


Barnett,T.P. and J.C.Wilkerson, (1967). "On the generation of Ocean Wind Waves as Inferred from Airborne Radar Measurements of Fetch Limited Spectra",*Journal of Marine Research* **25**, 292-321.

Carter,D.J.T.,1988,"A simple model for estimating the return value of wave height". *Modelling the Offshore Environment (Advances in underwater technology, ocean science and offshore engineering; v12)* pp 3 - 12, Graham and Trotman Limited, London.

Cox,C. and W.Munk. (1954). "Measurement of the Roughness of the Sea Surface from Photographs of the Sun's Glitter." *Journal of the Optical Society of America***44**, 838-850.

Donelan,M.A.,J.Hamilton and W.H.Hui. (1985). "Directional Spectra of Wind Generated Waves. "*Philosophical Transactions of the Royal Society, London,* **A315**, 509-562.

Fisher,R.A., and L.H.C.Tippet, 1928, "Limiting forms of the frequency distribution of the largest and smallest member of a sample". *Proc. Cambbridge Phil. Soc.*, **24**, 180-190.

Gumbel,E.J.,1958, *Statistics of Extremes*, Columbia University Press, New York.

Gumbel,E.J.,1954, "Statistical Theory of Droughts", *Proc. Am. Soc. Civ. Eng.*, **80**, sep. no. 439.

Hasselmann,K., T.P.Barnett, E.Bouws, H.Carlson, D.E.Cartwright, K.Enke, J.A.Ewing, H.Gienapp, D.E.Hasselmann, P.Kruseman, A.Meerburg, P.Muller, D.J.Olbers, K.Richter, W.Sell and H.Walden. (1973). "Measurements of Wind-Wave Growth and Swell Decay during the Joint North Sea Wave Project (JONSWAP)." *Deutsche Hydrographisce Zeitschrift* **A8**, 1-95.

Isaacson, M, de St. Q., M. ASCE and N.G.MacKenzie, 1981, "Long-Term Distributions of Ocean Waves: a Review" *Proc. Am. Soc. Civ. Eng.*, **107**, No WW2, pp 93-109.

Kinsman, B. (1965) *Wind Waves* Prentice-Hall, New Jersey.

Mollison, D. (1986), "Wave Climate and the Wave Power Resource" in *Proc. IUTAM Symposium on the Hydrodynamics of Wave Energy Utilization* ed. by D.V.Evans and A.F.de Falcao Springer-Verlag, Heidelberg.

Palao,I.,(1994), "Quality Control of Wave Data." *Technical Bulletin, National Data Buoy Center, National Oceanic and Atmosphere Administration, Mississippi 39529-6000* **20**,pp 6-8.

PIANC (1986). "List of Sea State Parameters." *Permanent International Association of Navigation Congresses, Residence Palace, Quartier Jordaens, rue de la Loi, 155, 1040 Brussels, Belgium.*

Pierson,W.J. and L.Moskwitz (1964). "A proposed spectral form for fully developed wind seas based on the similarity theory of S.A.Kitaigorodskii." *Journal of Geophysical Research* **69**, 5181-5190.

Reid,J.S. (1989). "Some Comments on Ocean Wave Statistics." *9th Australian Conference on Coastal and Ocean Engineering, Adelaide, 4-8 Dec 1989.*

Snodgrass,F.E., G.W.Groves, K.F.Hasselmann, G.R.Miller, W.H.Munk and W.H.Powers (1966). "Propagation of Swell across the Pacific." *Philosophical Transactions of the Royal Society* **A259**, 431-497.

Underwood, R. (1987),"Wave Power on the Tasmanian Coast - A Naive Analysis" *8th Australasian Conference on Coastal and Engineering, Launceston 30 November-4 December 1987.*

**CSIRO Marine Laboratories**

**Division of Oceanography**

Headquarters
Castray Esplanade, Hobart, Tasmania
GPO Box 1538, Hobart, Tasmania, 7001, Australia


ISBN 0 643 05623 8.
ISSN 0725–4598